



MONTREAL
NEUROLOGICAL
INSTITUTE
AND HOSPITAL
McGill University

INSTITUT ET
HÔPITAL
NEUROLOGIQUES
DE MONTRÉAL
Université McGill



McGill

**Axonal Migration and Turning Investigated through Surface-bound Digital Nanodot
Gradients**

Sébastien G. Ricoult
Integrated Program in Neuroscience
McGill University, Montréal

December 2014

*A thesis submitted to McGill University
in partial fulfillment of the requirements of the degree of
Doctor of Philosophy in Neuroscience*

© Sébastien Ricoult, 2014

TABLE OF CONTENTS

Table of Contents.....	2
List of Figures and Tables.....	5
Abstract.....	7
Resume.....	9
Acknowledgments.....	11
Contributions of Authors.....	13
Preface to CHAPTER 1.....	15
CHAPTER 1: In vitro Studies of Haptotaxis as a Regulatory Mechanism in Axon Guidance through Surface-bound Protein Gradients.....	16
1-1 Abstract.....	16
1-2 Introduction.....	17
1-3 Methods to create substrate-bound protein gradients to study haptotaxis.....	20
1-3.1 Microfluidics.....	22
1-3.1.1 Serial diluter.....	23
1-3.1.2 Microfluidic probes.....	24
1-3.1.3 Inkjet printing.....	24
1-3.1.4 Vesicle mixing to form supported lipid bilayers with protein gradients.....	25
1-3.2 Controlling protein adsorption to the surface.....	25
1-3.3 Protein doping of porous membranes.....	25
1-3.4 Gel diffusion.....	26
1-3.5 Microcontact/Nanocontact printing.....	26
1-3.6 Dip pen nanolithography.....	27
1-3.7 Colloid lithography.....	28
1-3.8 Light patterning.....	28
1-3.8.1 Laser-assisted adsorption by photobleaching.....	28
1-3.8.2 Laser scanning lithography.....	29
1-3.8.3 Photolithography.....	29
1-3.9 3D gradients.....	30
1-3.9.1 Polymer scaffolds.....	30
1-3.9.2 Spin coating fibrous scaffolds.....	30
1-3.10 Reference Surface.....	30
1-4 <i>In vitro</i> studies of axonal navigation on substrate-bound protein gradients...	31
1-4.1 Response to patterned molecules and concentrations.....	31
1-4.2 Intracellular response mechanism.....	33
1-4.3 Gradient characteristics to halt navigation.....	35
1-4.4 Combinatorial studies of haptotaxis and chemotaxis.....	35
1-5 Conclusions and Outlook.....	36
1-6 References.....	37
Preface to CHAPTER 2.....	43
CHAPTER 2: Large Dynamic Range Digital Nanodot Gradients of Biomolecules Made by Low-Cost Nanocontact Printing for Cell Haptotaxis.....	44
2-1 Abstract.....	44
2-2 Introduction.....	45
2-3 Results and Discussion.....	46

2-4 Conclusions.....	56
2-5 Experimental Section.....	57
2-6 References.....	59
Preface to CHAPTER 3.....	61
CHAPTER 3: Tuning Cell-Surface Affinity to Direct Cell Specific Responses to Patterned Proteins.....	63
3-1 Abstract.....	63
3-2 Introduction.....	65
3-3 Materials and Methods.....	68
3-4 Results.....	70
3-4.1 Tuning the cell-surface affinity of the RS by changing its composition.....	71
3-4.2 Cell adhesion, spreading, and motility in response to RS composition.....	71
3-4.3 RS affinity influences the cell response to patterned protein.....	75
3-4.4 RS affinity influences both cell body and axonal response in neurons.....	79
3-4.5 Cell-type specific biochemical signaling on RSs of intermediate affinity.....	81
3-5 Discussion.....	84
3-6 Conclusions.....	86
3-7 References.....	86
Preface to CHAPTER 4.....	91
CHAPTER 4: Neuron Navigation on Substrate-Bound Netrin-1 and Affinity Gradients	92
4-1 Abstract.....	92
4-2 Introduction.....	93
4-3 Materials and Methods.....	95
4-4 Results and Discussion.....	99
4-4.1 Patterning substrate-bound protein digital nanodot gradients for cell assays.....	99
4-4.2 Axonal navigation on DNG arrays.....	100
4-4.3 Axonal outgrowth and turning are maximized on shallow ordered gradients of netrin-1.....	103
4-4.4 Different neuron populations respond differently to substrate-bound netrin-1 gradients.....	106
4-4.5 Gradients of a permissive cue are sufficient to guide axonal navigation.....	107
4-4.6 Non-monotonic gradients guide neurons at specific periodicity.....	109
4-5 Conclusions.....	110
4-6 References.....	111
CHAPTER 5: Conclusions and Summary.....	114
5-1 Summary.....	114
5-2 Conclusions.....	115
5-3 Limitations.....	116
5-4 Outlook.....	119
5-5 References.....	120
Preface to APPENDIX I.....	121

APPENDIX I: Generation of MicroIsland Cultures using Microcontact Printing to Pattern Protein Substrates.....	122
AI-1 Abstract.....	122
AI-2 Introduction.....	124
AI-3 Materials and Methods.....	126
AI-4 Results.....	131
AI-4.1 Fabrication of stamps for microcontact printing.....	131
AI-4.2 Microcontact printing and background neutralization.....	132
AI-4.3 Cell co-culture and optimization of cell density.....	136
AI-5 Discussion.....	140
AI-6 Conclusions.....	142
AI-7 References.....	143
Preface to APPENDIX II.....	146
APPENDIX II: Ordered, Random, Monotonic and Non-monotonic Digital Nanodot Gradients	147
AII-1 Abstract.....	147
AII-2 Introduction.....	148
AII-3 Materials and Methods.....	154
AII-4 Results and Discussions.....	157
AII-4.1. Ordered Gradient Algorithm.....	157
AII-4.2. Random Gradient Algorithm.....	161
AII-4.3. Non-monotonic gradients.....	167
AII-4.4. One-Hundred-Gradient Array.....	170
AII-4.5. Gradient Array Fabrication.....	172
AII-5 Conclusion.....	176
AII-6 References.....	177

LIST OF FIGURES AND TABLES

Figure 1-1. Schematic representation of methods to form substrate-bound protein gradients.....	21
Table 1-1. Methods for forming substrate-bound protein gradients.....	22
Figure 2-1. DNG design.....	47
Figure 2-2. Schematic of the double replication process to make polymer replicas and their subsequent use as masters for lift-off nanocontact printing.....	48
Figure 2-3. SEM and AFM images of the Si master, the intermediate PDMS replica and the NOA replica.....	48
Figure 2-4. Liftoff microcontact printing of 200 and 100 nm dots.....	49
Figure 2-5. Comparison of prints obtained with lift-off stamps generated in the initial and a late replication cycles.....	50
Figure 2-6. Confocal fluorescence microscope and AFM images of a DNG patterned by lift-off nanocontact printing.....	51
Figure 2-7. C2C12 myoblast cell on a DNG of RGD peptides.....	52
Figure 2-8. Cell response to a DNG of RGD peptides.....	53
Figure 2-9. IgG DNG after seeding with cells and incubation.....	54
Figure 2-10. C2C12 myoblast migration on a netrin-1 DNG.....	55
Figure 2-11. C2C12 myoblast migration on a negative control IgG DNG.....	56
Figure 3-1. Cell response to fibronectin stripes on a RS with high affinity (typically adhesive) or low affinity (typically non-adhesive).....	66
Figure 3-2. Schematic of cell responses to a patterned cue and description of how cell distribution was quantified.....	70
Figure 3-3. Fluorescent characterization of the reference surfaces.....	71
Figure 3-4. Schematic of the assay format.....	72
Figure 3-5. Tuning cell-surface affinity to alter cell adhesion, spreading and motility.....	73
Figure 3-6. High affinity RSs result increased focal adhesions.....	75
Figure 3-7. Cell response to stripes of fibronectin patterned by incubation and by microcontact printing.....	76
Figure 3-8. Cell response to patterned cues is dependent on cell type, patterned protein and the affinity of the RS.....	78
Figure 3-9. Spinal commissural neurons respond to printed netrin-1 stripes based on the affinity of the RS.....	80
Figure 3-10. In the presence of an intermediate RS, the response of cells to protein patterns is driven by biologically appropriate signal transduction.....	83
Figure 3-11. Competitive Cell-surface affinity curves.....	85
Figure 4-1. Manual analysis process flow of axonal navigation on DNGs.....	98
Figure 4-2. Schematic of experimental process flow.....	100
Figure 4-3. Presentation of DNG array.....	101
Figure 4-4. Response plots of cortical neurons to netrin-1 DNGs.....	102
Figure 4-5. Response plots for cortical neurons to PDL DNGs.....	103
Figure 4-6. Cortical neurons make the strongest preferred response on shallow ordered exponential gradients of netrin-1.....	105

Figure 4-7. Cortical neurons turn specifically on netrin-1 DNGs.....	106
Figure 4-8. Response plots for spinal commissural neurons to netrin-1 DNGs	107
Figure 4-9. Axon navigation difference between cortical and spinal commissural neurons on netrin-1 DNGs.....	107
Figure 4-10. Neurons respond to non-monotonic netrin-1 and PDL gradients.....	110
Figure AI-1. Diagram of protein patterning technology used to generate microisland cultures.....	126
Figure AI-2. Mold and cross section of microcontact printing stamp.....	132
Figure AI-3. Array of microcontact printed islands.....	133
Figure AI-4. Recruitment of astrocytes to islands of different protein composition.....	135
Figure AI-5. MicroIsland foundation layer includes astrocytes and microglia.....	137
Figure AI-6. Hippocampal neurons grown on an astrocyte monolayer on printed islands of netrin-1	139
Figure AII-1. Random gradients produced by a random matrix threshold approach.....	152
Figure AII-2. Ordered gradient algorithm for continuously changing density in Digital Nanodot Gradients (DNGs) using a unit cell approach.....	158
Figure AII-3. Programmed and measured density for an ordered linear DNG.....	159
Figure AII-4. Ordered and random measured density matches programmed density over full range.....	160
Figure AII-5. Ordered and random DNGs superposed with their programmed exponential density function and actual, measured density.....	165
Figure AII-6. Ripley's K analysis for randomness and spatial homogeneity of a sample box produced with the ordered and random DNG algorithms.....	167
Figure AII-7. Non-monotonic random DNG superposed with its density function and actual, measured density.....	169
Figure AII-8. Density functions of the array of 100 DNGs.....	171
Figure AII-9. Optical images of the 100-gradient-array.....	173
Figure AII-10. Nanodot distribution in ordered and random DNGs.....	174
Figure AII-11. The printed nanodot pattern accurately replicates the design.....	175
Figure AII-12. Image processing procedure to assess alignment of the DNG design and print.....	176

ABSTRACT

Haptotaxis, or the directional motility of cells in response to a surface-bound cue, is a critical process in the wiring of the nervous system. Despite its importance, studies of this mechanism have been limited in large part due to the constraints of available methods to produce complex substrate-bound protein gradients. In this dissertation, we first developed a method to easily and reliably create substrate-bound protein gradients and then applied this method to investigate axonal navigation on netrin-1 and polylysine gradients. In chapter 2, we present novel designs to create gradients of protein nanodots where spacing between dots is changed in X and Y directions to change the density. We called these gradients digital nanodot gradients and achieved unprecedented dynamic range. We then report a low-cost lift-off nanocontact printing method to create substrate-bound protein gradients out of these designs with protein nanodots as small as 100 nm in diameter. In Chapter 3, we created quantitative tests to study the non-patterned surface, or the reference surface, which were used to draw comparisons among cells and surfaces as well as to articulate the concept of cell-surface affinity. We employed this method to identify an environment in which cells respond to substrate-bound protein patterns through specific biochemical transduction mechanisms. Implementing these methods we demonstrate that C2C12 myoblasts migrate up gradients of netrin-1. In Chapter 4, we used an array of 100 distinct gradients that can be printed within 10 minutes to investigate the navigation of cortical and spinal commissural neurons. The gradients in the array differ in geometry and the array was printed using either netrin-1 or polylysine. Implementation of the array revealed that cortical neurons exhibit a relatively strong turning response on netrin-1 digital nanodot gradients of ordered dot arrangement with shallow exponential curves.

The work reported in this thesis aimed to facilitate the study of haptotaxis. It provides an approach to create complex substrate-bound gradients through new algorithms, a means to convert these digital designs into printed protein gradients, and a means to control the reference surface to ensure desired cell response. Furthermore, the findings acquired from our large screen of the navigation of neurons on gradients of different geometries sets the foundation for further studies. Since the gradients are stably surface-bound, further components could easily be added to our process. For instance, pharmacological drugs could be applied in solution to identify a compound that promotes migration, transfected cells expressing fluorescent proteins could be

grown on our patterns and imaged in real time with a fluorescent microscope to study focal adhesion formation, or mutant neurons could be tested on the gradients to see how mutations in specific proteins impact navigation.

RESUME

L'haptotaxis, ou la migration de cellules en réponse à un repère lié à la surface, est un processus critique pour la connexion du système nerveux. Malgré son importance, les études de ce mécanisme ont été limitées en grande partie en raison des contraintes inhérentes aux méthodes disponibles pour produire des gradients complexes de protéines liées au substrat. Dans cette thèse, nous avons développé une méthode pour créer facilement et de manière fiable des gradients de protéines liées au substrat, puis appliqué cette méthode pour étudier la navigation axonale sur des gradients de nétrine-1 et de polylysine. Dans le chapitre 2, nous présentons de nouveaux modèles pour créer des dégradés de nanopoints de protéines où l'espacement entre les points est modifié dans des directions X et Y pour modifier la densité. Nous avons pu atteindre une plage dynamique sans précédent pour ces gradients numériques de nanodots. Nous rapportons ensuite une méthode d'impression par contact à l'échelle nanométrique de lift-off à faible coût pour créer des gradients de protéines liées au substrat avec des nanopoints de protéines aussi petites que 100 nm de diamètre. Dans le chapitre 3, nous avons créé des tests quantitatifs pour étudier la surface de référence non imprimée, ou la surface de référence, qui ont servi à établir des comparaisons entre la réponse de différentes cellules et surfaces ainsi que d'articuler le concept d'affinité cellulaire à la surface. Nous avons utilisé cette méthode pour identifier un environnement dans lequel les cellules répondent à des motifs protéiques liés au substrat par des mécanismes spécifiques de transduction biochimiques. Nous démontrons par l'application de ces méthodes que les myoblastes C2C12 migrent sur des gradients de nétrine-1. Dans le chapitre 4, nous avons utilisé une matrice de 100 gradients distincts, imprimés en 10 minutes, pour étudier la navigation de neurones corticaux et spinaux commissure. Les gradients dans la matrice diffèrent en géométrie et le tableau a été imprimé en utilisant soit la nétrine-1 ou polylysine. La mise en œuvre de la matrice a révélé que les neurones corticaux présentent une réponse de braquage relativement forte sur des gradients de nétrine-1 de nanopoints numériques d'arrangement ordonné aux courbes exponentielles peu profondes.

Le travail présenté dans cette thèse a pour objectif de faciliter l'étude de l'haptotaxis. Il fournit une approche pour créer des gradients liés au substrat par le biais de nouveaux algorithmes complexes, un moyen pour convertir ces designs numériques en gradients de protéines imprimés, et un moyen pour modifier la surface de référence pour assurer une réponse

cellulaire souhaitée. En outre, les résultats acquis de nos études sur la navigation de neurones sur des gradients de différentes géométries forment les bases pour de nouvelles études. Comme les gradients sont stables grâce à leur liaison à la surface, d'autres composants peuvent être facilement ajoutés à notre procédé. Par exemple, des médicaments pharmacologiques pourraient être appliqués en solution pour identifier un composé qui favorise la migration, les cellules transfectées exprimant des protéines fluorescentes peuvent être cultivées sur les schémas et visualisés en temps réel avec un microscope à fluorescence pour étudier la formation d'adhésions focales, ou des neurones avec des mutations génétiques pourraient être testés sur les gradients pour voir comment ces mutations impactent la navigation spécifique aux protéines liées à la surface.

ACKNOWLEDGMENTS

It would not have been possible for me to complete the work reported herein without the help and support of many outstanding friends and colleagues to whom I owe my sincerest gratitude. First and foremost, I thank my advisors, Profs. David Juncker and Tim Kennedy for granting me the opportunity to embark on this incredible scientific journey with them over the last 6 years and guiding my growth on so many levels along the way. I'm also particularly thankful that they encouraged me to let my scientific curiosity run wild and pursue side projects that are close to my heart.

Thanks to my committee members, Prof. Bruce Lennox and Prof. Craig Mandatto, for always asking the tough questions and ensuring that high standards were maintained in my research, presentations, and writings. I also wish to thank them for all the great suggestions they made towards my research.

I was also extremely fortunate to be part of two top notch laboratories that have been filled with amazing colleagues for the entirety of my tenure. So many lasting memories were written over the last 6 years and you all hold a special place in my heart. Special thanks go to my outstanding mentors who took the time to teach me: Mateu Pla Roca, Cécile Perrault, Ben Rappaz, Mohammad Qasaimeh, Rym Leulmi, Roozbeh Safavieh, Sébastien Bergeron, Dong Han, and Amir Sanati-Nezhad. In DJGROUPE, I want to express my gratitude to Grant Ongo for being an amazing friend and collaborator who brought all my crazy ideas to life and always provided the necessary humor along the way. The work herein would not have been possible without all your help. While in the Kennedy lab special thanks go to Nathalie Marcal, Jenea Bin, Karen Lai Wing Sun, James Correia, and Stephanie Harris for providing a constant supply of neurons and help completing experiments. I also want to thank my electrophysiology expert, Stephen Glasgow, for many great discussions and especially for teaching me the amazing game of hockey. Go Habs Go!

I hope to continue to find great collaborators like the ones I had the chance to work with here at McGill. Ben Rappaz and Angelica Gopal were fundamental in the success of the ligand-receptor colocalization experiments. I also want to thank Monserratt Lopez Ayon for making AFM fun and taking the time to teach me the workings of her big black box. I also always enjoyed the discussions with Tyler Sloan and Margaret Magdesian and I hope we continue our

discussions in the future. I also want to thank Marta Garnelo and Prof. Aldo Faisal at Imperial College for their help developing a means to analyse the massive data that I produced in my experiments and extract valuable information from it. At the Indian Institute of Sciences, I wish to acknowledge Prof. Shyamala Mani and her students Parthiv Haldepur, Anindo Chatterjee, Subahika Govindan, and Devesh Tewary who made me feel so welcome in their lab and guided me in the discovery of their beautiful country of India. I will return to continue my exploration.

I am also indebted to all the outstanding students that accepted to work with me and taught me how to become a better mentor. Special thanks to Levon Atoyian, Yannick Devaud, Abhishek Sinha, Greta Thompson-Steckel, and Henry Xu who made research fun and exciting.

This work could not have been completed without the help and guidance of my parents and brother who made sure I remained on the roller coaster throughout the ride. Lastly, I owe my greatest gratitude to Greta whose constant support, input, patience, and understanding continue to make my world go round on a daily basis.

CONTRIBUTIONS OF AUTHORS

In accordance with the “Guidelines for Thesis Preparation”, this thesis is presented as a collection of manuscripts written by the candidate with the collaboration of co-authors. The first chapter is an introduction to haptotaxis in the context of growth cone navigation which is intended for publication. The second, third and fourth chapters compose the results focused on (1) technique development for chapters 2 and 3 and (2) implementation of the presented method for the advancement of science in the fourth chapter. In the final chapter of this thesis, the impact of the contributions presented herein is discussed and potential further research avenues are suggested.

The manuscripts are based on experiments designed and conducted by the candidate who also carried out the collection and analysis of the obtained data. The candidate finally also interpreted the data and composed the herein presented articles. The PhD supervisors appear as co-authors on all manuscripts to reflect their supervisory role and involvement with result interpretation and manuscript editing.

In chapter 2, where we report a novel protein nanopatterning method and apply it to cell biology, Mateu Pla-Roca appears as a co-author for his contributions to the experimental design and insights into protein nanocontact printing. Roozbeh Safavieh produced the gradient designs that I edited to generate the gradients presented in the manuscript. Monserratt Lopez-Ayon and Prof. Peter Grütter helped acquire the Atomic Force Microscopy data presented in the manuscript.

In chapter 3, where we raise the importance of the non-patterned surface in cell response experiments and present an approach to alter the affinity of this surface by ratiometric mixing of low and high affinity molecules, Greta Thompson-Steckel appears as a co-author due to her contribution in performing some of the experiments, data collection, data analysis and help writing the manuscript. James Correia appears as a co-author to acknowledge that he conducted all the animal dissections that were required to obtain the neurons employed in the work.

In chapter 4, where we implement DNGs to investigate axonal navigation in cortical and spinal commissural neurons, Grant Ongo appears as a co-author to acknowledge that he coded the two algorithms needed to design complex digital nanodot gradients and to analyse/present in a legible manner the data obtained from the neuron navigation experiments. Karen Lai Wing Sun

appears as a co-author to acknowledge that she conducted all the animal dissections that were required to obtain the spinal commissural neurons employed in the work.

In Appendix I, where we present a method to create island co-cultures of neurons and astrocytes through microcontact printing, Jennifer Goldman appears as a co-author due to her contribution in performing both the patch clamping experiment and the microglia staining experiment, as well as conducting the analysis for the electrophysiology experiments. Prof. David Stellwagen is listed as a co-author for kindly granting access to his electrophysiology rig and providing feedback on the obtained results.

In Appendix II, Grant Ongco is listed as lead author for creating the algorithms to generate the digital nanodot gradients outlined in the paper, conducting all the computation and statistical analysis, and heading the writing efforts. I contributed with insights into the design, organization of the array, fabrication, patterning, image analysis and writing of the manuscript.

PREFACE TO CHAPTER 1

Chemotaxis and haptotaxis play equally important roles in guiding neurons through their environments, yet the latter has been investigated sparingly in comparison. A lack of adequate methods to create deterministic substrate-bound protein patterns *in vitro* has limited the study of haptotaxis.

In this chapter we introduce the currently available methods to create substrate-bound protein gradients and rate them based on a number of characteristics to assess where improvements are needed to facilitate haptotaxis studies. We then assess how some of these methods were implemented to investigate haptotaxis in neurons and review the findings to date.

This chapter serves as an introduction to facilitate comparison between the methods currently available and the ones we report in this thesis. Furthermore the review of the neuroscience findings also serves for comparison with the neuroscience findings we report herein.

This manuscript is intended for submission as a Review article in *Frontiers in Bioengineering and Biotechnology*, section *Biomaterials*.

Acknowledgements

We thank Greta Thompson-Steckel for feedback on the manuscript. We acknowledge support from CIHR (Regenerative and Nanomedicine grant), the Canadian Foundation for Innovation and the McGill Nanotools Microfabrication Laboratory (funded by CFI and McGill University). SGR was supported by the CREATE Integrated Sensor Systems and Neuroengineering programs funded both by NSERC and The Molson Foundation. TEK was supported by a Scholarship from the Killam Trust and by a Chercheur Nationaux Award from the Fonds de la Recherche en Santé du Québec. DJ holds a Canada Research Chair.

CHAPTER 1

In vitro Studies of Haptotaxis as a Regulatory Mechanism in Axon Guidance through Surface-bound Protein Gradients

Sébastien G. Ricoult,^{1,2} David Juncker^{1,2,3} and Timothy E. Kennedy^{1,*}

¹McGill Program in Neuroengineering, Department of Neurology and Neurosurgery, Montreal Neurological Institute, McGill University, 3801 University Ave, Montreal, Quebec, Canada H3A 2B4

²Genome Quebec Innovation Centre, McGill University, Montréal, Quebec, Canada H3A 0G1

³McGill Program in Neuroengineering, Department of Biomedical Engineering, McGill University, 740 Dr. Penfield Avenue, Montreal, Quebec, Canada H3A 0G1

1-1 Abstract

Cell navigation operates in response to inhomogeneous distributions of extracellular guidance cues. The cellular and molecular mechanisms underlying chemotaxis, migration in response to gradients of soluble cues, have been investigated for over a century. Haptotaxis, migration in response to gradients of immobilized cues, has received relatively less attention; however it is increasingly clear that many physiologically relevant guidance cues are presented *in vivo* bound to cellular surfaces or incorporated into extracellular matrix. Here, we review and compare a wide range of methods developed to pattern substrate-bound protein gradients *in vitro*. We review the findings reported using these gradients and classify them in three categories: 1) the molecules that can induce an axonal response and the gradient geometry required to achieve this response, 2) the molecular mechanism that underlies the capacity of a growth cone to respond to the gradient, and 3) the result of combinatorial presentation of chemotaxis and haptotaxis gradients simultaneously. Enhanced methods to study haptotaxis will extend our understanding of the underlying mechanism and its contribution to normal neural development and perhaps inform methods to promote axon regeneration following injury.

1-2 Introduction

Migrating cells rely on extracellular cues to direct their actions. Cues can influence cellular response in a wide variety of ways ranging from the presence of an electro-magnetic field in the environment to direct protein-protein interactions (Lara Rodriguez and Schneider 2013). The regulation of cytoskeletal rearrangement by such cues dictates the navigation of cells through the environment. To induce a directional change in navigation, cells may encounter gradients of molecular cues, where the concentration or density of a tropic protein determines the response (Kim and Peyton 2012). Protein gradients exist in two forms *in vivo*: diffusible, where proteins diffuse away from a source, or substrate-bound, where the cues are fastened either to cell surfaces or to the surrounding extracellular matrix (ECM). It is important to note that the same protein may be found in both forms. For example a secreted protein may diffuse a short distance, become bound, and then perhaps be released, travel further by diffusion, only to be bound again. Alternatively, a transmembrane protein that is initially firmly anchored to a cell membrane may be proteolyzed to release a soluble ectodomain that then becomes a diffusible cue.

Gradients of diffusible proteins have widely been investigated using a variety of methods (Wu, Wu et al. 2013). These have led to a better understanding of the chemotropic cell response that occurs through the activation of downstream signal transduction cascades that are activated by the formation of ligand-receptor complexes. However, these same guidance cues might also be bound to a surface, which allows a cell to develop traction force by using the immobilized protein as an anchor in a process called mechanotransduction. Durotaxis, navigation in response to the stiffness or modulus of a substrate, also relies on mechanotransduction, but has not yet been linked to specific receptors or protein interactions.

The investigation of chemotaxis has a long history, initially being described in the late 1800s (Engelmann 1881; Pfeffer 1884; Jennings 1906). Particularly well studied examples include: the migration of *E. coli* bacteria towards food sources (*e.g.* glucose) (Adler 1966), the common slime mold dictyostelium which uses secreted cAMP gradients to direct growth (Gerisch, Hulser et al. 1975), lymphocytes which respond to chemokine gradients to locate a site of immune response (Schall, Bacon et al. 1990). Based on his observations of lymphocyte navigation, S. Ramón y Cajal predicted in 1892 that neurons navigate through the environment in response to gradients of substrate-bound guidance cues (Sotelo 2002). However, it was not until 1965 that S.B. Carter defined haptotaxis, differentiating it from tropic responses to soluble cues

(Carter 1965). In this report, gradients of palladium patterned on glass were used to generate varied levels of substrate adhesion, and the impact of these gradients on cell navigation was then investigated. The mechanism was termed haptotaxis (from the Greek: ‘haptein’ to fasten and ‘taxis’ arrangement) to reflect that the cells were navigating in response to the relative strength of the adhesive contacts made with the substrate (Carter 1965). Carter suggested that all cell movements within a tissue could be considered haptotactic basis, including chemotaxis, where he speculated that the response observed might result from the adsorption of soluble gradients to form haptotactic gradients. Carter went on to further study and define haptotaxis in a subsequent article and proposed key roles for the leading and trailing edges of migrating cells (Carter 1967). As a result of these studies, Carter suggested that soluble chemotactic cues might alter the substrates on which cells were migrating and result in haptotaxis. Claims made by Carter that haptotaxis might underlie all cell movements, not surprisingly, generated controversy and drew counter arguments from those studying chemotaxis (Keller, Wissler et al. 1979). Various versions of this argument persist to the present day; however with contemporary tools, studies into the underlying mechanisms have the potential to provide more satisfying answers.

Protein gradients are of particular importance in neuroscience because they relay information to neurons regarding the trajectories that will lead them to desirable targets. The unique polarized morphology of neurons and the dynamics of growth cones, the specialized sensory structure at the tip of the axon, make these cells extremely proficient at rapidly restructuring the cytoskeleton in response to minute environmental changes (Rosoff, Urbach et al. 2004). This keen ability of axons to respond to graded distributions of guidance protein to navigate to their synaptic targets is critical for the formation of neural circuits during neural development, with particularly well studied examples being the embryonic spinal cord (Kennedy, Wang et al. 2006) and visual system (Cang, Kaneko et al. 2005). In addition to guiding axons to their targets, gradients direct the migration of neuronal and glial precursor cells (Paratcha, Ibanez et al. 2006). Although not addressed in detail here, gradients of highly conserved morphogens define the initial polarity of the early embryonic vertebrate CNS and regulate the proliferation and differentiation of precursor cells during neural development (Tanabe and Jessell 1996).

The visualization and functional characterization of substrate-bound gradients has been challenging; however several such gradients have been well documented *in vivo*. The ventral-

dorsal gradient of netrin-1 across the embryonic spinal cord arises from the secretion of netrin-1 by floor plate cells at the ventral midline and is a canonical example of a chemotropic cue that is captured by cell surface binding proteins and ECM following secretion. Alternatively, substrate-bound gradients may arise from graded expression by cells of transmembrane or GPI linked proteins. Ephrin gradients, that direct topographical mapping of retinal ganglion cell axons across the superior colliculus, are a well-studied example of a gradient formed by differential expression across a field of cells.

The members of the netrin family are essential axon guidance cues in the embryonic nervous system. Axon navigation directed by netrins include commissural axons in the embryonic spinal cord (Kennedy, Wang et al. 2006) and retinal ganglion cell axons at the optic nerve head (de la Torre, Hopker et al. 1997). Netrins are multifunctional proteins, mediating chemo-attractive or chemo-repellent responses based on the netrin receptors involved (Sun, Correia et al. 2011). For instance, the recruitment and multimerization of DCC or dimerization of neogenin result in attraction (Xu, Wu et al. 2014), whereas the cytoplasmic association of DCC with UNC5 leads to repulsion (Hong, Hinck et al. 1999).

Many studies investigating axon turning responses to netrin *in vitro* have utilized gradients formed by pulsatile ejection of protein from a micropipette (Ming, Song et al. 1997), secretion from a neighboring aggregate of cells (Kennedy et al., 1994), or microfluidics (Bhattacharjee, Li et al. 2010). The result interpretations of such assays are confounded due to the propensity of “sticky” molecules such as netrin-1 to adsorb to the surface. Further doubts over attributing these results strictly to chemotaxis were raised by the demonstration that forces required for the reorientation of the growth cone for netrin-1 mediated turning could only be achieved when the proteins were immobilized (Moore, Biais et al. 2009). Following up this initial study, evidence was then provided that mechanotransduction of these applied forces literally stretch out focal adhesion kinase, exposing sites that normally mask its kinase domain, thereby activating the protein (Moore, Zhang et al. 2012). To support this finding, when the adhesive C-terminal domain of netrin-1 is omitted, domains VI and V that bind netrin receptors are insufficient to promote outgrowth (Moore, Zhang et al. 2012; Bin, Rajasekharan et al. 2013). This therefore suggests that neurons respond to the reported netrin-1 protein gradient across the spinal cord via haptotaxis, where the netrin-1 proteins have been immobilized in the ECM. The immobilization

could potentially be via binding to heparin sulfate proteoglycans, for which the c-domain of netrin has a high binding affinity (KeinoMasu, Masu et al. 1996; Baker, Moore et al. 2006).

Here, we review a wide range of methods that have been developed to pattern substrate-bound protein gradients to investigate haptotaxis *in vitro*. We then summarize the work that has been conducted using these protein gradients and focus investigations of axon guidance that have been reported using these assays. We break down the findings into three sections: 1) the impact of geometry on navigation, 2) the haptotaxis response mechanism in neurons, and 3) combined studies of haptotaxis and chemotaxis.

1-3 Methods to create substrate-bound protein gradients to study haptotaxis

Unlike chemotaxis, where a wide range of methods has been developed to replicate freely-diffusible gradients *in vitro*, methods to pattern substrate-bound protein gradients to investigate haptotaxis *in vitro* are relatively limited (Genzer 2012). Of the developed methods capable of forming substrate-bound protein gradients (**Figure 1-1**), an ideal method that is low-cost, high throughput, and applicable to any desired protein with the ability to modify the gradient geometry and spot dimensions remains to be reported. Nevertheless, many of the reported methods are being used to investigate haptotaxis. Below we list several of these gradient patterning methods and report their pros and cons (**Table 1-1**). The gradients achieved through these methods occur in two classes: continuous, where the gradient is achieved through changes in protein concentration in a constant manner, or digital, where the gradient results from density changes of a patterned protein feature. Both have advantages and disadvantages. For instance, continuous gradients can easily be achieved through the diffusion of a protein from a source, but the accurate characterization of such gradients relies on fluorescence measurements and is therefore often inexact. On the other hand, digital gradients are deterministic, and as a result the exact local concentration can easily be calculated, however the geometry of digital gradients relies on patterned protein aggregates that are usually much larger than those present in nature.

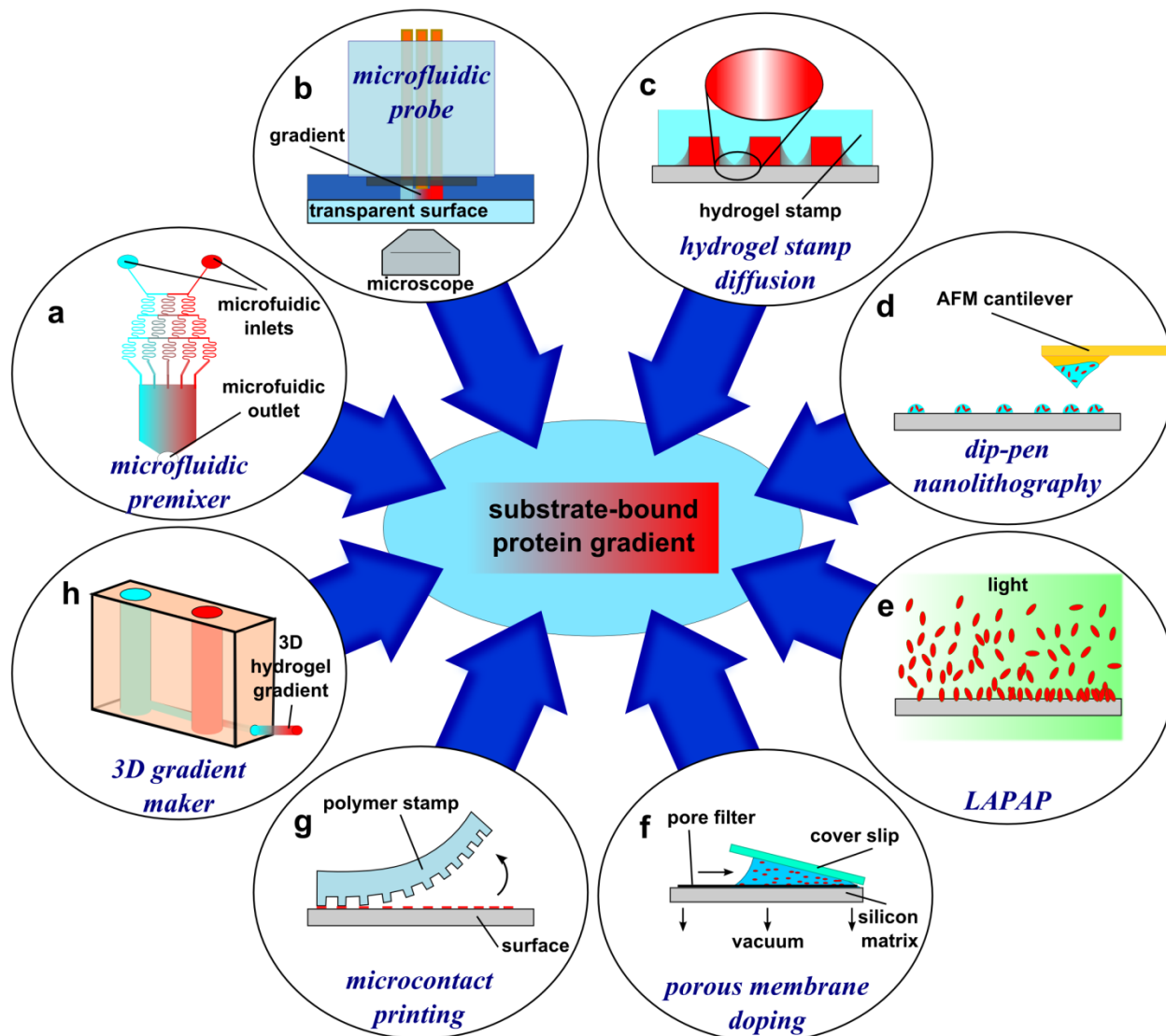


Figure 1-1: Schematic representation of methods to form substrate-bound protein gradients. (a) Micrograph image of a microfluidic premixer device where two solutions are inserted into the inlets and mix in a controlled fashion through the geometry of the premixer before forming a gradient in the chamber. With the appropriate surface chemistry, proteins will adsorb to the surface over time in a graded distribution. (b) A microfluidic probe with injection and aspiration apertures serves to create confined microfluidic flows that can serve to pattern gradients by controlling the lag time and position of the flow on the surface. (c) Hydrogel stamps in contact with the substrate create closed channels that can be filled with a protein solution. The proteins then diffuse through the hydrogel and adsorb to the surface in a graded distribution. (d) Dip-pen nanolithography employs an AFM cantilever inked with a protein solution to transfer

localized nanovolumes of protein solution on the surface in any desired geometry (e.g. dot gradient). (e) Controlled photobleaching of fluorescently-labeled proteins can also be used to increase the reactivity of the proteins with the surface in specific locations and by controlling light intensity or exposure, gradients can be formed. (f) By applying a vacuum, protein solutions can be aspirated through a silicon matrix where the proteins bind. By placing an angled coverslip on top of the solution; a protein gradient can be adsorbed to the matrix. (g) In microcontact printing, polymer stamps with topography are inked with a protein solution and used to stamp protein in a gradient geometry by limiting the regions of contact between the stamp and the surface. (h) A gradient maker forms 3D gradients by mixing two solutions: one containing the protein and the crosslinking agent, while the other contains the polymer base. Altering the mixing rate of the two solutions yields a 3D protein gradient.

Table 1-1: Methods for forming substrate-bound protein gradients.

Method	Throughput (serial → multiplex)	Low- cost	Patterning size	Capacity to adjust the local protein conc.	Resolution (milli → nano)	Geometry (fixed/flexibl e)	Gradient design complexity	[REF]
Serial diluters	+	+++	++	+++	micro	fixed	+	(Dertinger, Jiang et al. 2002)
Microfluidic probe	+	+	+++	+++	micro	flexible	+	(Juncker, Schmid et al. 2005; Qasaimeh, Ricoult et al. 2013)
Inkjet printing	+	+	+++	+++	micro	flexible	+	(Campbell, Miller et al. 2005)
Vesicle mixing	++	+++	++	+++	micro	fixed	+	(Kam and Boxer 2000)
Surface modification	+++	+	+++	++	micro-nano	fixed	+++	(Morgenthaler, Lee et al. 2003)
Protein doping of porous membranes	+	++	++	+	micro	fixed	+	(Baier and Bonhoeffer 1992)
Gel diffusion	++	+++	++	+	micro	fixed	+	(Mai, Fok et al. 2009)
Microcontact/ Nanocontact printing	+++	+++	++	+	micro-nano	fixed	+++	(Ricoult, Pla-Roca et al. 2013)
Dip-pen nanolithography	+	+	+	+	nano	flexible	++	(Senesi, Rozkiewicz et al. 2009)
Colloid lithography	+++	+++	+++	+	nano	N/A	+	(Taylor, Keay et al. 2012)
LAPAP	+	+	+	+++	nano	flexible	+++	(Belisle, Correia et al. 2008; B�elisle, Mazzaferri et al. 2013)
Laser scanning lithography	+	+	+	+++	micro	flexible	++	(Slater, Miller et al. 2011)
Photolithography	+++	+	+++	+	micro	fixed	++	(Herbert, McLernon et al. 1997)
Polymer scaffolds	+	++	+++	+++	milli	flexible	+	(Moore, MacSween et al. 2006) (Sundararaghavan, Masand et al. 2011)
3D electrospun gradients	+	+	+++	+++	micro	flexible	+	(Sundararaghavan and Burdick 2011)

1-3.1 Microfluidics

Microfluidics, where liquid flows are handled at the microscale, has been widely employed in biology due to 1) the small footprint of experiments, 2) rapidity of experiments, 3) multiplexing and high throughput characteristics, 4) high reproducibility, and 5) predictable design of devices for specific purposes. Most of these benefits arise from the fundamental principle that fluids at these scales follow laminar flows in the absence of turbulence, and that mixing occurs solely through diffusion (Whitesides 2006). Based on this, an assortment of microfluidic designs have been developed to create diffusible gradients suitable for chemotaxis studies, such as T-based devices, universal gradient generators, and premixer gradient generators. All of these microfluidic gradient generators create diffusible gradients, but over time protein-surface interactions will occur. In the presence of the appropriate surface, sufficiently stable interactions will result in the adsorption of proteins on the surface at a concentration that reflects the capacity of the substrate and the protein concentration in the solution (Jiang, Xu et al. 2005). As capillary flow continues in microfluidic devices, the adsorption of proteins to the surface will reach saturation and the gradient slope will no longer reflect the slope of the protein concentration in solution (Squires, Messinger et al. 2008).

1-3.1.1 Serial diluter

The simplest microfluidic design is a T-junction where two solutions merge into a perpendicular channel and a gradient is formed through the diffusion of the two laminar flows (Walker, Ozers et al. 2004). Further complexity in the design of the device can enhance the capacity to control the gradients of greater width. One such example is a microfluidic network premixing device where the channels branch and as a result mix two solutions in different ratios (**Figure 1-1a**). The result of this branching and mixing are a number of parallel flowing solutions of graded concentration, which then flow into a chamber where laminar flow maintains the concentration and diffusion enables smoothing of the gradient (Jeon, Dertinger et al. 2000). Substrate-bound protein gradients of the ECM protein laminin were created by flowing a gradient of laminin on a pre-coated poly-L-lysine substrate. These have been used to investigate how rat hippocampal neurons responded to monotonic surface-bound gradients of laminin (Dertinger, Jiang et al. 2002) and how *Xenopus* spinal neurons responded to non-monotonic gradients of laminin in the presence of a diffusible BDNF gradient (Joanne Wang, Li et al. 2008). Alternative geometries have been developed that easily create diffusible gradients, such as triangular microfluidic channels, where flow velocity changes across the channel (Park, Kim et al. 2010), and a

generalized serial dilution module, where device geometry creates a flow rate gradient that alters the mixing ratio (Lee, Kim et al. 2009). It is conceivable that such diffusible gradients could also be used to pattern substrate-bound gradients by flowing the gradient on the appropriate surface for extended periods.

1-3.1.2 Microfluidic probes

Despite the advantages of microfluidics listed above, it is restrained by the closed environment that confines the fluids, enables the formation of laminar flows, eliminated turbulent flows, and limits mixing to diffusion. The closed channel configuration of most microfluidic devices restricts the use of microfluidics to pattern surfaces (**Figure 1-1b**). To overcome this limitation, microfluidic probes were developed (Juncker, Schmid et al. 2005) that combines the attributes of microfluidic systems and scanning probes. The tool consists of a flat surface with inlet and outlet apertures where fluid is circulated. By 1) placing the apertures sufficiently close to one another, 2) maintaining an aspiration flow rate superior to the injection rate and 3) placing the probe surface parallel and in close contact with the patterning surface, confinement of the microflow can be maintained. The probe can be moved on the surface by either controlling the position of the microfluidic probe with micromanipulators or by moving the substrate with the motorized stage. Once an appropriate location is identified, flow can be turned on, and by controlling the flow rates and the lag rate of the probe on the surface, substrate-bound fluorescently-labeled IgG gradients can be patterned (Juncker, Schmid et al. 2005; Qasaimeh, Ricoult et al. 2013). One limitation of this method is that operation of the microfluidic probe requires significant expertise and relies on expensive equipment. Furthermore operation of the device is often complicated by the presence of air bubbles in the solution that disrupt the flow and the gradient geometry.

1-3.1.3 Inkjet printing

Inkjet printers are commonly employed to pattern surfaces, but the minimal dot size is dictated by the volume of a drop of solution, and the resulting patterned dots from conventional inkjet printers are therefore $\sim 100 \mu\text{m}$ in diameter with a resolution of $\sim 300 \mu\text{m}$ (Tan, Cipriany et al. 2010). By altering the concentration between adjacent printed dots of $\sim 75 \mu\text{m}$ diameter, a substrate-bound continuous concentration with a 1.7 fold increase in fluorescence intensity across a 1.75 mm gradient was patterned on glass (Campbell, Miller et al. 2005). To achieve the

high concentration portion of the gradient, the inkjet applied 20 different layers of the inking solution on the same location.

1-3.1.4 Vesicle mixing to form supported lipid bilayers with protein gradients

As an alternative to flowing protein solutions in the microfluidic channels, pools of vesicles can be loaded in the gradient generator device (Kam and Boxer 2000). Each vesicle pool expresses a different fluorescently labeled protein. The vesicles then bind to the substrate and fuse into a continuous lipid bilayer, allowing the membrane-bound receptors to diffuse laterally across the fluid membrane thereby creating a continuous gradient. Furthermore, by pre-patterning the substrate with a grid of fibronectin, boundaries could be defined to confine the diffusion of the receptors within each box. By employing two pools of either receptors or vesicles of different charge, a magnet could be used to separate the vesicles on each side of the confined region. As the vesicles in each confined area merge, an array of distinct substrate-bound receptor gradients forms. Despite the biological relevance of achieving protein gradients on a membrane surface, the complexity of the experiment at the molecular and technical levels, have made this approach hard to reproduce.

1-3.2 Controlling protein adsorption to the surface

Alterations to surface chemistry can also be employed to control protein adsorption to surfaces. One of the simplest ways to create protein gradients by changing the surface chemistry is to dip a gold coated surface at a controlled rate in a solution of alkanethiols to yield a gradient of wettability (Morgenthaler, Lee et al. 2003). A protein solution can then be incubated on the surface, and as a result of the difference in wettability and therefore the affinity of proteins for the surface, adsorption to the surface will occur in a graded geometry. Even though the ease and low-cost of this approach make it very appealing, the geometry of the gradient is limited to a staircase design.

1-3.3 Protein doping of porous membranes

One of the earlier methods to generate substrate-bound patterns, both stripes and gradients, was achieved by employing a vacuum and a capillary porous filter (**Figure 1-1f**) (Baier and Bonhoeffer 1992). The solution is incubated on one side of a porous capillary. A vacuum is then

applied which pulls the solution through the membrane to which the biomolecules bind as they flow through the porous material. By placing silicon masks with slits on top of the porous filter, the adsorption of proteins can be limited to homogeneous protein stripes. By placing an incubated coverslip on top of the droplet of solution, the amount of solution available for passage through the membrane changes in a graded fashion. As the vacuum is applied and the solution becomes flows through the matrix, the solution will first become depleted on the side of the coverslip with the biggest gap with the surface and move towards the smallest gap. This difference in the amount of protein that interacts with the matrix results in a substrate-bound protein gradient. This method was one of the earlier methods to achieve substrate-bound protein gradients, but other methods with greater control over the geometry, greater range of substrate materials, and a less complex experimental setup are now preferred.

1-3.4 Gel diffusion

The porous membranes through which molecules diffuse can also be made up of hydrogels (Mai, Fok et al. 2009). For instance, agarose stamps with channels were contacted with PLL-coated epoxy coverslips to create closed channels (**Figure 1-1c**). Proteins in solution were then injected into the microfluidic channels, diffused through the agarose gel, and bound to the surface. Proteins bound to the surface were more abundant closer to the source and became increasingly sparse further away from the source. Gradients achieved through this method are very simple to achieve, but the experiment requires specific chemistry between the hydrogel and the diffusing protein, and control over the geometry of the gradient is very limited.

1-3.5 Microcontact/Nanocontact printing

Microcontact printing is a technique where a polymer stamp with relief is used to create protein patterns of specific geometry (**Figure 1-1g**). The stamp is inked with a protein solution, incubated for the protein to adsorb to the surface, and subsequently contacted to the surface to transfer the protein only in the contacting areas. Different designs have been reported to date. One example is a dashed line with a centrally located node where the length of the dashes changed based on the distance from the central node (Fricke, Zentis et al. 2011). Alternatively, a gradient was formed by creating a range of dot arrays where spacing between dots changes in X

and Y, resulting in a range of 10% to 100% surface coverage (Hjortø, Hansen et al. 2009). A third approach employed microfluidics to flow different concentrations of a same molecule in parallel channels onto a flat polymer stamp, which led to the protein adsorption to the stamp which was subsequently used for microcontact printing (Lang, Philipsborn et al. 2008). To eliminate the sharp concentration changes between adjacent channels, gradient designs were developed where feature size, spacing or both changed over a greater distance (von Philipsborn, Lang et al. 2006). Despite these new designs, the dynamic range of the gradient remained limited to 25. To increase the dynamic range of the gradients to more accurately represent the expected dynamic range of gradients *in vivo*, digital nanodot gradient designs were developed, where the feature size is reduced to the nanoscale and where their spacing is changed in two directions instead of one (Ricoult, Pla-Roca et al. 2013). Using these new designs, the gradients reached an unprecedented dynamic range of 7250 (Ongo et al., 2014). More complex algorithms were also developed to introduce noise into the gradients at the nanoscale by pseudo-randomly distributing dots within a row of constant density and compensating for dot overlap based on the probability of overlap at the given density, or at the microscale by developing non-monotonic gradients. Despite the powerful designs that are now available for microcontact printing, the relative ease and high throughput of the technique, one of the main limitations of the method is the required time from design to print with the need for costly electron beam lithography to generate the digital nanodot gradient masters. Furthermore, microcontact printing remains limited to a single protein at a single concentration per print.

1-3.6 Dip pen nanolithography

In dip pen nanolithography, cantilevers are employed as reservoirs to pattern the surface (**Figure 1-1d**). By using an agarose solution embedded with protein, biologically active protein could be patterned on high energy, activated surfaces (Senesi, Rozkiewicz et al. 2009). By changing the contact time of the tip with the surface, the humidity level of the environment, viscosity of the agarose, the dot size can be controlled down to 50 nm in diameter. By changing these parameters from dot to dot, an array of protein dots with increasing size along a distance can be produced, thereby creating a gradient. Recently, polymer pyramid arrays have been employed in essentially the same way, which based on the applied force controls the portion of the pyramid that contacts the surface and therefore the size of the feature (Huo, Zheng et al. 2008). Furthermore, imbedded

heaters have been added to the polymer pyramid array to control polymer expansion under each pyramid individually to manipulate dot size (Brown, Eichelsdoerfer et al. 2013). Dip pen lithography provides one of the highest resolutions of the patterning techniques currently available and recent developments such as low-cost cantilever arrays or individually computer controlled cantilevers have made this method very promising. However, in its current state, the method remains quite challenging to carry out by the general community; but the Mirkin lab is pursuing the technique's development aimed at making it commercially available for the general public.

1-3.7 Colloid lithography

In this technique, polystyrene spheres in solution are deposited on a surface, and as the solvent evaporates, the spheres form a regular, packed monolayer (Taylor, Keay et al. 2012). Spheres are then deformed by exposing them to a temperature gradient, which melts the spheres differentially based on the heat applied. By having a heat source at one end that diffuses across the gradient surface, the extent of sphere melting goes from very high to not at all. A PEG silane is then evaporated on the surface and self assembles wherever the beads do not contact and protect the surface. Spheres are then detached and proteins incubated to fill the gaps previously protected by the beads. The colloid lithography approach yields very large patterned surfaces, however the low control over the placement of individual dots results in frequent defects. Furthermore, the heater approach to create gradients is limited to a linear geometry.

1-3.8 Light patterning

1-3.8.1 Laser-assisted adsorption by photobleaching

Here, a microscope is used to selectively photobleach fluorescently-labeled biotin, which renders the protein more reactive and causes it to bind to an underlying BSA-coated surface (**Figure 1-1e**) (Belisle, Correia et al. 2008; Bélisle, Mazzaferrri et al. 2013). Streptavidin can then be used to bind to the surface-bound biotin and serve as a binding site for navigational guidance cues. Any desired pattern of high complexity can be designed computationally and sent to a microscope to automatically create the surface-bound patterns. For instance, by altering the laser intensity and the displacement velocity of the fluorescence focal spot, gradients were produced. Notably, this

method combines a high level of flexibility with regard to the pattern produced, and the capacity to locally coat a substrate with different concentrations of protein. LAPAP is a very powerful technique where very intricate designs can be patterned, but the chemistry required to link the protein to the surface is not universal and therefore limits the proteins that can be patterned in the gradient.

1-3.8.2 Laser scanning lithography

Instead of using focused light to increase molecular reactivity with the surface, light can also be used to detach molecules from the surface. For example, Slater *et al.* (2011) developed a method whereby laser scanning lithography was used to form peptide patterns by selectively desorbing thiol SAM's from a gold surface by localized heating of the surface with light and replacing the displaced thiols with other thiols with a head group, which favors protein binding from solution. Through this approach, multi-protein gradients were achieved (Slater, Miller *et al.* 2011). Laser scanning lithography provides a relatively high resolution and the ability to create multi-protein patterns; however the method relies on the presence of thiols which might affect the response of the cells to the patterned protein.

1-3.8.3 Photolithography

An early technique for pattern with light is photolithography, a relatively harsh microfabrication method in which strong UV light is shone through a metal mask to expose specific regions on a surface. The surface may be coated with a photopolymer, or photoresist, that upon exposure to UV light will alter the level of polymer crosslinking. Alternatively, selective UV light exposure photolithography was employed to eradicate specific portions of self-assembled monolayers of thiols terminated with PEG end groups. The eradication of such groups then opens up available space on a surface for proteins to bind (Hynes and Maurer 2012). Peptides can also selectively adsorb to surfaces coated with thiol SAMs when exposed to light in a process called photoimmobilization. By selectively exposing the surface to light of a graded intensity with a photomask, surface-bound peptide gradients can be patterned (Herbert, McLernon *et al.* 1997). Photolithography provides a means to pattern very large surfaces in one step; however the method often requires a costly clean-room environment. Furthermore, its dependence on light, like the past two methods, also limits the resolution to the microscale.

1-3.9 3D gradients

3D substrates have grown in popularity due to their potential to generate patterns of even greater relevance to mechanisms that occur *in vivo*, however with the implementation of 3D systems, greater complexity in the system arises and data extraction and analysis becomes more complicated. Nevertheless, systems have been developed to create 3D gradients.

1-3.9.1 Polymer scaffolds

3D surface-bound gradients in a hydroxyethylmethacrylate (HEMA) scaffold were formed by using a gradient maker where two solutions are mixed and polymerized (**Figure 1-1h**). One of the two solutions is supplemented by a growth factor, and by altering the rate of mixing of the two solutions, a gradient is formed along the length of the 3D scaffold (Moore, MacSween et al. 2006). Alternatively, an H-shaped microfluidic channel was used to create collagen gels with a gradient of crosslinked peptides (Sundararaghavan, Masand et al. 2011). The formation of gradients imbedded in soft 3D matrices is very biologically relevant; however the dependence on microfluidics to create the gradients limits the geometry to very simple gradients.

1-3.9.2 Spin coating fibrous scaffolds

A popular method to create 3D scaffolds is to spin coat fibers on a surface. One such material that can be spin coated is hyaluronic acid (HA), a widespread ECM component in mammalian brain (Bignami, Hosley et al. 1993). Sundararaghavan *et al.* (2011) altered the conventional method of spin coating by adding a T-channel to the spinnerette of the machine, which allowed the two solutions to be mixed at different rates over time. By changing the mixing ratio as the fibers were deposited on the surface, a z gradient could be created within the 3D fibrous scaffold. By mixing either two HA solutions of different modulus or two HA solutions containing different proteins, mechanistic and chemical gradients were created that served to investigate durotaxis and haptotaxis, respectively (Sundararaghavan and Burdick 2011). This method of layering spin coated fibers provides a nice means to achieve more complex 3D gradients, however the scale of the gradients achieved through this method greatly exceed that of biological gradients and it is unclear whether cells will be able to sense such long gradients.

1-3.10 Reference surface

For all the methods where immobilized gradients are formed, it is critical to consider the reference surface (RS). Overlooking this parameter could drastically influence cell navigation. If the RS is of low affinity, cells will be pushed towards the higher density of the patterned protein regardless of activation of biochemical pathways, whereas when the affinity is excessively high, cell motility is reduced and the cellular responses to the patterns undermined. Instead of these extreme RSs, an intermediate RS should be identified where the response observed is the result of ligand-receptor interactions. To identify this ideal RS we developed an approach whereby two different solutions of high affinity (*e.g.* PDL) and of low affinity (*e.g.* polyethylene glycol (PEG)) are mixed ratiometrically to identify the ratio of the solution at which an ideal RS is achieved where cell response to the patterned gradient occurs through the activation of biochemical pathways (Ricoult, Thompson-Steckel et al. 2014).

1-4 *In vitro* studies of axonal navigation on substrate-bound protein gradients

A number of the above-mentioned methods have been used to investigate axonal navigation. By compiling the reported findings of axonal navigation on substrate-bound protein gradients, we can deduce basic haptotaxis mechanisms based on the patterned molecules that neurons will respond to, the molecular mechanism that ensues, the impact of geometry on navigation, and the repercussions of the presence of haptotaxis and chemotaxis simultaneously. Many of the substrate-bound gradients are challenging to characterize, and a comparative measure common to all does not exist. As a result, we report the geometrical parameters as they were reported in the literature. We also mention the RS for each study to contextualize the response.

1-4.1 Response to patterned molecules and concentrations

Various molecules have been patterned in substrate-bound gradients ranging from chemotropic guidance cues (*e.g.* netrin-1, ephrinA5, brain-derived neurotrophic factor (BDNF)), ECM proteins (*e.g.* laminin, proteoglycans), or synthetic molecules (*e.g.* poly-D-lysine). Neuronal responses to these various patterned molecules depend on the patterned protein, its density, and the receptors expressed by the specific neuron challenged in the assay.

The earliest studies demonstrating the propensity of molecules secreted by cells to guide axonal navigation were conducted by spraying skeletal muscle conditioned medium on a surface in front of a growing axon and demonstrating directed spinal cord neuron outgrowth on the

adsorbed protein gradients (Gundersen and Park 1984). Later, gradients of basal lamina rich in ECM proteins and of the laminin-2 subunit merosin were created with either steep (50-25 %) or a shallow (17-10%) slope on polylysine (PDL)-treated cellulose ester membrane filters (Halfter 1996). Retinal ganglia neurons grown on these gradients exhibited no response to gradients of basal lamina but did respond strongly to shallow merosin gradients at the initial outgrowth; however, neurons did not turn towards higher concentrations after initial outgrowth. Hippocampal neurons were reported to be attracted towards higher concentrations of the full length laminin protein when the gradient slope exceeded $0.6 \mu\text{g/ml}/\mu\text{m}$ with a RS of bovine serum albumin (Dertinger, Jiang et al. 2002). After axonal specification, the attractive response to laminin disappears, and neurons no longer respond to the gradient. The most convincing evidence of the ability of ECM proteins to guide neurons came in 2005 when Adams *et al.* patterned gradients of the laminin peptide IKVAV in two different slopes: shallow and steep (Adams, Kao et al. 2005). Dorsal root ganglions (DRG) seeded outside the gradients and turning into the gradients were reported to pause as the growth cone first entered the gradient and then exhibit the strongest turning response on shallow gradients, with an angle of $30\text{-}45^\circ$ towards the higher laminin density. The speed of the growth cone did not differ for either the different slopes or the different turning angles. By combining the YIGSR peptide with the IKVAV peptide in a single 3D substrate-bound collagen gradient, the directed outgrowth of DRG neurons was stronger than the response observed with either of the peptides alone (Sundararaghavan, Masand et al. 2011).

Comparatively, very shallow laminin gradients ($0.12\text{-}0.52 \text{ ng/mm}^2/100 \mu\text{m}$) with an RS of hemoglobin did not induce turning by axons of embryonic sympathetic ganglion neurons (McKenna and Raper 1988). To induce an axonal response on shallow gradients, the laminin patterns were supplemented with PDL to induce a stronger response than laminin alone on an RS of glass. Surprisingly, it was shown that even greater outgrowth of the rat embryonic cortical neurons could be achieved with affinity gradients of PDL alone without the addition of ECM proteins (Fricke, Zentis et al. 2011). The gradient that induced the strongest response had a slope of 0.04, a width of $4 \mu\text{m}$ and was composed of PDL alone.

The permissive protein laminin has also been coated with a step gradient of Chondroitin sulfate proteoglycans to replicate the proteoglycan gradient expected to form at a glial scar following injury, which inhibits axon regeneration back to their proper targets (Lee, Kalinski et

al. 2014). Outgrowth inhibition occurs within a wide variety of neurons (DRGs, RGCs, and forebrain neurons) on these substrates as the concentration of inhibitory heparin sulfate proteoglycan (HSPG) increases (Snow and Letourneau 1992). Similar work where DRGs were grown on a gradient of the HSPG molecule aggrecan with a RS of laminin resulted in the axons forming dystrophic endballs, which continuously and actively attempted to proceed with outgrowth of the axon but could not successfully exit this inhibitory surface (Tom, Steinmetz et al. 2004). Surprisingly, the endballs could be transformed into active migrating growth cones with a rapid turnaround of point contacts by inactivating PKA and phosphorylation of paxillin (Kuboyama, Luo et al. 2013). Outgrowth inhibition was also observed in RGC temporal axons on a gradient of tectal cell membranes containing the repellent guidance protein ephrin (Baier and Bonhoeffer 1992).

Axon initiation and growth cone turning in hippocampal neurons were both shown to be polarized towards the higher density portions of netrin-1 and BDNF substrate-bound gradients with a RS of PDL (Mai, Fok et al. 2009). Furthermore, on gradients of BDNF, a threshold seemed to exist where at the highest density portion of the gradient, neurons were repelled, at the threshold level, the turning response was non-specific, and below the threshold, axons were attracted. Substrate-bound gradients of the chemotropic guidance proteins nerve growth factor (NGF) and Sema3a also mediate a slope specific response where DRG explants turned towards and away from the high density portion of steep gradients of NGF and Sema3a, respectively (Joddar, Guy et al. 2013). In contrast, on shallow gradients, the response was abolished for both proteins. Furthermore, dissociated DRG neurons did not respond to Sema3a gradients altogether, whereas the same response observed in explants was reproduced on the NGF gradients.

When sympathetic neurons were grown in heart conditioned media on patterned gradients of laminin backfilled with hemoglobin, no role in navigation was observed, but outgrowth was shown to be controlled by the surface density of laminin, where outgrowth became inhibited at laminin surface densities inferior to 0.5 ng/mm^2 (McKenna and Raper 1988).

1-4.2 Intracellular response mechanism

At the molecular level, growth cone movement is controlled by the polymerization and depolymerization of actin monomers at the leading and trailing edges of the growth cone, respectively (Lambert de Rouvroit and Goffinet 2001). For actin polymerization to result in a

forward movement, the filamentous actin must be linked to the exterior of the cell and immobilized so that elongation can occur instead of static cycling of the actin filaments (Chen, Tan et al. 2004). The complex of proteins that enables the formation of actin protrusions, such as those present in filopodia, is collectively called the “clutch mechanism” (Wang 2007). This “clutch” is not only needed to form centers of protein organization but is also essential for the cell to apply force in a process called mechanotransduction (Gomez and Letourneau 2014). Once focal adhesions are formed, the cell uses these adhesions to pull its cytoskeleton forward. The cell achieves this feat by using molecular motors such as myosin that pull parallel actin filaments in opposite directions and thereby haul the cytoskeleton forward (Small, Stradal et al. 2002). The mechanism and the constituents of the adhesion sites that enable this movement have been studied in depth (Giannone, Mege et al. 2009), and the findings thus far seem to suggest that a universal mechanism controls the interaction between the cell and its surroundings, which can be engaged by a variety of different receptor protein present at the surface.

Cells first interact and bind via transmembrane receptors (*e.g.* integrin, cadherin, or DCC) with cues expressed either on the surface of other cells or integrated into the ECM (Geiger, Spatz et al. 2009). This interaction leads to the recruitment of a number of other proteins (*e.g.* paxillin, talin, and vinculin) which aggregate to this location to stabilize the adhesion site (*i.e.* point contact) (Geiger and Bershadsky 2001). As more proteins are recruited and the adhesion matures (*i.e.* focal adhesion), large forces can be applied by the growth cone onto the adhesion site to propel the cytoskeleton forward (Critchley 2000). At the same time, the cytoskeleton simultaneously extends at the leading edge of the cell through the merging of vesicles trafficked to the leading edge via microtubules (Goode, Drubin et al. 2000). There is a long standing debate of whether the navigation of the growth cone results from the localized incorporation of membrane through direct vesicle trafficking and insertion, or whether the recruitment of vesicles occurs as a result of the directed reorganization of the cytoskeleton (Horn and Kennedy 2012).

Among one of the first proteins recruited to the site of interaction between a ligand and a receptor is the Src family tyrosine kinase Fyn, which is thought to regulate the activity of Rho GTPases by the activation of downstream guanine nucleotide exchange factors (GEFs) such as LARG or GEF-H1 (Guilluy, Swaminathan et al. 2011). As a result of GEF activation, RAC1 and CDC42 become upregulated predominantly at the leading edge of a navigating growth cone, whereas RHOA is upregulated at the trailing edge, where disassembly of focal adhesions takes

place (Raftopoulou and Hall 2004). RAC1 and CDC42 interact with a number of proteins associated with filopodia and lamellipodia extension, whereas RHOA is associated with the disassembly of focal adhesions.

Through the expression of substrate-bound protein gradients with disproportionate protein densities, the local enrichment of these intracellular molecular mechanisms is thought to result in the restructuring of the cell cytoskeleton and cell navigation up a gradient of attractant.

1-4.3 Gradient characteristics to halt navigation

The most informative body of work was produced by von Phillipsborn *et al.* where they patterned ephrinA5 gradients to investigate the mechanism through which growth cones sense gradient direction (Von Philipsborn, Lang et al. 2006; von Philipsborn, Lang et al. 2007). They showed that RGC neurons form stop zones in these gradients and that the location of the stop zone was determined by the slope of the gradient (von Philipsborn, Lang et al. 2006). Regardless of the average protein concentration, as the slope became shallower, the stop zone was shifted toward higher density portions of the gradient. By using stripes of different sizes, the authors determined that the stop zone location was defined by the amount of protein encountered by the growth cone along its navigational route as well as the local concentration of the protein. Despite this suggested mechanism, lower protein concentrations were required in shallow gradients than were required to establish the stop zone in steep gradients. This difference seems to be due to different sensitivities of neurons based on the gradient steepness, where shallower gradients seem to result in greater biochemical sensitization (Lang, von Philipsborn et al. 2008). The authors even suggested that the observed difference might result from lower desensitization/adaptation levels in shallower gradients. Lastly, the location of the stop zone in a gradient of a specific slope did not depend on the location of RGCs in the retina as they all stopped on the gradients at the same location, suggesting that no graded response to EphrinA5 gradients exists in temporal RGCs.

1-4.4 Combinatorial studies of haptotaxis and chemotaxis

Substrate-bound laminin gradients with a RS of PDL have also been combined with soluble non-monotonic gradients of BDNF (Joanne Wang, Li et al. 2008). When exposed to the laminin

gradient alone with a slope of 30 ng/ml/mm, more than 60% of the *Xenopus* embryonic spinal neuron axons extended towards the higher laminin density. However, when the soluble gradient was applied in an opposite direction to the laminin gradient, at the high density portion of the laminin gradient, axons were repelled by the laminin gradient (-18%), while at the low density, neurons were strongly attracted (+33%). Similar to the findings reported with the single gradients of IKVAV, no difference in outgrowth speed was observed.

In a second example, a topography gradient coated with PDL was overlaid with a soluble gradient of either an attractive molecule (netrin-1) or repulsive molecule (Sema3A) going in the same direction as the substrate-bound gradient or in an opposite direction (Kundu, Micholt et al. 2013). Mouse embryonic hippocampal neurons seeded on the substrate-bound gradients of PDL showed a neurite turning response to the gradient and maximal outgrowth when the pillars were spaced 1.4 μm apart in X and Y. Substrate topography directed axon extension and very strongly synergized with a superimposed microfluidic gradient of netrin-1. However, when the chemotactic gradient was presented at a 90° angle from the substrate-bound PDL gradient, the haptotactic response was reduced, but remained significant. Surprisingly, when a co-directional Sema3a gradient was added to the PDL gradient, the density of bound protein was shown to define the neuron response to the chemotropic gradient. At the optimal pillar density, the repulsive effect of Sema3a was inhibited, while at lower or higher densities, the repulsive response was maintained. These results suggest that substrate-bound gradients can enhance attraction, but inhibit repulsion in optimal spacing conditions.

1-5 Conclusions and Outlook

There is a high incentive to better understand cell navigation because not only will it allow us to better understand how the organism develops, but as regenerative medicine becomes more and more clinically relevant, a clear understanding on how to control and direct navigation will become essential. Significant strides have been made toward understanding the mechanism of chemotaxis, whereby cells respond to diffusible cues; however, many proteins are bound to cell surfaces and the ECM, and the mechanism at play is haptotaxis instead of chemotaxis. Due to a limitation in available methods to pattern substrate-bound gradients, *in vitro* studies investigating haptotaxis in growth cones are limited.

Preliminary studies have produced a list of molecules that can be patterned and induce axonal navigation responses in neurons. The extensive studies on laminin and ephrinA5 have even given us some insights into the gradient geometries required to induce a response and how this response occurs at a cellular level and molecular level. These results only scrape the tip of the iceberg, and significant work will need to follow to provide us with an accurate understanding of how haptotaxis works.

The numerous technologies that are now available to form substrate-bound protein gradients provide hope that this goal will be reached in the near future. Patterning techniques such as LAPAP or dip-pen nanolithography offer a staggering resolution and an option to alter gradient geometry on the spot, whereas substrate-bound gradients achieved through microfluidic gradients or microcontact printing can pattern large surfaces at a rapid rate and at a low-cost without any specialized equipment. Furthermore, by implementing the concept of digital nanodot gradients, large arrays of distinct gradients can be patterned onto a same substrate, and multi-point live imaging of fluorescently transfected neurons will yield large data sets that will shed light on the mechanisms underlying haptotaxis.

1-6 References

- Adams, D. N., E. Y. Kao, et al. (2005). "Growth cones turn and migrate up an immobilized gradient of the laminin IKVAV peptide." *J Neurobiol* **62**(1): 134-147.
- Adler, J. (1966). "Chemotaxis in Bacteria." *Science* **153**(3737): 708-&.
- Baier, H. and F. Bonhoeffer (1992). "Axon Guidance by Gradients of a Target-Derived Component." *Science* **255**(5043): 472-475.
- Baker, K. A., S. W. Moore, et al. (2006). "When a diffusible axon guidance cue stops diffusing: roles for netrins in adhesion and morphogenesis." *Current Opinion in Neurobiology* **16**(5): 529-534.
- Bélisle, J., J. Mazzaferri, et al. (2013). "Laser-assisted adsorption by photobleaching." *Methods in cell biology* **119**: 125-140.
- Belisle, J. M., J. P. Correia, et al. (2008). "Patterning protein concentration using laser-assisted adsorption by photobleaching, LAPAP." *Lab on a Chip* **8**(12): 2164-2167.
- Bhattacharjee, N., N. Li, et al. (2010). "A neuron-benign microfluidic gradient generator for studying the response of mammalian neurons towards axon guidance factors." *Integrative Biology* **2**(11-12): 669-679.
- Bignami, A., M. Hosley, et al. (1993). "Hyaluronic-Acid and Hyaluronic Acid-Binding Proteins in Brain Extracellular-Matrix." *Anatomy and Embryology* **188**(5): 419-433.
- Bin, J. M., S. Rajasekharan, et al. (2013). "Full-Length and Fragmented Netrin-1 in Multiple Sclerosis Plaques Are Inhibitors of Oligodendrocyte Precursor Cell Migration." *American Journal of Pathology* **183**(3): 673-680.

Brown, K. A., D. J. Eichelsdoerfer, et al. (2013). "A cantilever-free approach to dot-matrix nanoprinting." Proceedings of the National Academy of Sciences of the United States of America **110**(32): 12921-12924.

Campbell, P. G., E. D. Miller, et al. (2005). "Engineered spatial patterns of FGF-2 immobilized on fibrin direct cell organization." Biomaterials **26**(33): 6762-6770.

Cang, J. H., M. Kaneko, et al. (2005). "Ephrin-As guide the formation of functional maps in the visual cortex." Neuron **48**(4): 577-589.

Carter, S. B. (1965). "Principles of cell motility: the direction of cell movement and cancer invasion." Nature **208**(5016): 1183-1187.

Carter, S. B. (1967). "Haptotaxis and the mechanism of cell motility." Nature **213**(5073): 256-260.

Chen, C. S., J. Tan, et al. (2004). "Mechanotransduction at cell-matrix and cell-cell contacts." Annual Review of Biomedical Engineering **6**: 275-302.

Critchley, D. R. (2000). "Focal adhesions - the cytoskeletal connection." Current Opinion in Cell Biology **12**(1): 133-139.

de la Torre, J. R., V. H. Hopker, et al. (1997). "Turning of retinal growth cones in a netrin-1 gradient mediated by the netrin receptor DCC." Neuron **19**(6): 1211-1224.

Dertinger, S. K. W., X. Jiang, et al. (2002). "Gradients of substrate-bound laminin orient axonal specification of neurons." Proceedings of the National Academy of Sciences **99**(20): 12542-12547.

Engelmann, T. W. (1881). "Neue Methode zur Untersuchung der Sauerstoffausscheidung pflanzlicher und thierischer Organismen." Pflügers Archiv European Journal of Physiology **25**(1): 285-292.

Fricke, R., P. D. Zentis, et al. (2011). "Axon guidance of rat cortical neurons by microcontact printed gradients." Biomaterials **32**(8): 2070-2076.

Geiger, B. and A. Bershadsky (2001). "Assembly and mechanosensory function of focal contacts." Current Opinion in Cell Biology **13**(5): 584-592.

Geiger, B., J. P. Spatz, et al. (2009). "Environmental sensing through focal adhesions." Nat Rev Mol Cell Biol **10**(1): 21-33.

Genzer, J. (2012). "Surface-Bound Gradients for Studies of Soft Materials Behavior." Annual Review of Materials Research **42**(1): 435-468.

Gerisch, G., D. Hulser, et al. (1975). "Cell Communication by Periodic Cyclic-Amp Pulses." Philosophical Transactions of the Royal Society of London Series B-Biological Sciences **272**(915): 181-&.

Giannone, G., R. M. Mege, et al. (2009). "Multi-level molecular clutches in motile cell processes." Trends in Cell Biology **19**(9): 475-486.

Gomez, T. M. and P. C. Letourneau (2014). "Actin dynamics in growth cone motility and navigation." Journal of Neurochemistry **129**(2): 221-234.

Goode, B. L., D. G. Drubin, et al. (2000). "Functional cooperation between the microtubule and actin cytoskeletons." Current Opinion in Cell Biology **12**(1): 63-71.

Guilluy, C., V. Swaminathan, et al. (2011). "The Rho GEFs LARG and GEF-H1 regulate the mechanical response to force on integrins." Nature Cell Biology **13**(6): 722-U211.

Gundersen, R. W. and K. H. Park (1984). "The effects of conditioned media on spinal neurites: substrate-associated changes in neurite direction and adherence." Dev Biol **104**(1): 18-27.

Halfter, W. (1996). "The behavior of optic axons on substrate gradients of retinal basal lamina proteins and merosin." Journal of Neuroscience **16**(14): 4389-4401.

Herbert, C. B., T. L. McLernon, et al. (1997). "Micropatterning gradients and controlling surface densities of photoactivatable biomolecules on self-assembled monolayers of oligo(ethylene glycol) alkanethiolates." Chemistry & Biology **4**(10): 731-737.

Hjortø, G. M., M. Hansen, et al. (2009). "Generating substrate bound functional chemokine gradients in vitro." Biomaterials **30**(29): 5305-5311.

Hong, K. S., L. Hinck, et al. (1999). "A ligand-gated association between cytoplasmic domains of UNC5 and DCC family receptors converts netrin-induced growth cone attraction to repulsion." Cell **97**(7): 927-941.

Horn, K. E. and T. E. Kennedy (2012). "Putting flesh on the bones: DCC combines membrane insertion with cytoskeletal reorganization to promote chemoattraction (Commentary on Cotrufo et al.)." European Journal of Neuroscience **36**(9): 3151-3151.

Huo, F. W., Z. J. Zheng, et al. (2008). "Polymer pen lithography." Science **321**(5896): 1658-1660.

Hynes, M. J. and J. A. Maurer (2012). "Photoinduced Monolayer Patterning for the Creation of Complex Protein Patterns." Langmuir **28**(47): 16237-16242.

Jennings, H. S. (1906). "Behavior of the Lower Organisms." New York: 366.

Jeon, N. L., S. K. W. Dertinger, et al. (2000). "Generation of Solution and Surface Gradients Using Microfluidic Systems." Langmuir **16**(22): 8311-8316.

Jiang, X. Y., Q. B. Xu, et al. (2005). "A general method for patterning gradients of biomolecules on surfaces using microfluidic networks." Analytical Chemistry **77**(8): 2338-2347.

Joanne Wang, C., X. Li, et al. (2008). "A microfluidics-based turning assay reveals complex growth cone responses to integrated gradients of substrate-bound ECM molecules and diffusible guidance cues." Lab on a Chip **8**(2): 227-237.

Joddar, B., A. T. Guy, et al. (2013). "Spatial gradients of chemotropic factors from immobilized patterns to guide axonal growth and regeneration." Biomaterials **34**(37): 9593-9601.

Juncker, D., H. Schmid, et al. (2005). "Multipurpose microfluidic probe." Nature materials **4**(8): 622-628.

Kam, L. and S. G. Boxer (2000). "Formation of supported lipid bilayer composition arrays by controlled mixing and surface capture." Journal of the American Chemical Society **122**(51): 12901-12902.

KeinoMasu, K., M. Masu, et al. (1996). "Deleted in Colorectal Cancer (DCC) encodes a netrin receptor." Cell **87**(2): 175-185.

Keller, H. U., J. H. Wissler, et al. (1979). "Chemotaxis is not a special case of haptotaxis." Experientia **35**(12): 1669-1671.

Kennedy, T. E., H. Wang, et al. (2006). "Axon guidance by diffusible chemoattractants: A gradient of netrin protein in the developing spinal cord." Journal of Neuroscience **26**(34): 8866-8874.

Kim, H.-D. and S. R. Peyton (2012). "Bio-inspired materials for parsing matrix physicochemical control of cell migration: A Review." Integrative Biology **4**(1): 37-52.

Kuboyama, T., X. T. Luo, et al. (2013). "Paxillin phosphorylation counteracts proteoglycan-mediated inhibition of axon regeneration." Experimental Neurology **248**: 157-169.

Kundu, A., L. Micholt, et al. (2013). "Superimposed topographic and chemical cues synergistically guide neurite outgrowth." Lab on a Chip **13**(15): 3070-3081.

Lambert de Rouvroit, C. and A. M. Goffinet (2001). "Neuronal migration." Mechanisms of Development **105**(1-2): 47-56.

Lang, S., A. Philipsborn, et al. (2008). "Growth cone response to ephrin gradients produced by microfluidic networks." Analytical and Bioanalytical Chemistry **390**(3): 809-816.

Lang, S., A. C. von Philipsborn, et al. (2008). "Growth cone response to ephrin gradients produced by microfluidic networks." Analytical and Bioanalytical Chemistry **390**(3): 809-816.

Lara Rodriguez, L. and I. C. Schneider (2013). "Directed cell migration in multi-cue environments." Integrative Biology **5**(11): 1306-1323.

Lee, K., C. Kim, et al. (2009). "Generalized serial dilution module for monotonic and arbitrary microfluidic gradient generators." Lab on a Chip **9**(5): 709-717.

Lee, S. J., A. L. Kalinski, et al. (2014). "Awakening the stalled axon — Surprises in CSPG gradients." Experimental Neurology **254**(0): 12-17.

Mai, J., L. Fok, et al. (2009). "Axon Initiation and Growth Cone Turning on Bound Protein Gradients." The Journal of Neuroscience **29**(23): 7450-7458.

McKenna, M. P. and J. A. Raper (1988). "Growth cone behavior on gradients of substratum bound laminin." Developmental Biology **130**(1): 232-236.

Ming, G. L., H. J. Song, et al. (1997). "CAMP-dependent growth cone guidance by netrin-1." Neuron **19**(6): 1225-1235.

Moore, K., M. MacSween, et al. (2006). "Immobilized concentration gradients of neurotrophic factors guide neurite outgrowth of primary neurons in macroporous scaffolds." Tissue Eng **12**(2): 267-278.

Moore, S. W., N. Biais, et al. (2009). "Traction on Immobilized Netrin-1 Is Sufficient to Reorient Axons." Science **325**(5937): 166.

Moore, S. W., X. Zhang, et al. (2012). "Netrin-1 Attracts Axons through FAK-Dependent Mechanotransduction." Journal of Neuroscience **32**(34): 11574-11585.

Morgenthaler, S., S. W. Lee, et al. (2003). "A simple, reproducible approach to the preparation of surface-chemical gradients." Langmuir **19**(25): 10459-10462.

Ongo, G., S. G. Ricoult, et al. (2014). "Ordered, Random, Monotonic and Non-monotonic Digital Nanodot Gradients". Plos One, Accepted.

Paratcha, G., C. F. Ibanez, et al. (2006). "GDNF is a chemoattractant factor for neuronal precursor cells in the rostral migratory stream." Molecular and Cellular Neuroscience **31**(3): 505-514.

Park, J., D. H. Kim, et al. (2010). "Simple haptotactic gradient generation within a triangular microfluidic channel." Lab on a Chip **10**(16): 2130-2138.

Pfeffer, W. F. P. (1884). Locomotorische richtungsbewegungen durch chemische reize.

Qasaimeh, M. A., S. G. Ricoult, et al. (2013). "Microfluidic probes for use in life sciences and medicine." Lab on a Chip **13**(1): 40-50.

Raftopoulou, M. and A. Hall (2004). "Cell migration: Rho GTPases lead the way." Developmental Biology **265**(1): 23-32.

Ricoult, S. G., M. Pla-Roca, et al. (2013). "Large Dynamic Range Digital Nanodot Gradients of Biomolecules Made by Low-Cost Nanocontact Printing for Cell Haptotaxis." Small **9**(19): 3308-3313.

Ricoult, S. G., G. Thompson-Steckel, et al. (2014). "Tuning cell-surface affinity to direct cell specific responses to patterned proteins." Biomaterials **35**(2): 727-736.

Rosoff, W. J., J. S. Urbach, et al. (2004). "A new chemotaxis assay shows the extreme sensitivity of axons to molecular gradients (vol 7, pg 678, 2004)." Nature Neuroscience **7**(7): 785-785.

Schall, T. J., K. Bacon, et al. (1990). "Selective Attraction of Monocytes and Lymphocytes-T of the Memory Phenotype by Cytokine Rantes." Nature **347**(6294): 669-671.

Senesi, A. J., D. I. Rozkiewicz, et al. (2009). "Agarose-Assisted Dip-Pen Nanolithography of Oligonucleotides and Proteins." ACS Nano **3**(8): 2394-2402.

Slater, J. H., J. S. Miller, et al. (2011). "Fabrication of Multifaceted Micropatterned Surfaces with Laser Scanning Lithography." Advanced Functional Materials **21**(15): 2876-2888.

Small, J. V., T. Stradal, et al. (2002). "The lamellipodium: where motility begins." Trends in Cell Biology **12**(3): 112-120.

Snow, D. M. and P. C. Letourneau (1992). "Neurite Outgrowth on a Step Gradient of Chondroitin Sulfate Proteoglycan (Cs-Pg)." J Neurobiol **23**(3): 322-336.

Sotelo, C. (2002). "The chemotactic hypothesis of Cajal: a century behind." Changing Views of Cajal's Neuron **136**: 11-20.

Squires, T. M., R. J. Messinger, et al. (2008). "Making it stick: convection, reaction and diffusion in surface-based biosensors." Nature Biotechnology **26**(4): 417-426.

Sun, K. L. W., J. P. Correia, et al. (2011). "Netrins: versatile extracellular cues with diverse functions." Development **138**(11): 2153-2169.

Sundararaghavan, H. G. and J. A. Burdick (2011). "Gradients with Depth in Electrospun Fibrous Scaffolds for Directed Cell Behavior." Biomacromolecules **12**(6): 2344-2350.

Sundararaghavan, H. G., S. N. Masand, et al. (2011). "Microfluidic Generation of Haptotactic Gradients through 3D Collagen Gels for Enhanced Neurite Growth." Journal of Neurotrauma **28**(11): 2377-2387.

Tan, C. P., B. R. Cipriany, et al. (2010). "Nanoscale Resolution, Multicomponent Biomolecular Arrays Generated By Aligned Printing With Parylene Peel-Off." Nano Letters **10**(2): 719-725.

Tanabe, Y. and T. M. Jessell (1996). "Diversity and pattern in the developing spinal cord." Science **274**(5290): 1115-1123.

Taylor, Z. R., J. C. Keay, et al. (2012). "Independently Controlling Protein Dot Size and Spacing in Particle Lithography." Langmuir **28**(25): 9656-9663.

Tom, V. J., M. P. Steinmetz, et al. (2004). "Studies on the development and behavior of the dystrophic growth cone, the hallmark of regeneration failure, in an in vitro model of the glial scar and after spinal cord injury." Journal of Neuroscience **24**(29): 6531-6539.

Von Philipsborn, A. C., S. Lang, et al. (2006). "Microcontact printing of axon guidance molecules for generation of graded patterns." Nature Protocols **1**(3): 1322-1328.

von Philipsborn, A. C., S. Lang, et al. (2007). "Substrate-Bound Protein Gradients for Cell Culture Fabricated by Microfluidic Networks and Microcontact Printing." Sci. STKE **2007**(414): pl6-.

von Philipsborn, A. C., S. Lang, et al. (2006). "Growth cone navigation in substrate-bound ephrin gradients." Development **133**(13): 2487-2495.

Walker, G. M., M. S. Ozers, et al. (2004). "Cell infection within a microfluidic device using virus gradients." Sensors and Actuators B: Chemical **98**(2-3): 347-355.

Wang, Y.-l. (2007). Flux at Focal Adhesions: Slippage Clutch, Mechanical Gauge, or Signal Depot.

Whitesides, G. M. (2006). "The origins and the future of microfluidics." Nature **442**(7101): 368-373.

Wu, J., X. Wu, et al. (2013). "Recent developments in microfluidics-based chemotaxis studies." Lab on a Chip **13**(13): 2484-2499.

Xu, K., Z. Wu, et al. (2014). "Structures of netrin-1 bound to two receptors provide insight into its axon guidance mechanism." Science.

PREFACE TO CHAPTER 2

In the previous chapter, we introduced haptotaxis and reviewed the methods that have been developed to date to investigate haptotaxis. We also pointed out the limitations in the currently available methods that have limited the study of haptotaxis in neuroscience. This chapter provided the incentives to develop an easy and low-cost method to form substrate-bound protein gradients of complex geometries and high dynamic range (Chapter 1).

In the following chapter, we present novel algorithms which facilitate the creation of digital nanodot gradients (DNG) of any desired geometry composed of 200 nm dots with spacing ranging from 0 nm to 12 μm that reach a dynamic range of 3.6 orders of magnitude. We then developed a simple and low-cost lift-off nanocontact printing technique to rapidly pattern large surfaces with protein nanofeatures in any desired geometry. Lastly, we show that the lift-off nanocontact printing method and the digital nanodot gradient designs can be implemented to yield substrate-bound protein gradients that we used to probe C2C12 myoblast adhesion and migration on arginine-glycine-aspartic acid peptide and netrin-1 protein, respectively.

Our contributions provide a method which will render nanopatterning feasible to the general scientific community. Furthermore, DNGs will lead to more in depth studies of axonal navigation and more generally cell migration on substrate-bound protein gradients.

This chapter was published as a research article in *Small* (Ricoult et al., 2013).

Acknowledgements

The authors wish to thank Yannick Devaud, Levon Atoyan and Natalia Tansky for their contributions to nanocontact printing, Tohid Fatanat Didar for providing RGD peptides and Prof. Craig Mandato for providing C2C12 cells. We acknowledge support from CIHR (Regenerative and Nanomedicine grant), the Canadian Foundation for Innovation and the McGill Nanotools Microfabrication Laboratory (funded by CFI and McGill University). SGR was supported by a Jeanne Timmins Costello Studentship, the NSERC-Create Integrated Sensor System Program and the Neuroengineering program funded by CIHR and The Molson Foundation. TEK is a Killam Foundation Scholar and holds a Chercheur National award from the Fonds de la Recherche en Santé du Québec. DJ holds a Canada Research Chair.

CHAPTER 2

Large Dynamic Range Digital Nanodot Gradients of Biomolecules Made by Low-Cost Nanocontact Printing for Cell Haptotaxis

Sébastien G. Ricoult^{1,2}, Mateu Pla-Roca¹, Roozbeh Safavieh¹, G. Monserratt Lopez-Ayon³, Peter Grütter³, Timothy E. Kennedy², David Juncker^{1,2}

¹*Department of Biomedical Engineering, McGill University and Génome Québec Innovation Centre, McGill University, 740 Dr. Penfield Avenue, Montréal, Québec H3A 0G1, Canada;*

²*Department of Neuroscience, McGill University, 3801 University Avenue, Montréal, Québec H3A 0G1, Canada;* ³*Center for the Physics of Materials and the Department of Physics, McGill University, Montréal, Québec H3A 2T8, Canada.*

2-1 Abstract

A novel method is introduced for ultrahigh throughput and ultralow cost patterning of biomolecules with nanometer resolution and novel 2D digital nanodot gradients (DNGs) with mathematically defined slopes are created. The technique is based on lift-off nanocontact printing while using high-resolution photopolymer stamps that are rapidly produced at a low cost through double replication from Si originals. Printed patterns with 100 nm features are shown. DNGs with varying spacing between the dots and a record dynamic range of 4400 are produced; 64 unique DNGs, each with hundreds of thousands of dots, are inked and printed in 5.5 min. The adhesive response and haptotaxis of C2C12 myoblast cells on DNGs demonstrated their biofunctionality. The great flexibility in pattern design, the massive parallel ability, the ultra low cost, and the extreme ease of polymer lift-off nanocontact printing will facilitate its use for various biological and medical applications.

2-2 Introduction

Patterning of biomolecules and notably proteins on surfaces has been critical to advances in microarrays, biosensors, and cell biology.[1, 2] Proteins are the main effectors in cells and are important for bioanalysis, but they are labile and cannot be exposed to harsh conditions due to risks of denaturation which results in a loss in biological activity. Patterning of proteins cannot be done by photolithography, and alternative methods, such as Inkjet printing, are now well established, but the resolution is typically limited to 100 μm . [3] Interestingly, proteins can be patterned by microcontact printing by first inking of a soft stamp by incubating it in a protein solution, briefly drying it, and placing it onto a target substrate so as to effect the transfer of proteins from the stamp to the substrate. However, conventional microcontact printing suffers from a number of limitations and it is for example difficult to achieve resolution $< 1 \mu\text{m}$ or large spacing in the pattern due to the risk, and occurrence, of collapse of the soft, elastomeric stamps.[4] Alternative methods with greater flexibility such as dip pen lithography were developed,[5] but they are slow and cumbersome. Recently, parallel dip-pen patterning was introduced,[6] which helped improve the throughput, however it does not allow for direct control of the tips and is thus limited to the replication of patterns no larger than the spacing between two tips. More recently, high resolution Si stencil was introduced to make nanoarrays,[7] but so far only small arrays with each only one ink were made, and the stencils are fragile and costly to make.

A modified microcontact printing method called lift-off printing has increased resolution and overcome the limitations of aspect ratio and stamp collapse.[8] For proteins, a lift-off printing has been conducted by pressing a hard, Si “master” stamp containing recesses against a flat stamp coated with protein, thus lifting-off proteins in the contact areas, but leaving untouched the ones located below a recess. These proteins can then be transferred onto a glass surface by printing the flat stamp without risk of collapse. Recently, the use of PDMS stamps has been introduced for reactive lift-off of thiols on gold,[9] but only Si stamps have been used for protein lift-off to date. Coyer et al. used lift-off printing to produce digital gradients by varying the spacing of dots along one axis perpendicular to the gradient direction from 1 μm to 64 μm , corresponding to a 63 fold change, which expressed in Log 10 corresponds to a dynamic range of 1.8 orders of magnitude (OM). [7, 10] However, Si lift-off masters are expensive to make, and their lifetime is limited as they get contaminated by each print, and thus only a restricted number

of patterns can be produced, keeping the overall costs of patterning high and limiting their usefulness.

Here, we introduce two significant advances. Firstly, we use photo-crosslinked polymer masters for lift-off nanocontact printing of proteins and peptides with feature sizes down to 100 nm. The polymer masters are double-replicated from a Si master where at each step multiple copies can be made, to produce a very large number of prints exceeding 400 from a single Si nanopattern. Secondly, we present a novel DNG that while being unidirectional varies in two-dimension and has the greatest dynamic range of any single gradient produced to date to our knowledge, and which could be further expanded. The response and haptotaxis of C2C12 muscle cells to both peptide and protein DNGs was established.

2-3 Results and Discussion

DNGs, each between 200 and 400 μm long depending on the slope, and 400 μm wide, were designed using 200 nm wide dots with varying spacing between the dots. To increase the dynamic range of the gradient, the spacing of the dots was changed in two-dimensions, both parallel and perpendicular to the gradient direction. We developed an algorithm to create such patterns while producing a continuous gradient. The DNGs were formed by subdividing the gradient into “boxes” each 400 μm long and with a height $\sim 8 \mu\text{m}$ (depending on the gradient and the position). The spacing of nanodots within one box is constant, while in each box it was adjusted to depend on the position of the box so as to match the density corresponding to the position in the gradient. **Figure 2-1** shows one such gradient composed of 53 rectangles that are 400 μm long and 7.5 μm wide while the center-to-center spacing of the dots in each rectangle varies from 0.3 μm to 4.83 μm along both X and Y. Here, the spacing d of the dots within each box follows the power law $d = 3 \mu\text{m} \times (\text{box number})^{\sqrt{2}/2}$. The dynamic range of this DNG is 259 or 2.4 OM. Linear, exponential, or power-law gradients can be produced by using the appropriate function to calculate the dot spacing in each box. The DNG with the highest dynamic range extended from full coverage at one end to one 200 nm dot ($= 0.0314 \mu\text{m}^2$) within an area of $11.75 \times 11.75 = 138 \mu\text{m}^2$ at the other end, corresponding to a dynamic range of 4400, or 3.6 OM. This constitutes the highest dynamic range reported to date for a single continuous surface gradient to the best of our knowledge, while the maximal spacing is relevant to cell migration. Indeed, the maximal spacing was limited to $\sim 12 \mu\text{m}$ between the dots so that a cell would be in contact with at least one dot. Larger spacing could easily be produced if desired. By changing the

various parameters such as minimal and maximal spacing and the slope, 64 different gradients were designed and collectively occupied an area of $5.4 \times 5.8 \text{ mm}^2$.

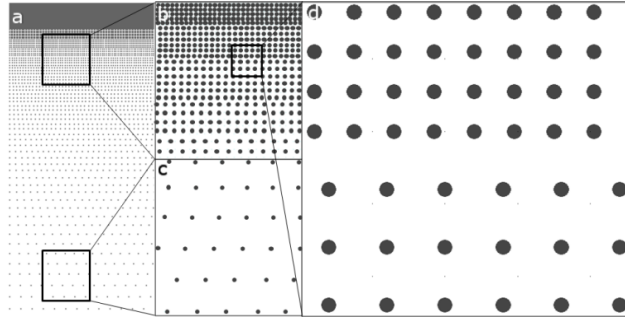


Figure 2-1. DNG design. (a) Excerpt of a DNG made up of 88,521 200 nm dots with center-to-center spacing decreasing from $4.85 \mu\text{m}$ to 300 nm . The gradient is composed of 53 rectangular boxes $7.5 \times 400 \mu\text{m}^2$ in size with an array of dots of constant spacing in both X and Y directions within each box. (b, c) Close-up views from the high and low density regions at the top and bottom of the gradient, respectively. (d) Close-up view of a section of the gradient showing 200 nm dots with a center-to-center spacing of 792 nm for the top 4 rows and 926 nm for the bottom 3 rows.

An accurate polymer copy of the Si wafer with the etched nanopatterns was obtained after double replication using poly(dimethylsiloxane) (PDMS) and a UV sensitive photopolymer (Norland Optical Adhesive 63 (NOA)), (**Figure 2-2**).^[11] The details of the process are provided in the accompanying methods. Scanning electron microscopy (SEM) and atomic force microscopy (AFM) images of the original Si master, the intermediate, and the final replicate, show a high fidelity (**Figure 2-3**). In addition to the 200 nm dots, we also produced stamps with 100 nm features and successfully printed them, **Figure 2-4**. However, for cells to recognize the nanodots and efficiently form focal adhesions, it has been shown that protein aggregates less than 200 nm large fail to elicit a cell response,^[12] thus 200 nm dots were used for the DNGs.

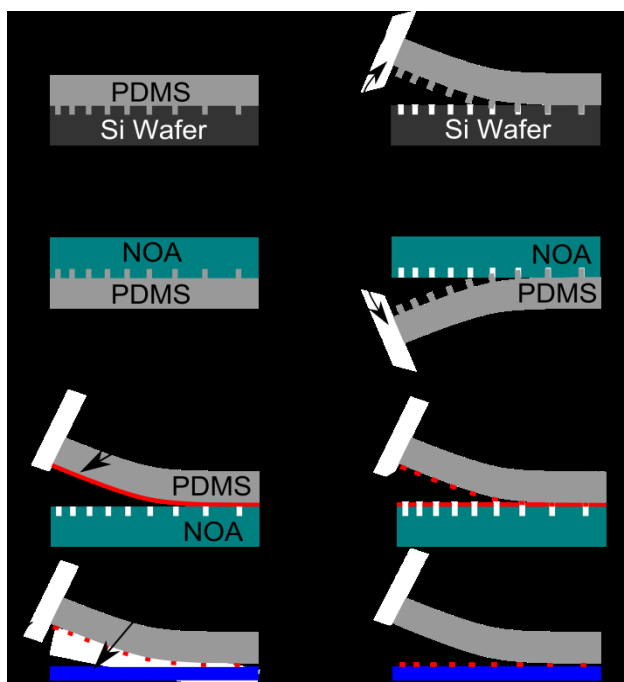


Figure 2-2. Schematic of the double replication process to make polymer replicas and their subsequent use as masters for lift-off nanocontact printing. (a) A Si wafer with a DNG of 200 nm holes is covered with PDMS, which is cured, and (b) separated from the wafer. The PDMS is in turn covered with a photo-sensitive polymer (NOA), exposed to light, and (d) the NOA replica separated. A planar PDMS stamp is incubated with a protein solution, blown dry, and (e) quickly brought into contact with a NOA replica that was plasma activated, and separated to lift-off proteins in the contact areas. (g) The flat PDMS stamp is then printed onto a glass slide and (h) separated, producing a DNG of protein on the slide.

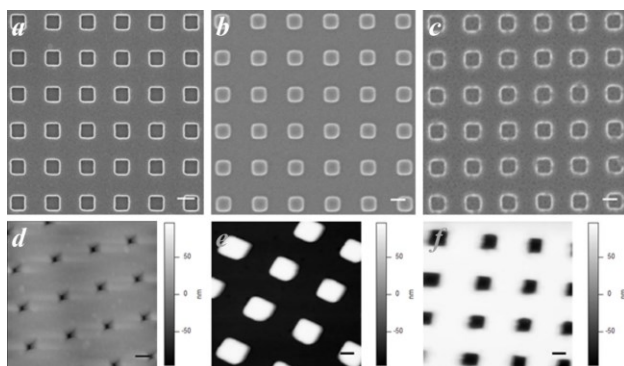


Figure 2-3. SEM and AFM images of the Si master, the intermediate PDMS replica and the NOA replica. (a-c) SEM images of the pattern on (a) the silicon wafer, (b) the intermediate replica and (c) the second photoadhesive replica. (d-e) AFM micrographs of the topography on

(d) the Silicon wafer, (e) the intermediate replica and (f) the second photoadhesive replica. Scale bars (a-f) are 200 nm.

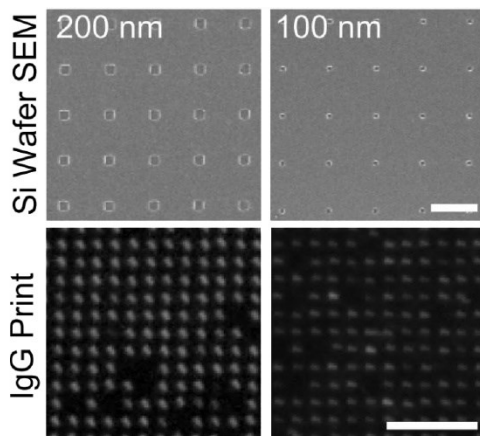


Figure 2-4. Liftoff microcontact printing of 200 and 100 nm dots. SEM micrograph of the Si wafer etched with 200 nm and 100 nm in diameter dots with 1 μm pitch. The corresponding prints of fluorescently labeled IgG protein are shown below. The streaked dot geometry seen in the fluorescent patterns is exclusively attributable to the imaging process since AFM of the dots does not reveal any consistent deformation of the pattern (Figure 3b). Scale bars are 1 μm for the SEM micrographs and 5 μm for the fluorescence images.

The throughput and cost of nanocontact printing benefit from multiple replications and the massive parallelism of printing. To test the possibility for making multiple copies, the Si wafer was replicated over 20 times into PDMS, and the 20th copy in turn replicated into NOA more than 20 times (**Figure 2-5**). We believe that well over 400 replicates could be made but did not pursue the experiment further. It takes ~ 1 min for PDMS to NOA replication, allowing tens of NOA copies to be rapidly produced. All 64 gradients which comprise 7.6×10^6 dots can be printed in parallel in a 5 s lift-off step. The material cost of an NOA replica with the 64 gradients (0.8 ml) is only \$0.13. We paid \$450 for the Si wafer patterned by e-beam. The material cost of a PDMS replica (50 ml) is ~ \$6. The combined material cost for each replica with 64 DNGs, assuming 400 copies, is thus \$1.55, or 2.4 cents per gradient. Whereas until now production of arbitrary nanopatterns has been very cost and time intensive, DNGs can be produced with great ease and at low cost. Indeed, once the double-replication nanopatterning procedure had been optimized, the time, efforts and cost of DNG production were negligible compared to the needs of cell culture, imaging and data analysis.

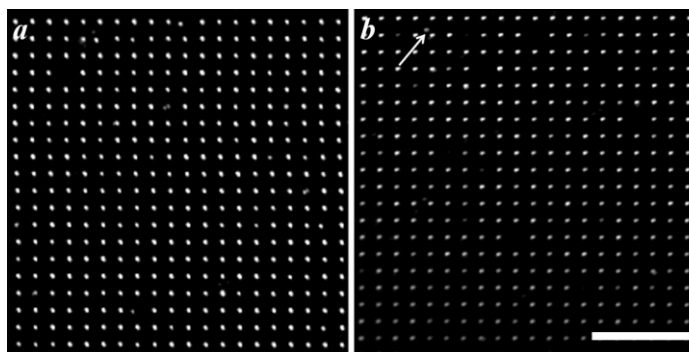


Figure 2-5. Comparison of prints obtained with lift-off stamps generated in the initial and a late replication cycles. Fluorescent micrographs of protein patterned made using lift-off stamps that were (a) the 1st NOA replicate from the 1st PDMS intermediate replica (of the original Si wafer) and (b) the 20th NOA replica obtained from the (at least) 20th PDMS intermediate replica. The lift-off stamps feature an array of 200 nm holes with 2 μm pitch in X and Y. Following lift-off and the printing of fluorescently labeled IgGs, dots of proteins were produced that are similar to the ones shown in Figure 3 in the main text. Many of the missing dots in (b) are due to the degradation of the original Si wafer with many holes getting clogged up following multiple replications, in excess of 20 times. Spots that appear between the dots of the array (see arrow) originate in the PDMS-to-NOA replication step and become more prevalent with replication numbers, and are likely due to dust particles adsorbing on the PDMS stamp. Scale bar 10 μm .

A solution of Arginine-Glycine-Aspartic acid (RGD) peptide mixed with fluorescently-labelled immunoglobulin G (IgGs) for visualization was used as “ink” for the printing process, **Figure 2-1e-f**. Following optimization, high yields were achieved for protein nanopatterning with a minimal number of defects, **Figure 2-6a**. These results indicate that NOA, and by extension other hard polymeric materials, may serve as efficient and reliable masters for lift-off nanocontact printing of biomolecules. Defects were rare and could be attributed to dust particles that adsorbed to the PDMS during replication, and might be further reduced by working in a clean room. Whereas Si masters may be used repeatedly for lift-off printing,[10] recycling NOA stamps was not effective as the second print displayed multiple defects. It may be possible to overcome this limitation using more harsh cleaning procedures, but it was not pursued here given that NOA masters were inexpensive and plentiful.

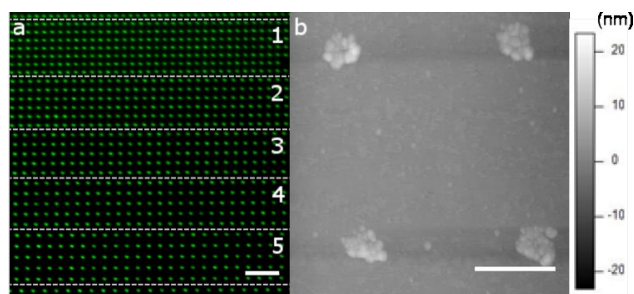


Figure 2-6. Confocal fluorescence microscope and AFM images of a DNG patterned by lift-off nanocontact printing. (a) Grids of 200 nm dots of a peptide-protein “ink” made of RGD peptide mixed 1:1 by mass with a fluorescently labeled antibody. The image shows 5 rectangular boxes of the DNG with a grid size of 1052 nm, 1171 nm, 1286 nm, 1397 nm and 1504 nm for boxes labeled 1 - 5, respectively. (b) AFM image of box 1. The image reveals the rugged shape of individual dots and features within the dot that delineates individual IgG proteins. The height of the dots was measured to be 5 nm on average. Scale bar for (a) is 3 μm and (b) 500 nm.

The nanodots were characterized using an AFM operated in tapping mode. The nanodots have rugged edges due to the globular nature of the proteins (**Figure 2-6b**). The diameter of the dots was established using an image recognition algorithm (“analyze particle” function in Image J, NIH) for 16 dots and found to be $210 \text{ nm} \pm 18 \text{ nm}$, thus closely matching the original design of 200 nm. Variability in dot size may be contributed by minor imprecision during replication, the finite size of proteins which may only partially contact the lift-off stamp at the edges and thus add to the variability, as well as lateral interactions between proteins that may entrain or restrain adjacent proteins. Dot size is however not expected to vary with the change in gradient density since proteins are adsorbed evenly on a flat surface and lifted off, and hence the pattern density is not apparent during the incubation and lift-off steps.

To test the bioactivity of the printed proteins and the utility of DNGs for cell biology, we first studied cellular migration on DNGs of RGD peptides. The amino acid sequence RGD is a binding site for transmembrane integrins that form a molecular link between the ECM and the cytoskeleton and is found in ECM proteins such as fibronectin[13] and laminin.[14] Surface gradients of laminin guide the migration of rat hippocampal neurons,[15] embryonic *Xenopus* spinal neurons[16] and rat intestinal IEC-6 cells,[17] while RGD peptides have been demonstrated to orient fibroblast migration.[18]

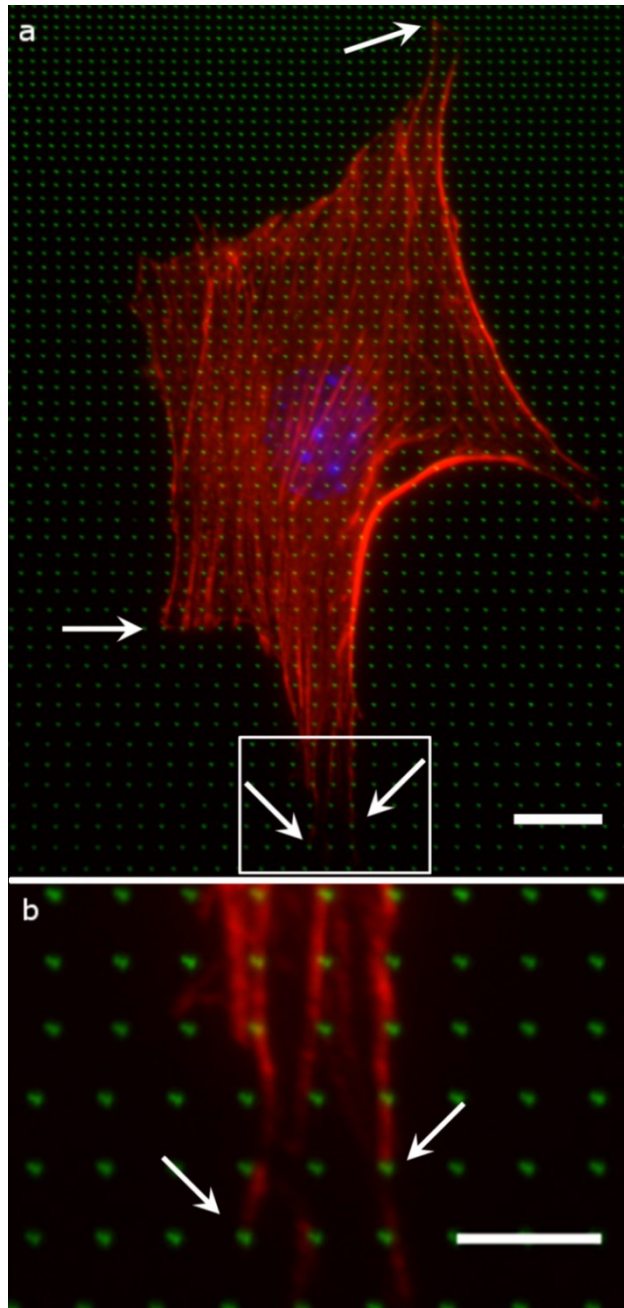


Figure 2-7. C2C12 myoblast cell on a DNG of RGD peptides. (a) Fluorescent micrograph of a DNG or RGD peptides mixed with fluorescent IgG (green dots) and a C2C12 cell grown for 18 h, fixed and stained to reveal actin filaments (red) and the cell nucleus (blue). (b) Close-up of the frame in (a) showing that actin filaments align with the nanodot patterns. Arrows indicate areas where cell shape or structures strikingly coincide with the nanodot pattern. Scale bar for (a) is 10 μm and (b) 5 μm .

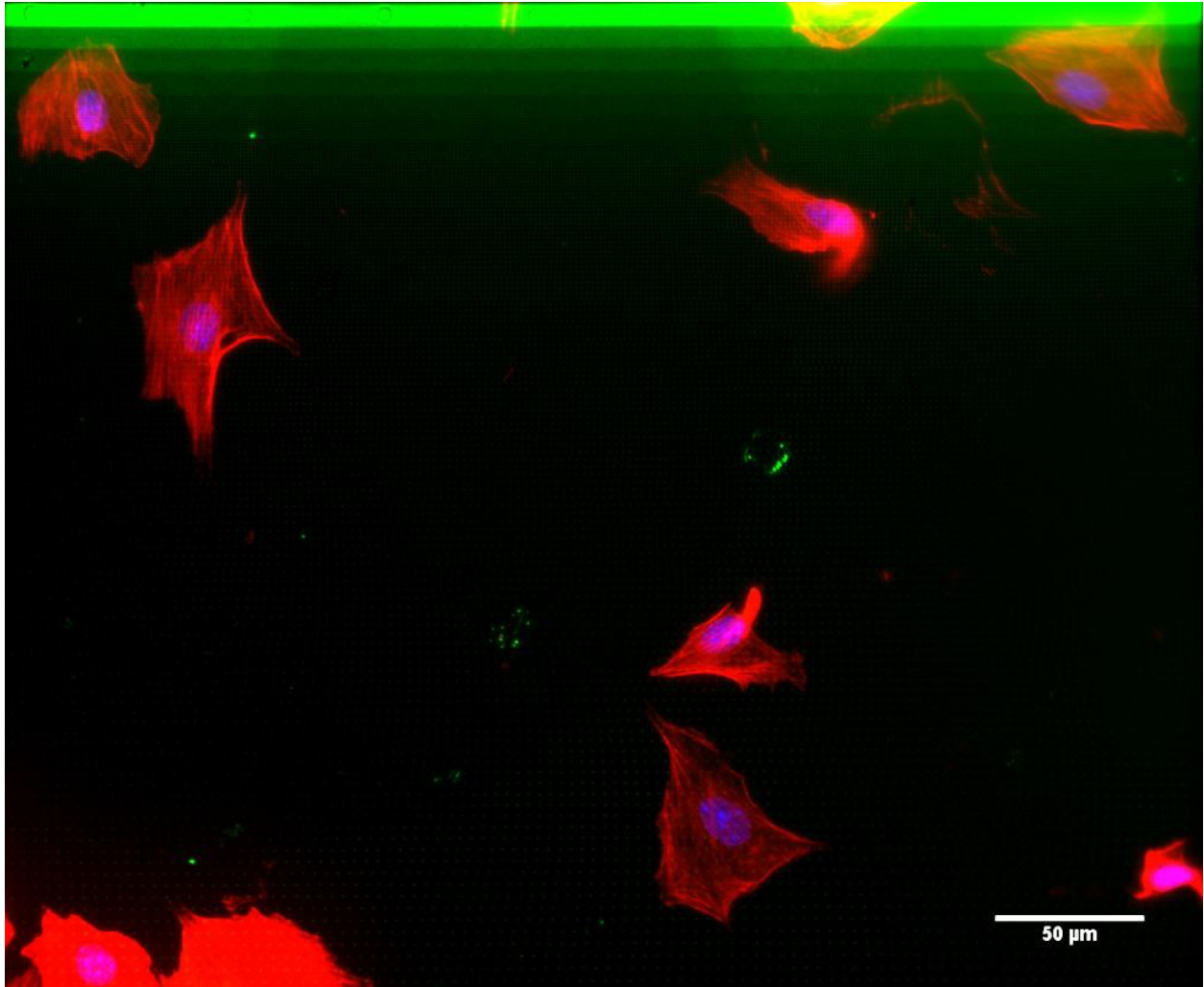


Figure 2-8. Cell response to a DNG of RGD peptides. Fluorescent micrograph of an entire DNG with C2C12 cells that were grown for 18 h, fixed and stained to reveal actin filaments (red) and cell nuclei (blue). The DNG is visible at the top (high density) because fluorescently labeled IgGs (green) were mixed with the RGD peptides; the gradient appears continuous at the top because the nanodot spacing is smaller than the resolution of the microscope.

DNGs of RGD peptides were patterned by lift-off nanocontact printing as described above. Next, a solution of 75% poly-L-lysine grafted with polyethylene glycol (PLL-g-PEG)[19, 20] and 25% Poly-d-lysine (PDL) by volume was applied to the coverslip to backfill the surface with an appropriate background for maximizing the cell response to the DNG (the development of this method and the rationale will be discussed in detail elsewhere). C2C12 myoblast cells were seeded on the coverslip and grown for 18 h. The response of C2C12 cells to DNGs was assessed

by fluorescence microscopy (**Figure 2-7 and 2-8**). C2C12 cells adhered to the surface, extended filopodia, and migrated along the gradient. Negative control experiments were performed by replacing the RGD peptide with Immunoglobulin G (IgG) proteins and lead to a loss of cell adhesion (**Figure 2-9**), thus confirming that cells specifically responded to the peptide. In order to show the generality of the method in terms of both patterning and applications, the protein netrin-1 was patterned as DNG to study cell haptotaxis [21] that is a chemoattractant for C2C12 myoblasts.[22] Cells were imaged 20 min after seeding immediately after attachment to the substrate and after 18 h. Whereas cells were initially distributed over the entire netrin-1 DNG, they were subsequently preferentially located in the high density area, **Figure 2-10a&b**. Cell haptotaxis on DNGs was quantified by recording cell distribution on 30 gradients in 8 separate experiments upon seeding and after 18 h of incubation, **Figure 2-10c**. Cells were distributed almost equally throughout the gradient initially, while 50% of the cells were localized within 30 μm of the highest density edge of the netrin-1 gradients. There were $n=133$, cells on the netrin-1 gradients at the beginning, and $n=68$ at the end of the experiment. Whereas we observed cells from the center of the gradient migrate in the direction of higher density, cells at the lower end migrated in all directions and many left the gradient into the relatively vast surrounding space. Additional experiments with live imaging to quantify cell responses to various gradient slopes and as a function of the initial position are in progress, but are beyond the scope of this manuscript and will be reported elsewhere. On control gradients composed of patterned IgG, the cells appeared randomly distributed at the beginning. At the end, relatively few cells remained on the gradients, but were randomly scattered throughout the gradient (**Figure 2-11**).

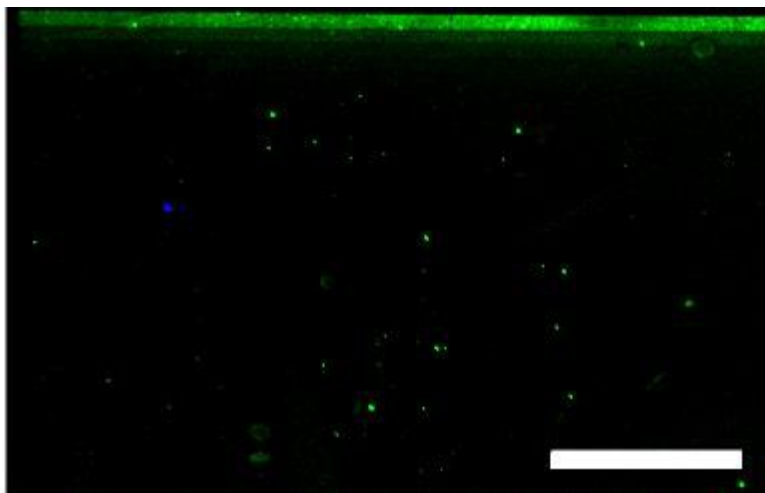


Figure 2-9. IgG DNG after seeding with cells and incubation. Fluorescent micrograph of a full IgG DNG that was seeded with C2C12 cells that were grown for 18 h, fixed and stained to reveal actin filaments (red) and cell nuclei (blue). The protocol used here was identical to the one used for RGD DNGs however due to the lack of cell adhesion on IgGs, the cells migrate outside of the patterned DNG region and were observed to migrate to the cell culture dish or to detach due to the lack of adhesion. The DNG is visible at the top (high density) because the patterned IgGs are fluorescently labeled (green). The DNG dots are not visible because the image was taken with a 10 × objective for easy cell quantification. Scale bar is 100 μm.

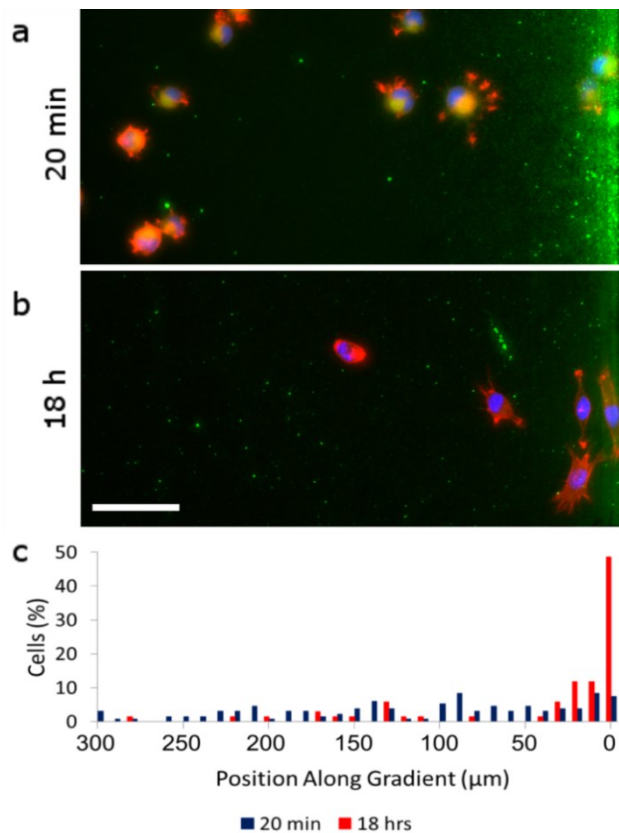


Figure 2-10. C2C12 myoblast migration on a netrin-1 DNG. Netrin-1 was mixed with fluorescent IgG (9:1 ratio) for visualization (green dots) and the C2C12 cells were fixed and stained to reveal actin filaments (red) and the cell nucleus (blue). C2C12 cells were seeded on the coverslip with the DNGs and one set fixed and imaged after (a) 20 min and the other after (b) 18 h. (c) Distribution of cells on 30 DNGs 20 min and 18 h after seeding. Over time, cells

accumulate at the top of the gradient where the density of dots is the highest ($p=1.89 \times 10^{-9} < 0.05$, netrin-1 start $n=133$, netrin-1 end $n=68$ in 9 separate experiments). Scale bar is 65 μm .



Figure 2-11. C2C12 myoblast migration on a negative control IgG DNG. C2C12 cells were grown on an IgG gradient and imaged 20 min and 18 h after seeding. The IgG was fluorescently labeled to identify the gradient, while the C2C12 cells were fixed and stained to reveal actin filaments and the cell nucleus. The distribution of cells found on 30 different gradients after seeding and after 18 h growth on IgG DNG's is shown. Over time, cells on the IgG gradient do not exhibit directed migration, however cells lack adhesion sites and as a result migrate away from the gradients resulting in a very low number of cells localized on gradients and analyzed despite analysis of 30 different gradients. ($p=0.29 > 0.05$, IgG start $n=51$, IgG end $n=6$ in 8 separate experiments).

2-4 Conclusions

In conclusion, we have developed a novel versatile, ultra low cost and massively parallel nanocontact printing process that can produce 100 nm features. The polymer masters are made by double replication of Si wafers and features replicated with ~ 30 nm accuracy, indicating that much higher resolution are feasible.[11] We developed protocols for printing DNGs of proteins covering large areas at a material cost of a few cents per gradient. The 7.6×10^6 dots of all gradients were printed in a 5 s lift-off step at a rate of 1.3×10^5 dots s^{-1} , which makes it one of the fastest nanopatterning methods; during the course of the optimization we estimate that we produced over 900 prints. The surface gradients presented here span a dynamic range of up to 3.6 OM, which is the highest reported to date and represents an 80 fold increase over previous digital gradients,[10] and represents the maximum for cell migration studies given the upper and lower

bounds. Smaller patterns and higher resolutions are readily achievable, and the dynamic range may thus be further expanded if desired. The biological relevance of DNGs was established by observing C2C12 mouse myoblasts spreading and migrating on DNGs of RGD peptides and netrin-1 protein, respectively. DNGs will be useful for studying how cells, including lymphocytes and neurons, respond to both attractive and repellent gradients while monitoring their response in real time. DNGs may also be combined with microfluidic devices[16] or microfluidic probes[23] to apply a combination of cues to cells. The implementation of DNGs for repulsive assays will be technically more challenging since cells will need to attach to the surface, and be precisely positioned at the high density portion of the gradient to reveal directed motion away from the cue. The low cost and ease-of-use of polymer nanocontact lift-off printing will allow its widespread adoption, including in laboratories without access to nanofabrication facilities, and routine use for a variety biological and medical applications.

2-5 Experimental Section

Preparation of Lift-off Stamps: A computer generated design of the DNGs with 200 nm dots was created in Clewin Pro 4.0 (Wieweb software, Hengelo, Netherlands). A 4" silicon wafer was coated with PMMA resist and the dot arrays patterned by electron beam lithography (VB6 UHR EWF, Vistec), followed by 100 nm reactive ion etching (System100 ICP380, Plasmalab) into the Si. After cleaning, the wafer was coated with an anti-adhesive layer by exposing it to Perfluorooctyltriethoxysilane (Sigma-Aldrich, Oakville, ON, Canada) in vapor phase in a desiccator. An accurate polymer copy of the Si wafer was obtained after double replication using poly(dimethylsiloxane) (PDMS) and a UV sensitive polyurethane (Figure 1).[24] Firstly, a ~ 6 mm layer of 1:10 PDMS (Dow Corning, Corning, NY, USA) was poured on the wafer inside a Petri dish, followed by removal of bubbles under vacuum in a desiccator for 10 min. Next, the PDMS was cured in an oven for 24 h at 60 °C (VWR, Montreal, QC, Canada), and then peeled off of the wafer. To remove un-crosslinked extractables, the PDMS replica was bathed in 70% ethanol for 24 h and then baked at 60°C for 4 h. Secondly, a large drop of UV sensitive polyurethane (Norland Optical Adhesive 63 (NOA); Norland Products, Cranbury, NJ) was poured on the PDMS and cured by exposing it to 600 W of UV light (Uvitron International, Inc., West Springfield, MA) for 50 s. The PDMS was then peeled off, thus yielding an NOA replica of the Si pattern.

Lift-off Microcontact Printing: A flat PDMS stamp cured against a Si wafer treated with a perfluorooctyltriethoxysilane anti-adhesive layer was used for lift-off nanocontact printing against the NOA replicas – now serving as master - with 200 nm holes. Following removal of the extractables as described above, the flat PDMS stamp was inked with a 10 μ drop of phosphate buffered saline solution (PBS) containing either 25 μ g/ml of the Arginine-Glycine-Aspartic acid (RGD) peptide (CHI Scientific Inc., Maynard, MA) or 25 μ g/ml of netrin-1 (12.5 μ g/ml, produced and purified as described [25, 26]), both mixed with 25 μ g/ml of chicken immunoglobulin G (IgG) conjugated to Alexa Fluor 488 (Invitrogen, Burlington, ON, Canada) for visualization or IgG alone for the negative control experiments. A plasma activated hydrophilic coverslip was then placed on the drop to spread the solution evenly on the surface of the hydrophobic PDMS stamp during a 5 min incubation period. After rinsing with PBS and double distilled water for 30 s, the inked stamps were briefly dried under a stream of N₂ and immediately brought into contact with a plasma activated (Plasmaline 415, Tegal, Petaluma, CA, USA) NOA master for 5 s. The PDMS was separated and the proteins in the contact areas were transferred to the NOA, while the remaining proteins transferred to the final substrate by printing the PDMS stamp for 5 s onto a plasma activated glass coverslip.

Cell Culture: Patterned RGD DNGs used in our experiments were backfilled by coating the areas between the nanodots with a solution composed of 75% poly-L-lysine (PLL) conjugated with polyethylene glycol (PEG) (PLL(20)-g[3.5]-PEG[2], Surface Solutions, Grande Prairie, AB, Canada)[27, 28] and 25% poly-D-lysine (PDL, 70-150 kDa, Sigma-Aldrich, Oakville, ON, Canada) by volume, which was done by incubating the coverslip with the mixture at a concentration of 10 μ g/ml. We seeded 50,000 C2C12 myoblast cells per coverslip and grew them on the patterned substrate for 18 h at 37°C in 5% CO₂ in high glucose DMEM, 10% Fetal Bovine Serum and 1% Penicillin/Streptomycin (all from Invitrogen) growth media. Cells were fixed after 18 h of growth with 4% paraformaldehyde for 1 min, permeabilized with triton-X 100 for 5 min and blocked with Horse Serum for 1 h. C2C12 myoblasts were labeled with phalloidin conjugated to Alexa Fluor 555 (1:250, Invitrogen, Burlington, ON, Canada) and with Hoechst stain (1:10,000, Invitrogen, Burlington, ON, Canada). Protein dots were colocalized with a secondary chicken anti-goat antibody conjugated to Alexa Fluor 488 (polyclonal, 1:20, Invitrogen, Burlington, ON, Canada).

Imaging: Images of the original Si master, and the intermediate and final replicates were collected using scanning electron microscopy (SEM, Hitachi, Mississauga, ON) and Atomic Force Microscopy (AFM, Asylum Research, Santa Barbara, CA). DNGs of fluorescent IgG and C2C12 myoblasts grown on the DNGs were imaged by fluorescence microscopy (TE2000, Nikon). The location of fixed cells was determined by the center of the nucleus of the stained cells. Their position on the gradient was measured from the edge of the gradient at the highest density.

2-6 References

1. Sassolas, A.; Leca-Bouvier, B. D.; Blum, L. J., *Chemical Reviews* **2007**, *108* (1), 109-139. DOI 10.1021/cr0684467.
2. Blawas, A. S.; Reichert, W. M., *Biomaterials* **1998**, *19* (7-9), 595-609. DOI 10.1016/s0142-9612(97)00218-4.
3. Delaney, J. T.; Smith, P. J.; Schubert, U. S., *Soft Matter* **2009**, *5* (24), 4866-4877.
4. Perl, A.; Reinhoudt, D. N.; Huskens, J., *Adv Mater* **2009**, *21* (22), 2257-2268. DOI DOI 10.1002/adma.200801864.
5. Piner, R. D.; Zhu, J.; Xu, F.; Hong, S.; Mirkin, C. A., *Science* **1999**, *283* (5402), 661-663. DOI 10.1126/science.283.5402.661.
6. Zheng, Z.; Daniel, W. L.; Giam, L. R.; Huo, F.; Senesi, A. J.; Zheng, G.; Mirkin, C. A., *Angewandte Chemie International Edition* **2009**, *48* (41), 7626-7629. DOI 10.1002/anie.200902649.
7. Huang, M.; Galarreta, B. C.; Artar, A.; Adato, R.; Aksu, S.; Altug, H., *Nano Lett* **2012**, *12* (9), 4817-4822. DOI 10.1021/nl302266u.
8. Renault, J.; Bernard, A.; Juncker, D.; Michel, B.; Bosshard, H.; Delamarche, E., *Angewandte Chemie* **2002**, *114* (13), 2426-2429.
9. Liao, W.-S.; Cheunkar, S.; Cao, H. H.; Bednar, H. R.; Weiss, P. S.; Andrews, A. M., *Science* **2012**, *337* (6101), 1517-1521. DOI 10.1126/science.1221774.
10. Coyer, S. R.; Garcia, A. J.; Delamarche, E., *Angew Chem Int Edit* **2007**, *46* (36), 6837-6840. DOI DOI 10.1002/anie.200700989.
11. Xia, Y. N.; McClelland, J. J.; Gupta, R.; Qin, D.; Zhao, X. M.; Sohn, L. L.; Celotta, R. J.; Whitesides, G. M., *Adv Mater* **1997**, *9* (2), 147-149.

12. Geiger, B.; Spatz, J. P.; Bershadsky, A. D., *Nat Rev Mol Cell Bio* **2009**, *10* (1), 21-33. DOI Doi 10.1038/Nrm2593.
13. Linask, K.; Lash, J., *Dev Biol* **1986**, *114* (1), 87-101.
14. McCarthy, J.; Palm, S.; Furcht, L., *The Journal of Cell Biology* **1983**, *97* (3), 772.
15. Dertinger, S.; Jiang, X.; Li, Z.; Murthy, V.; Whitesides, G., *P Natl Acad Sci USA* **2002**, *99* (20), 12542.
16. Wang, C. J.; Li, X.; Lin, B.; Shim, S.; Ming, G. L.; Levchenko, A., *Lab Chip* **2008**, *8* (2), 227-237. DOI Doi 10.1039/B713945d.
17. Gunawan, R. C.; Silvestre, J.; Gaskins, H. R.; Kenis, P. J. A.; Leckband, D. E., *Langmuir* **2006**, *22* (9), 4250-4258. DOI 10.1021/la0531493.
18. Kang, C. E.; Gemeinhart, E. J.; Gemeinhart, R. A., *Journal of Biomedical Materials Research Part A* **2004**, *71A* (3), 403-411. DOI 10.1002/jbm.a.30137.
19. Saravia, V.; Küpcü, S.; Nolte, M.; Huber, C.; Pum, D.; Fery, A.; Sleytr, U.; Toca-Herrera, J., *Journal of biotechnology* **2007**, *130* (3), 247-252.
20. Senaratne, W.; Sengupta, P.; Harnett, C.; Craighead, H.; Baird, B.; Ober, C., *NanoBioTechnology* **2005**, *1* (1), 23-33. DOI 10.1385/nbt:1:1:023.
21. Sun, K. L. W.; Correia, J. P.; Kennedy, T. E., *Development* **2011**, *138* (11), 2153-2169. DOI 10.1242/dev.044529.
22. Kang, J.-S.; Yi, M.-J.; Zhang, W.; Feinleib, J. L.; Cole, F.; Krauss, R. S., *The Journal of Cell Biology* **2004**, *167* (3), 493-504. DOI 10.1083/jcb.200405039.
23. Qasaimeh, M. A.; Ricoult, S. G.; Juncker, D., *Lab on a Chip* **2013**.
24. Xia, Y. N.; McClelland, J. J.; Gupta, R.; Qin, D.; Zhao, X. M.; Sohn, L. L.; Celotta, R. J.; Whitesides, G. M., *Adv. Mater.* **1997**, *9* (2), 147-149.
25. Serafini, T.; Kennedy, T. E.; Galko, M. J.; Mirzayan, C.; Jessell, T. M.; Tessierlavigne, M., *Cell* **1994**, *78* (3), 409-424.
26. Shirasaki, R.; Mirzayan, C.; TessierLavigne, M.; Murakami, F., *Neuron* **1996**, *17* (6), 1079-1088.
27. Saravia, V.; Küpcü, S.; Nolte, M.; Huber, C.; Pum, D.; Fery, A.; Sleytr, U.; Toca-Herrera, J., *J Biotech* **2007**, *130* (3), 247-252.
28. Senaratne, W.; Sengupta, P.; Harnett, C.; Craighead, H.; Baird, B.; Ober, C., *J Nanobiotechnology* **2005**, *1* (1), 23-33. DOI 10.1385/nbt:1:1:023.

PREFACE TO CHAPTER 3

In the previous chapter, we presented a low-cost lift-off nanocontact printing method where protein nanodots as small as 100 nm in diameter can be printed rapidly and in a high throughput format. We then designed digital nanodot gradients (DNGs) where the spacing between nanodots is increased from 0 nm to 12 μm in X and Y direction, resulting in an unprecedented dynamic range of 3.6 orders of magnitude. The reported method renders controlled protein nanopatterning accessible to the general scientific community for the first time and the patterning of DNGs enables in depth haptotaxis studies (Chapter 2).

In the following chapter, we investigate the impact of the non-patterned surface, or the reference surface (RS), on cell response to the printed protein patterns. It has long been understood that this experimental parameter critically impacts the cell response, but its extent has thus far never been characterized. Furthermore an easy and universal approach to control the RS in substrate-bound experiments is desirable.

To create RSs of different affinities we developed an approach whereby we mix two solutions – one of high affinity and one of low affinity – to identify an RS of intermediate affinity at which cells respond to the patterned protein through specific biochemical pathways. We then present cell-surface affinity curves, which graphically present cell response to a printed protein in the context of the RS.

This chapter was published as a research article in *Biomaterials* (Ricoult et al., 2014).

Acknowledgements

We acknowledge support from CIHR (Regenerative and Nanomedicine grant), the Canadian Foundation for Innovation and the McGill Nanotools Microfabrication Laboratory (funded by CFI and McGill University). Some images were collected in the McGill University Life Sciences Complex Imaging Facility. Purchase of equipment in the facility was made possible with funding from the Canadian Foundation for Innovation (CFI) and the Ministère du Développement Économique, Innovation et Exportation Québec (MDEIE). SGR and GTS were supported by the Integrated Sensor System NSERC program and SGR and JPC were also supported by the

Neuroengineering program funded by CIHR and The Molson Foundation. TEK holds a Killam Foundation Scholar award and a Chercheur National award from the Fonds de la Recherche en Santé du Québec. DJ holds a Canada Research Chair.

CHAPTER 3

Tuning Cell-Surface Affinity to Direct Cell Specific Responses to Patterned Proteins

Sébastien G. Ricoult^{1,2,3,‡}, Greta Thompson-Steckel^{1,2,3,‡}, James P. Correia³, Timothy E. Kennedy³ and David Juncker^{1,2,3}

¹McGill Program in NeuroEngineering, Department of Biomedical Engineering, McGill University, 740 Dr. Penfield Avenue, Montreal, Quebec H3A 0G1, Canada; ²Genome Quebec Innovation Centre, McGill University, Montréal, Quebec H3A 0G1, Canada; ³McGill Program in NeuroEngineering, Department of Neurology and Neurosurgery, Montreal Neurological Institute, McGill University, 3801 University Ave., Montreal, Quebec H3A 2B4, Canada; [‡]SGR and GTS contributed equally.

3-1 Abstract

Interactions with local extracellular cues direct cell migration. A versatile method to study cell response to a protein consists of patterning the protein cue on a substrate and quantifying the distribution of cells between patterned and non-patterned areas. Here, we define the concepts of (i) cell-surface affinity to describe cell choices, and of (ii) reference surface (RS) to clarify that the choice is made relative to a reference. Furthermore, we report a method to systematically tune the RS and show that it can dominate the experimental cell response to a protein cue. The cell response to a cue can be switched from strong preference to strong aversion by only changing the RS. Using microcontact printing, we patterned the extracellular matrix proteins fibronectin or netrin-1 adjacent to a series of RSs with different ratios of poly-D-lysine (PDL) and polyethylene glycol (PEG), which are of high affinity and of low-affinity for cells, respectively. C2C12 myoblasts or primary neurons seeded on substrates with a high affinity RS (high % PDL) did not respond to a printed protein of interest, and conversely on RSs of low affinity (high % PEG) the cells preferred the printed protein even in the absence of a specific interaction. However, when testing cell response to a standardized series of RSs varying from high to low affinity, a specific response curve was obtained that was unique to each cell type–protein pair. Importantly, for intermediate RSs with moderate affinity, the cell response to the

cue was dependent on the activation of biologically relevant protein-specific biochemical signal transduction pathways. Our results establish that choices made by cells in response to a surface bound cue must take into account, and be interpreted in the context of, the RS. The use of a series of RSs with varying cell-surface affinity reveals specific response curves of cells to a cue that can be compared quantitatively, and that may help gain new insights into cellular responses to extracellular proteins.

3-2 Introduction

Cell migration *in vivo* is a complex process in which multiple extracellular cues may be integrated to evoke a cellular response (Ridley, Schwartz et al. 2003). Interactions with cues surrounding the cell activate signaling pathways that regulate adhesion and migration (Hood and Cheresh 2002). Adhesion is essential for many forms of cell migration and is regulated through transmembrane adhesion proteins that bind to ligands presented on cell surfaces or components of the extracellular matrix (ECM), such as fibronectin and laminins (Larsen, Artym et al. 2006). Contact-mediated adhesion and signaling trigger the assembly of intracellular macromolecular complexes around the site of adhesion that transmit both mechanical force and regulatory signals to the cytoskeleton (Geiger, Spatz et al. 2009). Using similar mechanisms, gradients of secreted chemotropic guidance cues like netrin-1 (Kennedy, Serafini et al. 1994) promote directional cell migration, in part through a mechanism dependent on cell-substrate adhesion (Moore, Correia et al. 2008).

In order to study the mechanisms involved in contact-mediated cell responses, *in vitro* assays have been developed that employ patterned substrate-bound proteins to challenge cells with precise spatial distributions of molecular cues (Falconnet, Csucs et al. 2006; Ricoult, Goldman et al. 2012). While these assays fall short of duplicating the complexity of the *in vivo* environment, they can succeed in isolating the influence of one or a limited number of extracellular cues (Roy, Kennedy et al. 2013). Cells preferentially attach and migrate onto surfaces due to a combination of differential adhesion and signal transduction mechanisms that reorganize the cytoskeleton (Lauffenburger and Horwitz 1996). While the strength of the adhesive interaction plays an important role, cells sometimes prefer a less adhesive surface. Laminin-1, for example, was shown to be less adhesive than fibronectin, but cells subjected to a choice assay between both surfaces preferably moved onto the laminin pattern (Calof and Lander 1991). Thus, in consideration that higher adhesion does not always equate preference, we use the purely descriptive term "cell-surface affinity" which characterizes the interaction free of mechanistic assumptions. Although this term had been used previously in the context of cell choice assays for neurons between two surfaces, neither the meaning nor the underlying concept were well-defined, and its functional significance has not been investigated relative to the contiguous surface (Vielmetter, Stolze et al. 1990; Lemmon, Burden et al. 1992; Fereol, Fodil et al. 2009; Fereol, Fodil et al. 2011).

In addition to affinity, we introduce the concept of a reference surface (RS) and report a method to tune the cell-surface affinity of the RS. The surface contiguous to a patterned protein has a widely accepted but rarely discussed role in the responses cells make to patterned protein substrates. **Figure 3-1** shows that the cell response can be switched from strong affinity to strong aversion simply by tuning the RS.

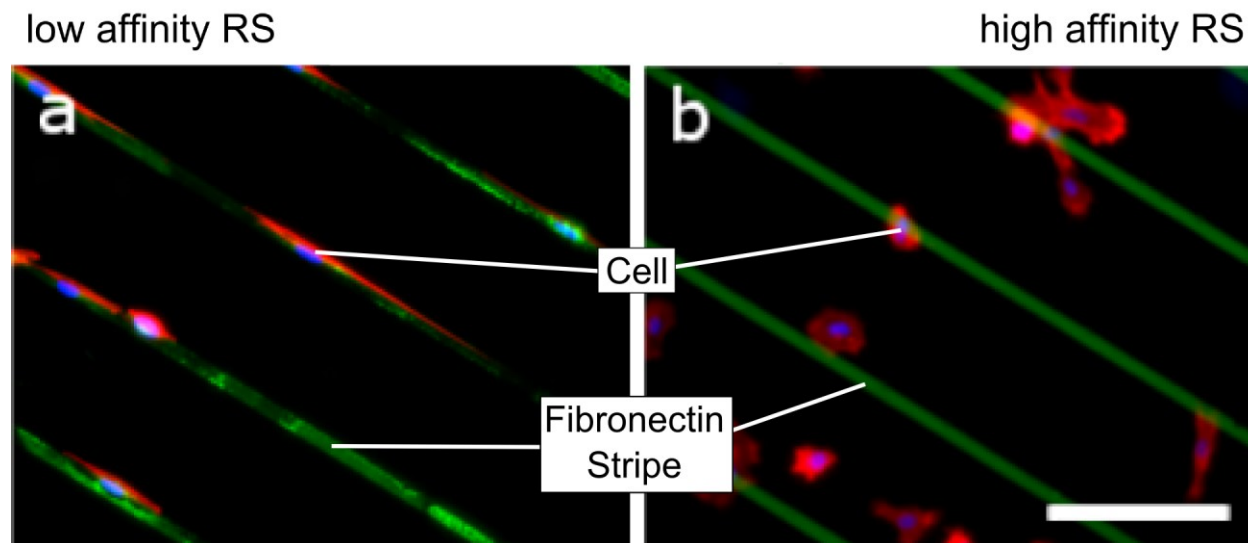


Figure 3-1. Cell response to fibronectin stripes on a RS with high affinity (typically adhesive) or low affinity (typically non-adhesive). Illustrative images of Rat2 fibroblasts responding to stripes of substrate-bound fibronectin protein (green) showing the differences in cell response obtained by altering the RS to widely different levels of cell-surface affinity. Cells were stained with phalloidin to visualize F-actin (red) and Hoechst to label nuclei (blue). (a) On non-adhesive RSs, cells preferentially stick to the cue lines whereas (b) on adhesive surfaces they stick to the RS. Scale bar is 100 μm .

Whereas it is expected that the cell response depends on the RS, many manuscripts fail to report the composition of the RS or how it was produced (Vogt, Stefani et al. 2004). Although its importance has not been broadly recognized, the RS should be considered as it will help to qualify the findings, compare studies conducted in different laboratories, and account for discrepancies. Despite cells typically having a low affinity for untreated glass or polystyrene, and therefore preferentially adhere to almost any protein substrate (Curtis, Forrester et al. 1983), such RSs have often been used in studies of cell migration. For example, a polystyrene RS was used to examine the response of neurons to a patterned grid of the laminin peptide IKVAV (Adams,

Kao et al. 2005)., To better control the RS, cell culture surfaces are thus often coated with poly-D-lysine (PDL) (Oliva, James et al. 2003) and polyethylene glycol (PEG) (Zhang, Desai et al. 1998; They, Racine et al. 2005; Saravia, Kupcu et al. 2007) that are known for their very high and very low affinity to cells, respectively. For example, an RS of polylysine was used to investigate neurite preference between laminin and fibronectin in a juxtaposed stripe assay and migration on substrate-bound netrin-1 gradients (Evans, Euteneuer et al. 2007; Mai, Fok et al. 2009). Conversely, an RS made of PEG was used to investigate neurite outgrowth on patterns of RGD peptide and fibronectin (Zhang, Yoo et al. 2005). In these two studies, since one of the surfaces had a high affinity and the other a low affinity, one might expect that the RS could influence the outcome and the conclusions made. Another study, which examined the capacity of melanoma cells to form sites of adhesion on geometric arrangements of fibronectin and vitronectin surface-bound dots, used a RS formed of hydrophilic alkanethiols that may act as a cell repellent, akin to glass (Lehnert, Wehrle-Haller et al. 2004). Another case had EphrinA5 gradients formed with an RS of perpendicular laminin tracks (a high affinity surface) to demonstrate repulsion of RGD neurons (von Philipsborn, Lang et al. 2006). Increasing concentrations of EphrinA5 would be expected to mask the laminin, an effect that may have contributed to responses that were solely attributed to EphrinA5. The absence of understanding and control of the RS may have confounded the design and conclusions of certain studies in more subtle ways as well. For example, Evans *et al.* used microchannels to flow different concentrations of fibronectin and laminin to form stripes on a substrate, followed by backfilling with a fixed concentration of Poly-l-lysine (PLL), in effect serving as the RS (Evans, Euteneuer et al. 2007). The higher affinity of the neurons for PLL may have masked their response to fibronectin and laminin, and the use of a RS with a high affinity may have prevented the use of lower concentrations of fibronectin and laminin, which may have led to a stronger differential response and a more convincing result.

Here, in addition to clarifying and formally defining the concepts of cell-surface affinity and RS, we also present a novel standardized protocol to tune the RS by using mixtures of PDL (high affinity) and PLL-g-PEG (low affinity, named PEG hereafter for brevity) with varying ratios of %PEG:%PDL ranging from 0:100 (highest affinity) to 100:0 (lowest affinity). We tested the set of RSs in a stripe assay (Knoll, Weigl et al. 2007) with lines of either fibronectin or netrin-1 patterned using microcontact printing (von Philipsborn, Lang et al. 2006) surrounded by

a specific %PEG:%PDL ratio in each experiment. We characterized the adhesion, spreading, migration and focal adhesions of cells on various RSs, and observed that for intermediate cell-surface affinity of the RS, both migratory and polarized cells (*i.e.* neurons) respond in a physiologically appropriate manner to the patterned surface-bound proteins. For extreme affinity values, *e.g.* highest and lowest affinity, cells universally adhere to or avoid the patterned protein cues, respectively, indicating that the RS dominates the response and has the capacity to mask specific cellular responses. It follows that optimal RS composition can be selected to maximize the capacity of a particular cell type to respond to a printed protein of interest via ligand-receptor interactions. A graphical representation of the cell response to a protein as function of the RSs yielded an affinity “binding curve” that was specific for each cell and each surface. This affinity curve not only constitutes a quantitative and reproducible way of characterizing the cell response to a cue, but also creates new defined parameters for measuring cellular responses including magnitude, range and slope of the response.

3-3 Materials and Methods

Microcontact printing: A pattern of stripes of 10 μm width and 100 μm spacing was produced using Clewin Pro 4.0 (Wieweb software, Hengelo, Netherlands). A 4” silicon wafer (University Wafers, Boston, MA, USA) was coated with a layer of SU-8 photoresist (Microchem, Newton, MA, USA), and stripe arrays patterned using photolithography. After baking and cleaning, the wafer was coated with an anti-adhesive layer by exposing it to Perfluorooctyltriethoxysilane (Sigma-Aldrich, Oakville, ON, Canada) in vapor phase in a desiccator. To obtain flat stamps, a native Si wafer was employed. Stamps bearing an inverse copy of the pattern on the Si wafer were obtained by pouring 10:1 poly(dimethylsiloxane) (PDMS) onto the wafer and curing the polymer for 6 h at 60°C. The stamps were then cut and cleaned in 70 % Ethanol for 6 h and baked for 1 h at 60°C to evaporate all traces of solvent. The stamps were then ultrasonicated for 5 min in 70% Ethanol prior to the experiment and dried using compressed N₂. After drying, stamps were inked for 5 min onto a plasma activated coverslip coated with 10 μl of either poly-D-lysine (5 $\mu\text{g/ml}$, PDL, 70-150 kDa, Sigma-Aldrich, Oakville, ON, Canada), fibronectin (25 $\mu\text{g/ml}$, mouse, Biopur, Bubendorf, Switzerland) fluorescently labeled IgG (25 $\mu\text{g/ml}$, chicken, Invitrogen, Burlington, ON, Canada), or netrin-1 (12.5 $\mu\text{g/ml}$, produced and purified as described (Serafini, Kennedy et al. 1994; Shirasaki, Mirzayan et al. 1996)). A fluorescent secondary IgG was mixed into the protein ink as a fiducial marker to facilitate the localization of

the stripes. Stamps were then rinsed with 1x PBS and ddH₂O for 10 s each before being rapidly dried with a strong pulse of N₂ gas and contacted for 5 s with plasma activated coverslips to transfer the protein.

Backfilling: To create the different RSs, various ratios based on % volumes of poly-L-lysine grafted polyethylene glycol (10 µg/ml, PLL(20 KDa)-g[3.5]-PEG(2 KDa), abbreviated as PEG), Surface Solutions, Dübendorf, Switzerland) and poly-D-lysine (10 µg/ml, PDL, 70-150 kDa, Sigma-Aldrich, Oakville, ON, Canada) were incubated on the coverslip on a rocking plate for 15 min before washing off unbound PEG and PDL with 1xPBS.

Cell culture: C2C12 myoblasts and Rat2 fibroblasts were seeded at a concentration of 50,000 cells per coverslip and grown at 37°C in 5% CO₂ for 6 h in neurobasal media (Invitrogen, Burlington, ON, Canada), 1% B27 (Invitrogen, Burlington, ON, Canada), 0.5% N2 (Invitrogen, Burlington, ON, Canada), 1% Penn/Strep (Invitrogen, Burlington, ON, Canada), 0.2% Fungizone (Invitrogen, Burlington, ON, Canada) and 0.25% L-glutamine (Invitrogen, Burlington, ON, Canada). Embryonic rat spinal commissural neurons were isolated and cultured as described (Moore and Kennedy 2001), seeded at 50,000 cells per coverslip, and grown at 37°C in 5% CO₂ for 2 DIV in neurobasal media. In function blocking experiments, cells were exposed to the following inhibitors: function blocking monoclonal antibody against DCC (2 µg/ml), or the src family kinase inhibitor PP2 (2 µM) and its inactive analogue PP3 (2 µM), when the cells were seeded on the patterned substrates.

Immunocytochemistry: Cells were fixed with 4% paraformaldehyde (PFA) for 1 min, permeabilized with 0.1% triton-X 100 for 5 min and blocked with 5% milk overnight at 4°C. Cells were labeled with phalloidin conjugated to Alexa Fluor 555 (1:250, Invitrogen, Burlington, ON, Canada) and with Hoechst dye (1:10,000, Invitrogen, Burlington, ON, Canada). Protein stripes were mixed with a secondary chicken anti-goat antibody conjugated to Alexa Fluor 488 (polyclonal, 1:20, Invitrogen, Burlington, ON, Canada). C2C12 myoblasts in focal adhesion assays were immunolabelled for paxillin (monoclonal, 1:500, BD biosciences, Franklin Lakes, NJ, USA) detected with a secondary fluorescent goat anti-mouse antibody conjugated to Alexa Fluor 488 (polyclonal, 1:500, Invitrogen, Burlington, ON, Canada).

Imaging: Standard epifluorescence microscopy was performed using a 20× objective on a TE 2000 inverted fluorescence microscope (Nikon, Saint-Laurent, QC, Canada). Confocal microscopy was conducted on a LSM 710 using a 1.4 n.a. 100× oil immersion objective (Carl

Zeiss, Toronto, ON, Canada). Live imaging time-lapse studies were conducted on an Axiovert 200M (Carl Zeiss, Toronto, ON, Canada) using phase contrast optics, with images captured at 10 min intervals for 6 h and analyzed with MtrackJ (Meijering, Dzyubachyk et al. 2012).

Quantification of Cells on Printed Stripes: Non polar C2C12 myoblasts and Rat2 fibroblasts were characterized as on or off a stripe based on the overlap of the visualized F-actin cytoskeleton with the stripe. If more than half the cell was localized on the stripe, the cell was deemed to be “on” the stripe, whereas if more than half of the cell was off the stripe, the cell was “off” the stripe. Clusters of two or more cells were excluded from the analysis (**Figure 3-2**). Control studies to determine random cell response values were conducted on PDL coated coverslips.

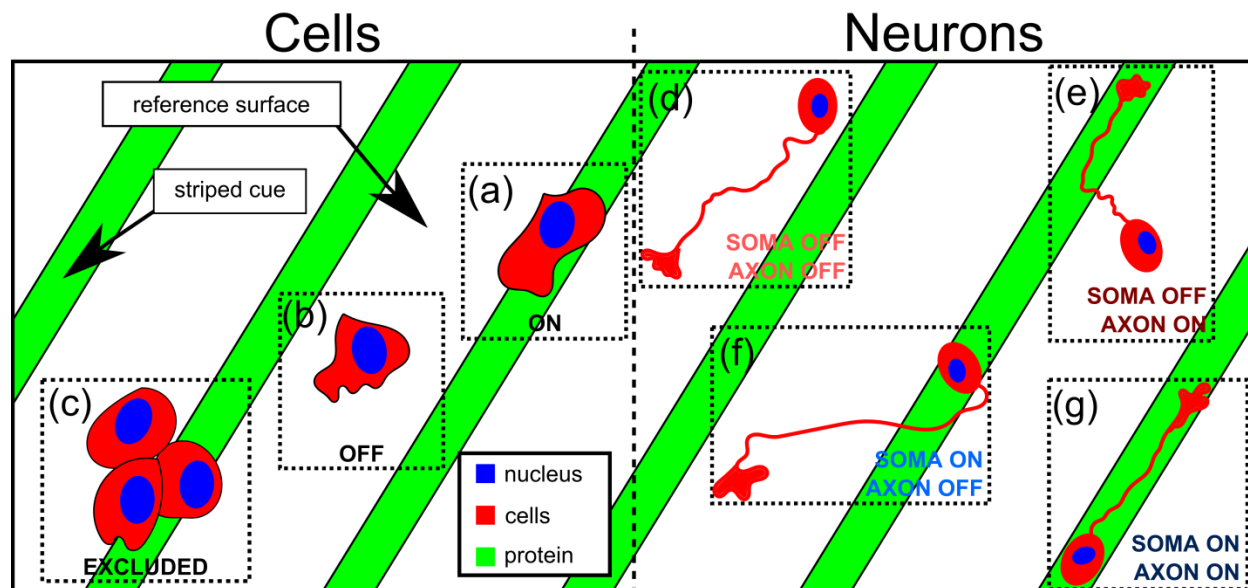


Figure 3-2. Schematic of cell responses to a patterned cue and description of how cell distribution was quantified. The schematic demonstrates the various cell responses (red blobs with blue nuclei) to a patterned striped cue (green) and a reference surface (RS) (white). (a) A representative image of a cell that is considered to be on the stripe, and (b) of a cell counted as being on the RS, while (c) cell clusters and ambiguous cells are eliminated from the count. In studies with polarized primary cells such as neurons, both the positions of the cell soma and of the axon tip were recorded. Thus cells were classified according to combinatorial possibilities: (d) soma off/ axon off, (e) soma off/axon on, (f) soma on/axon off, and (g) soma on/axon on.

3-4 Results

3-4.1 Tuning the cell-surface affinity of the RS by changing its composition

To investigate the functional significance of the RS, the substrate contiguous to the microcontact printed proteins, we developed a method to systematically vary its affinity by mixing different ratios of PDL and PEG, which are known to be high-affinity and low-affinity substrates, respectively. Mixtures of PEG and PDL solutions were incubated on glass coverslips to produce RSs with intermediate levels of affinity. RSs composed of increasingly higher ratios of PEG:PDL (100:0, 95:5, 90:10, 75:25, 50:50, 0:100; all corresponding to the %PEG:%PDL) were tested. Considering that PEG is in fact a PEG-PDL molecule, and that the surface adsorption is driven by the PDL moiety, we expected that the surface coverage would closely match the PEG:PDL ratio in solution. This hypothesis was confirmed experimentally by measuring the adsorption of fluorescently labeled PDL and PEG for various ratios of PEG:PDL (**Figure 4-3**).

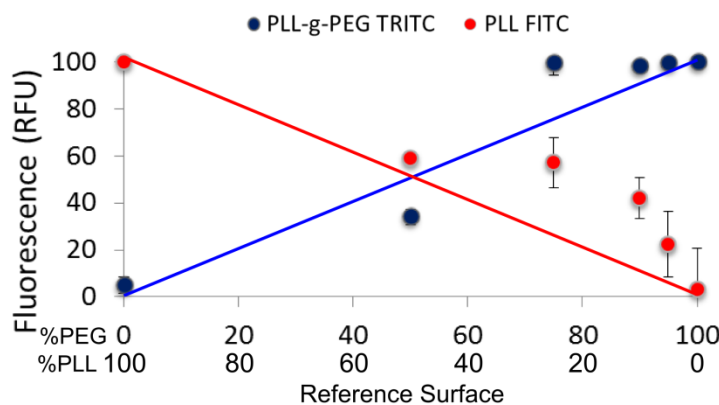


Figure 3-3. Fluorescent characterization of the reference surfaces. Fluorescence quantification of PDL and PLL-g-PEG determined by incubating FITC-PLL with non-fluorescently-labeled PLL-g-PEG and PLL-g-PEG- TRITC with PLL at the different ratios investigated. (n=3, mean \pm standard error). Lines represent the expected fluorescence levels. The non-linearity of the data points can be attributed to the method of quantification where photobleaching of the fluorophores or background fluorescence from the surface are likely present. Despite the variations in the characterization, the trend can successfully be confirmed with this approach.

3-4.2 Cell adhesion, spreading, and motility in response to RS composition

First, uniform substrates of RS were formed and cells were then plated. These tests and subsequent ones were performed in parallel using a multi-well format with a coverslip of a particular RS in each well (**Figure 3-4**). Depending on the composition of the RS, the number of adhered myoblast or fibroblast cells following a wash could be readily manipulated (**Figure 3-5a**). The numbers of cells that adhered to RSs of high PDL content and high-affinity were comparable to those of cells plated on fibronectin surfaces. Adherent cells also differed in the extent that they spread on these surfaces; on high PEG content and low-affinity surfaces, cells spread minimally, while cells on high-affinity surfaces increased their average surface area up to 4 to 5 fold (**Figure 3-5b**). Cell motility was strongly affected by cell-surface affinity. Cells grown on surfaces predicted to have either very high or very low-affinity had the slowest speeds. RS surfaces with predicted intermediate affinity resulted in the highest rates of cell migration (**Figure 3-5c**). These results are consistent with other studies and reflect that migration requires both sufficient adhesion at the migration front for cells to pull, which is not possible on low affinity surfaces, as well as a way to detach the back of the cell from the surface it is residing on, which is inhibited on the high affinity surfaces.

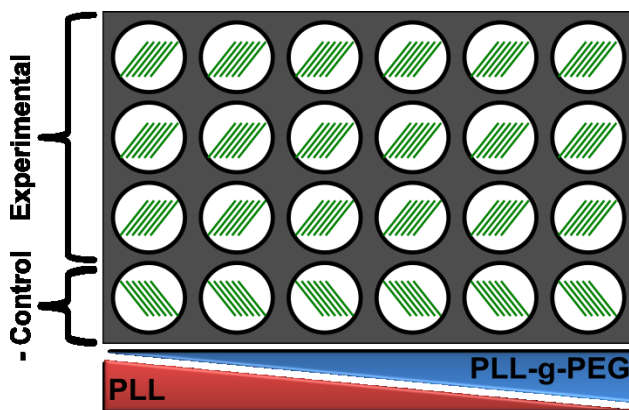


Figure 3-4. Schematic of the assay format. A 24-well plate illustrating microcontact printed stripe patterns on 18 coverslips of the experimental protein and 6 of the negative control, backfilled with various RS mixtures of low affinity PEG and high affinity PDL at different ratios across the plate.

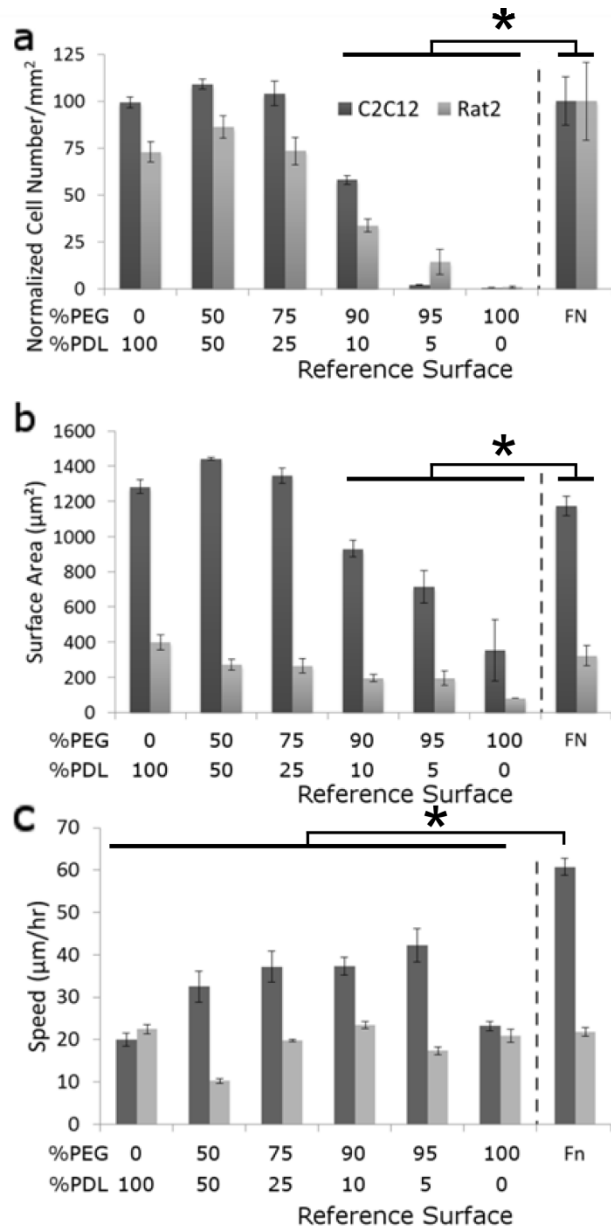


Figure 3-5. Tuning cell-surface affinity to alter cell adhesion, spreading and motility.

C2C12 myoblasts (dark grey) and Rat2 fibroblasts (light grey) were grown on the different substrates. Quantification of (a) cell number indicates that both cell types follow a similar trend where in the presence of 0:100 to 75:25 RSs, there was no significant difference in comparison to the cell numbers on fibronectin surfaces. A sharp decrease in cell numbers occurred at 90:10 and continued to 100:0 where less than 1% of the seeded cells remain after 16 hours of growth. Cell numbers were normalized to the number of cells on the fibronectin surface. Fewer cells were present on the 90:10, 95:5, and 100:0 RSs in comparison to cells plated on fibronectin surfaces for C2C12 myoblasts and Rat2 fibroblasts (b) Cell spreading followed the same trend

observed with cell numbers and cells on the same RSs as the cell number comparison were shown to be significantly smaller than on fibronectin surfaces for Rat 2 fibroblasts and C2C12 myoblasts. (c) The speed of cell migration was also investigated for C2C12 myoblasts and Rat2 fibroblasts over 6 hours on the different surfaces and the speed of cells was shown to be statistically slower on all the RSs when compared to the speed on fibronectin for C2C12 myoblasts.

To further characterize the effect of altering the RS we characterized sites of cell-substrate adhesion by staining for the focal adhesion marker paxillin (**Figure 3-6a-d**). Focal adhesion formation was quantified by comparing the surface area of the cell to the surface area of punctate paxillin staining, providing a measure of the percentage of the cell surface area positive for paxillin (**Figure 3-6e**). The C2C12 myoblast cells are relatively large, which facilitates the identification of focal adhesions, and focal adhesion formation in response to fibronectin has been well studied in these cells. RSs composed of a relatively high percentage of PEG resulted in the formation of fewer focal adhesions, consistent with these surfaces being of relatively low-affinity. In contrast, RSs containing relatively high levels of PDL resulted in a 3-fold increase in focal adhesions, consistent with these being high-affinity surfaces. Cells plated on fibronectin exhibited a 5-fold increase in paxillin positive surface area compared to that evoked by low-affinity surfaces. These results suggest that cells can more readily produce focal adhesions and adhere on fibronectin surfaces than they do on synthetic PDL surfaces, consistent with the difference in adhesive response between these two surfaces previously described in the literature (Grashoff, Hoffman et al. 2010).

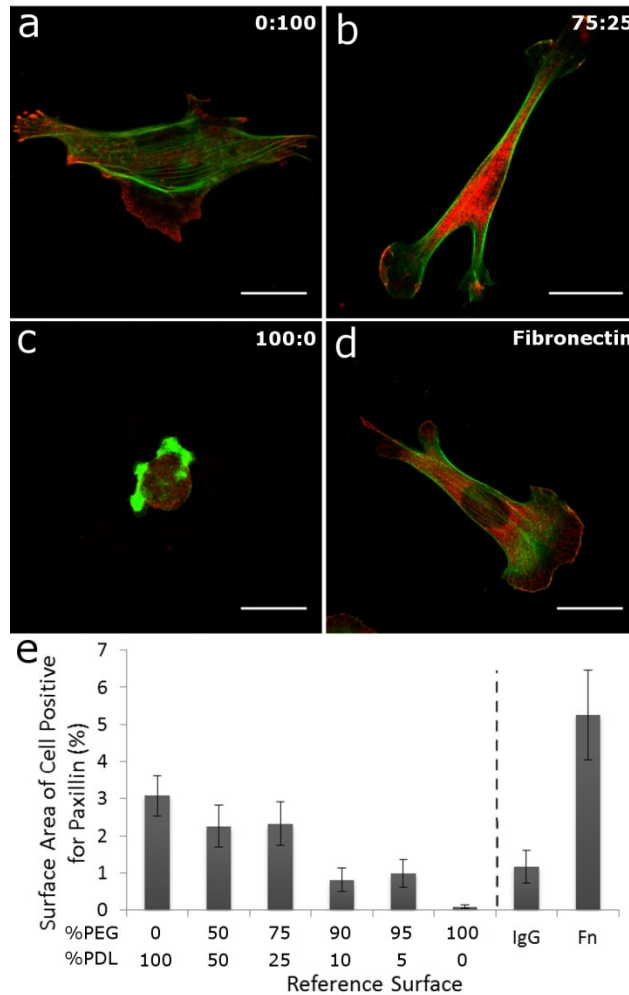


Figure 3-6. High affinity RSs result increased focal adhesions. Fluorescent images of C2C12 myoblasts stained for paxillin (red) and filamentous actin (green) on substrates of (a) 0:100, (b) 75:25, (c) 100: 0 and (d) fibronectin. (e) Quantification of the focal adhesion ratio to the cell surface area based on paxillin density and the cell cytoskeleton surface area determined via phalloidin in C2C12 myoblasts determined that the RS is statistically significant in defining the extent of focal adhesions that a cell can form with $p=2.54 \times 10^{-5} < 0.05$ ($n=5$, mean \pm standard error). Scale bars (a-d) are 20 μ m.

3-4.3 RS affinity influences the cell response to patterned protein

To compare the impact of changes in the RS affinity, we printed striped patterns of proteins along with different RS ratio combinations. While fibronectin, one of the proteins we tested, is a well-studied extracellular matrix protein, microcontact printing of fibronectin has been reported to result in the loss of functional activity, attributed to partial denaturation during stamping (von

Philipsborn, Lang et al. 2006). We therefore developed methods to limit stress on the protein during patterning and assayed the effectiveness of these protocols using fibronectin to ensure that protein integrity was not impaired by the patterning process. It was critical in our approach to not allow the fibronectin solution to dry onto the stamp, as in previous studies (von Philipsborn, Lang et al. 2006), so we reduced the time that the protein was incubated on the stamp. Juxtaposed alternating stripes of fibronectin were patterned using either microcontact printing, which might denature the protein, or via standard adsorption from solution, which maintains protein activity. C2C12 myoblasts grown on the alternating stripe patterns were then fixed and stained for F-actin using phalloidin (**Figure 3-7a**). No difference in the percentage of cells found on each type of substrate was found, indicating no preference for the printed or adsorbed fibronectin substrates (**Figure 3-7b**). Furthermore, immunostaining of cells on both substrates revealed equivalent distributions of paxillin, marking the formation of FAs (**Figure 3-7c**). These results confirmed that microcontact printed proteins, including fibronectin, maintain protein function.

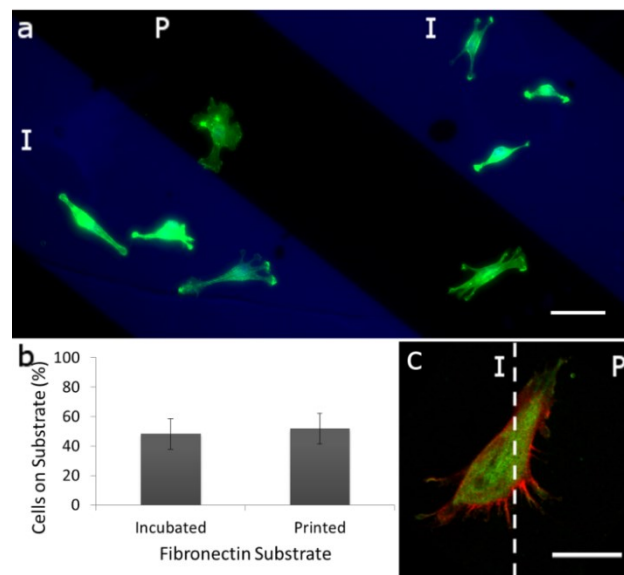


Figure 3-7. Cell response to stripes of fibronectin patterned by incubation and by microcontact printing. (a) Alternating 125 μm wide stripes of patterned fibronectin either incubated (I, blue) or microcontact printed (P, black) on the substrate. C2C12 myoblasts were grown on the substrate backfilled with a 100:0 PEG: PDL RS and stained for filamentous actin (green). (b) Fibronectin deposition through incubation or through printing is shown to not be statistically significant ($p=0.83>0.05$) as per the percentage of cells on incubated and printed

fibronectin ($n=4$, mean \pm standard error). (c) High magnification image of a single cell grown on the substrates and stained for the focal adhesion marker paxillin (red) and filamentous actin (green). The dashed line indicates the separation between the stripes. Scale bars are (a) 50 μm and (c) 20 μm .

Next, striped patterns of fibronectin, PDL, or IgG, along with different RS ratio combinations were formed. C2C12 myoblasts or Rat2 fibroblasts were then seeded and grown on the patterned coverslips for 6 h before fixation and staining to visualize F-actin and nuclei (**Figure 3-8a**). Cells responded to the stripes consistent with the predicted affinity of the RS. With very-low affinity RSs, cells were exclusively localized on printed fibronectin or PDL stripes. When presented with a high-affinity RS, cells did not bind preferentially to the RS or patterned stripes of fibronectin or PDL, but were randomly distributed. In contrast, at intermediate levels of PEG, the RS was neither excessively sticky nor “slippery”, and therefore did not exert confounding effects on the cellular response to fibronectin stripes.

Cellular responses to fluorescently labeled stripes of fibronectin were assessed by determining the percentage of cells in each RS condition that showed preference for the printed protein based on the location of the cell soma. With a low-affinity RS, cells were almost exclusively located on the patterned stripes of PDL or fibronectin (**Figure 3-8b**). In contrast, when presented with a high affinity RS, ~18% of the cells were found on stripes of patterned PDL or fibronectin. Importantly, this value is consistent with a random distribution of cells across the surface, determined by calculating relative surface area of the stripes and also determined experimentally by imaging cells grown on homogeneous PDL substrates and overlaying images of virtual stripes to find the percentage of cells that were located on stripes. This implies that both surfaces are indistinguishable from the seeded cells. Cellular responses to the patterned protein were also investigated by conducting the same experiments on patterned stripes of antibodies (IgG). To a limited extent, IgG stripes also appeared to follow the same trend as stripes of fibronectin or PDL. As the affinity of the RS decreases, there was a slight increase in preference of cell adhesion to the IgG stripe over the RS, but since the cell numbers on the stripes were distributed close to the level of randomness across all RS conditions, the change in cell response was not substantial. This indicates that the trend was largely due to the effect of the RS and not to a specific response to IgG. In general, the responses of Rat2 fibroblasts and C2C12 myoblasts to

fibronectin or PDL decreased as the affinity of the RS increased (**Figure 3-8c**). We also note that the trend in responsiveness of C2C12 myoblasts was more abrupt than that for Rat2 fibroblasts, illustrating the specificity of the responses made by these two cells types to the patterned substrate.

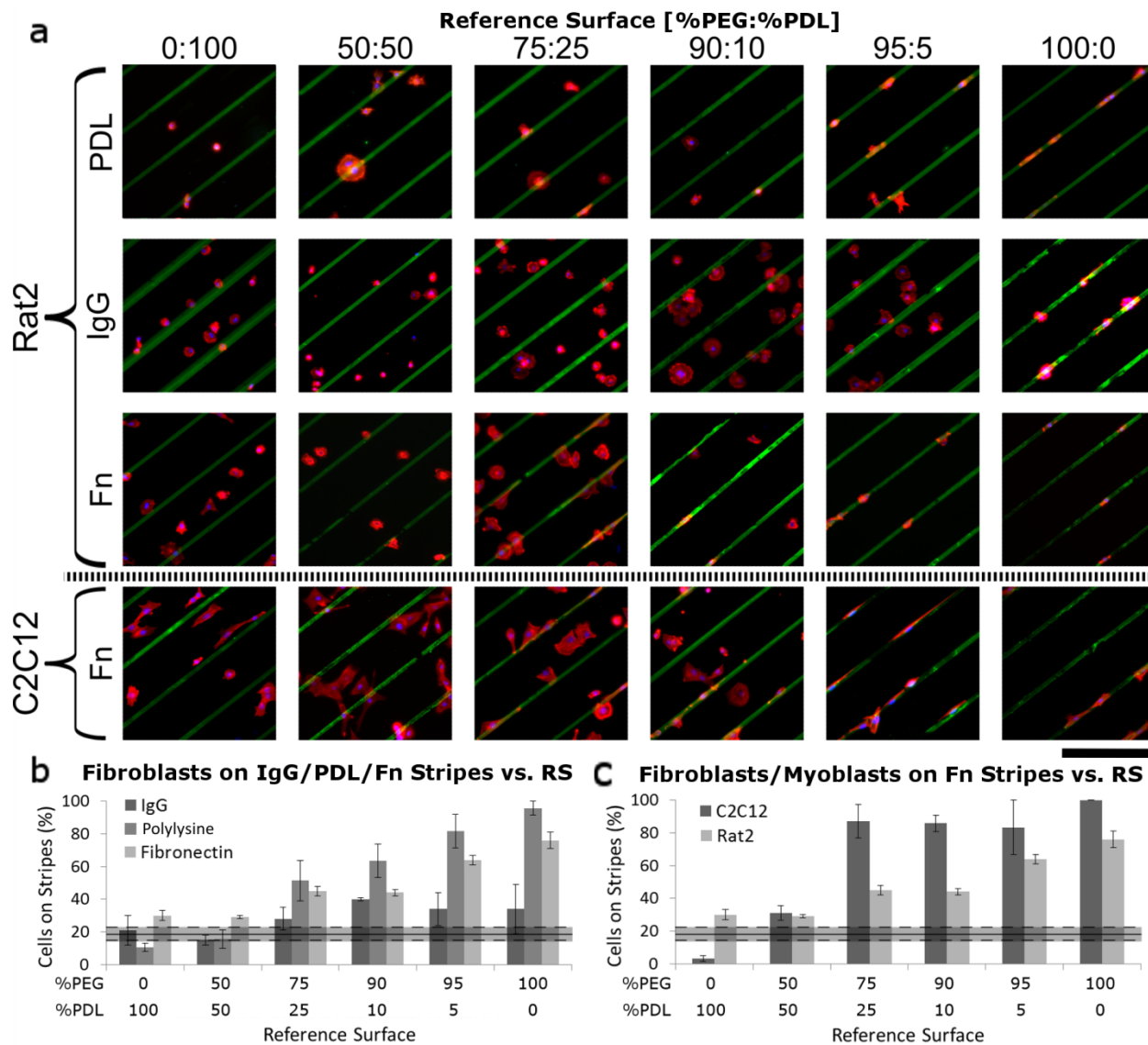


Figure 3-8. Cell response to patterned cues is dependent on cell type, patterned protein and the affinity of the RS. Rat2 fibroblasts were grown on printed PDL, fibronectin and IgG stripes and C2C12 myoblasts on fibronectin. For each condition, the RSs were varied to compositions of %PEG:%PDL 100:0, 95:5, 90:10, 75:25, 50:50, 0:100. Representative fluorescent images of each condition show the cells stained for F-actin (red) and Hoechst (blue) on the printed stripes (green). (b) Rat2 Cells were grown on printed IgG, PDL, fibronectin stripes on RSs of varying

percentages of %PEG:%PDL 100:0, 95:5, 90:10, 75:25, 50:50, 0:100. The difference in the response to the RS was statistically significant for Rat2 fibroblasts on PDL stripes ($p=4.36 \times 10^{-5} < 0.05$, $n=3$, mean \pm standard error), fibronectin ($p=4.26 \times 10^{-2} < 0.05$, $n=6-9$, mean \pm standard error) and there was no significant difference found for the RS for Rat2 cells compared to IgG stripes ($p=7.48 \times 10^{-2} > 0.05$, $n=6$, mean \pm standard error). (c) The difference between the response of C2C12 and Rat2 cells seeded on fibronectin stripes with different RSs shows that the cell response to the same patterned protein will vary based on the cell type used. With both cell lines, the cell response to patterned stripes in the presence of different RSs was found to be statistically significant across all conditions (c2c12: $p=1.44 \times 10^{-5} < 0.05$, Rat2: $p=2.12 \times 10^{-5} < 0.05$, $n=6$, mean \pm standard error). Solid lines represent the expected distribution of cells solely due to a random distribution with dotted lines representing the standard error ($n=3-6$, mean \pm standard error). (a) Scale bar is 200 μm .

3-4.4 RS affinity influences both cell body and axonal response in neurons

We also tested the effect of RSs of different affinity on neurons from embryonic rat spinal cords, illustrating the applicability of this method to primary cells and different cell types. The axonal growth cones of embryonic rat spinal commissural neurons respond to immobilized substrate bound netrin-1 (Shekarabi, Moore et al. 2005; Moore, Correia et al. 2008; Moore, Biais et al. 2009; Moore, Zhang et al. 2012). To investigate the significance of the RS to the guidance response, we patterned stripes of netrin-1 and plated spinal commissural neurons that were then grown for 48 h. Following cell fixation and staining, the location of the cell body and the axon were determined relative to the stripes (**Figure 3-2**).

The commissural neuron axon guidance response to either netrin-1 or control IgG stripes was quantified by averaging the percentage of cells in each of four possible categories (soma on/axon on, soma on/axon off, soma off/axon on, soma off/axon off) across 3 trials for netrin-1 ($n=9$ coverslips, $n=1,345$ neurons) and control ($n=3$ coverslips, $n=327$ neurons) (**Figure 3-9**). Each image analyzed contained an average of 25 neurons, ranging from 6 to 44 cells. When presented with a low affinity RS, $\sim 98\%$ of the neuronal cell bodies were positioned on netrin-1 stripes, while $\sim 57\%$ of cell bodies were found on IgG stripes, suggesting specificity in the response to netrin-1. As the proportion of PDL in the RS increased along with its affinity, the percentage of cells located on the netrin-1 stripe decreased to as low as $\sim 18\%$ on the highest affinity RS,

essentially becoming randomly distributed across the substrate. A similar but much less drastic decrease in the percentage of cell somas located on the stripes was observed on IgG patterns, which further supports our claim that the RS has a potent effect on cell response, since cell response to a non-specific cue like IgG would normally not change on its own.

The positioning of axons was similar to the cell soma, with ~98% of axons located on the netrin-1 stripes when presented with a low affinity RS, and ~40% of the axons located on the stripes in the context of a high affinity RS. On IgG stripes, ~66 % of the axons terminated on stripes when the RS was of low affinity, and only ~9% when it was high affinity, indicating that in this case the affinity to the RS surface was significantly higher.

The guidance response when an axon is directed onto a substrate bound cue is best indicated by the condition Soma Off/Axon On. When challenged with stripes of netrin-1, a RS composed of 75:25 %PEG:%PDL yielded the highest percentage of cells classified as having their soma off the stripe and their axon on the stripe for it allowed cell somas to bind to the RS while maintaining high affinity of the axons for the patterned netrin-1. Higher affinity RSs resulted in a loss of axonal affinity for netrin-1, while lower affinity RSs reduced cell adhesion. At the 75:25 %PEG:%PDL condition, ~50% of the cells matched the Soma Off/Axon On category (**Figure 3-9b**). Notably, the same RS with patterned IgG stripes resulted in only ~13% of the neurons in this same category (**Figure 3-9c**), consistent with a substantial cell specific response to netrin-1 (**Figure 3-9d**).

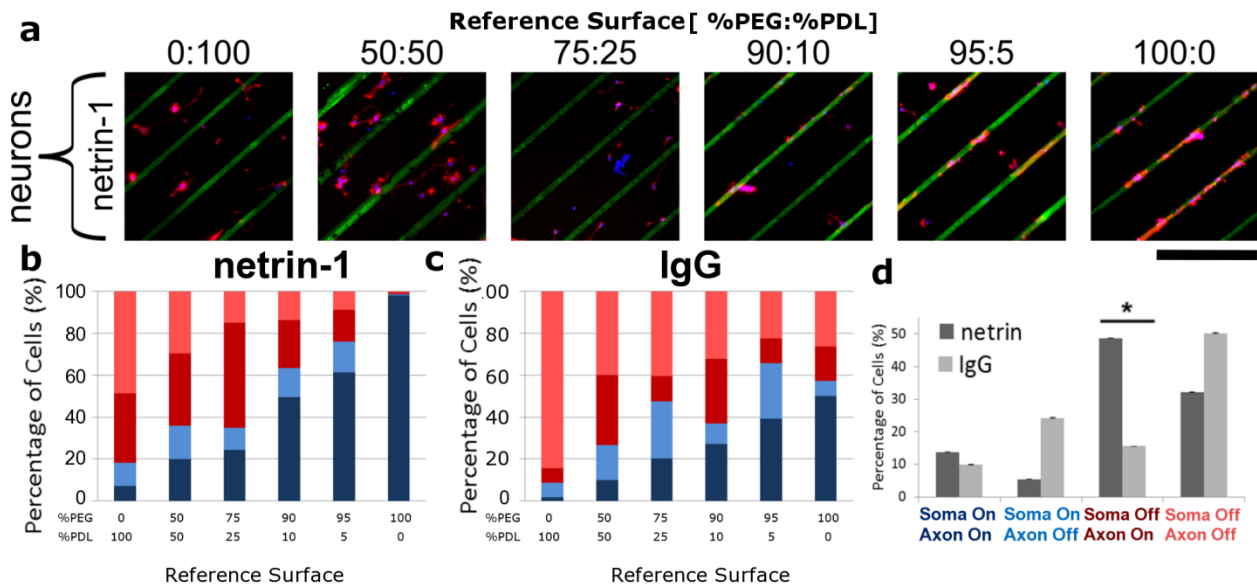


Figure 3-9. Spinal commissural neurons respond to printed netrin-1 stripes based on the affinity of the RS. (a) neurons were grown on printed netrin-1 stripes and the RS was varied to compositions of %PEG:%PDL 100:0, 95:5, 90:10, 75:25, 50:50, 0:100. Representative fluorescent images of each condition show the cells stained for F-actin (red) and Hoechst (blue) on the printed stripes (green). Characterization of neurons based on the location of their soma and axon relative to the stripes. The two conditions with soma on the stripes are blue with Soma On/Axon On in dark blue and Soma On/Axon Off in light blue. The two conditions with soma on the RS are Soma Off/Axon On in dark red and Soma Off/Axon Off in light red. The percentage of neurons in each category for the different RSs is reported for (b) netrin-1 (n=9 coverslips, n=1,345 neurons) or (c) IgG stripes (n=3 coverslips, n=327 neurons). (d) The optimal RS to investigate the navigation of spinal commissural neurons on netrin-1 patterns was determined to be 75:25 where significantly more neurons fit the category soma off-axon on for netrin-1 (n=24 coverslips, n=551 neurons) than for IgG stripes (n=8 coverslips, n=149 neurons). *indicates statistical significance where $p=1.2 \times 10^{-4} < 0.05$, mean \pm standard error). Scale bar (a) is 200 μ m.

3-4.5 Cell-type specific biochemical signaling on RSs of intermediate affinity

To confirm that the responses observed were driven by the patterned protein of interest, rather than solely the RS, function blocking experiments were conducted where Rat2 fibroblasts (**Figure 3-10a**) and C2C12 myoblasts (**Figure 3-10b**) were grown on stripes of fibronectin or IgG in the presence of a RS composed of 75:25 %PEG:%PDL. Integrin-mediated cellular responses to fibronectin activate src family tyrosine kinases (Salazar and Rozengurt 2001). Before plating, one third of the cells were exposed to the src family tyrosine kinase inhibitor PP2 (Hanke, Gardner et al. 1996), one third to its inactive analogue PP3, and the final third remained unexposed as a native condition. Cells plated on IgG stripes were not significantly affected by either PP2 or PP3, exhibiting a similar response to the patterns in all conditions. On stripes of fibronectin, significantly more cells were located on the stripes in control and PP3 conditions; however, incubation with PP2 resulted in significantly fewer cells being located on the stripes. No significant difference in cell numbers was recorded for the same condition on IgG stripes, indicating a difference in the distribution of cells and not a change in cell survival or proliferation. Collectively, these experiments illustrate that cell preference is linked to the activation of integrins.

Netrin-1 signals through its receptor deleted in colorectal cancer (DCC) to activate src family kinases (Li, Lee et al. 2004; Liu, Beggs et al. 2004). Embryonic rat spinal commissural neurons were similarly grown on netrin-1 and IgG stripes bounded by an RS of 75:25 %PEG:%PDL, with the addition of either PP2, PP3 or a DCC function blocking monoclonal antibody (Jarjour, Durko et al. 2011) (**Figure 3-10c**). Spinal commissural neurons grown on stripes of netrin-1 in control and PP3 conditions exhibited significantly more neurons with the soma on the RS and the axon on the netrin-1 stripe than did cells grown in the PP2 or DCC function blocking antibody conditions. Similarly, the inclusion of the DCC function blocking antibody blocked the preference for the axons to grow on stripes of netrin-1. Although the findings presented above (**Figure 3-9**) indicate that at relatively high- or low-affinities the RS dominates axonal responses to stripes of netrin-1, these findings (**Figure 3-10**) reveal biochemically appropriate axon guidance responses to microcontact printed stripes of netrin-1 when presented with a RS composed of intermediate affinity. These experiments confirm that the response of primary polarized cells such as neurons to patterns of substrate-bound cues is driven by these established adhesive cues, which are linked to migratory signaling pathways.

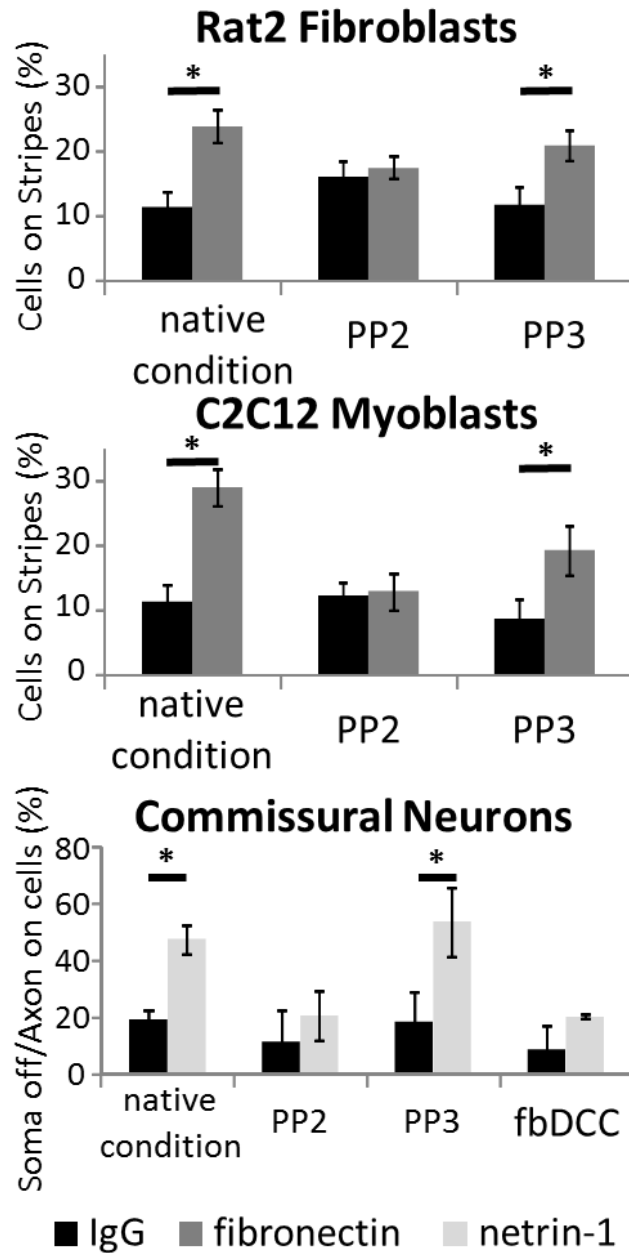


Figure 3-10. In the presence of an intermediate RS, the response of cells to protein patterns is driven by biologically appropriate signal transduction. Function blocking experiments for (a) Rat2 fibroblasts and (b) C2C12 myoblasts grown on fibronectin and IgG stripes in the presence of a RS of 75:25 %PEG:%PDL. Cells were cultured with the addition of PBS in the native condition, PP2 or PP3. (c) Spinal commissural neurons grown on netrin-1 and IgG stripes all on a RS of 75:25 %PEG:%PDL. The cells were cultured with PBS in the native condition, PP2, PP3 or a function blocking antibody specific for the receptor DCC. The percentage of cells

that fit the soma off/axon on category were recorded. * indicates statistical significance, mean± standard error. n=9 for (a) and (b) and n=3 for (c).

3-5 Discussion

Information explicitly describing the RS used in cell culture studies is often lacking in the literature, indicating that the functional significance of the RS may be overlooked. The current lack of consideration for the RS may account for difficulties in reproducing experiments and interpreting functional outcomes. Here, we describe a method to tune the cell-surface affinity of the RS that is contiguous to the printed protein. Our method allows the RS to be tuned from 100:0 PDL:PEG to 0:100 %PEG:%PDL. Whereas at high or low affinity the RS dictates cell response, at intermediate affinities cells respond in a physiologically appropriate manner to patterned proteins. Strong specific cell responses were observed in our experiments for a RS of 75:25 %PEG:%PDL. The number of increments and range of RSs sampled can be easily adjusted for particular experimental questions.

The technique to produce tunable RSs has a number of benefits that will facilitate the study of substrate-bound cues *in vitro*. By employing PEG and PLL as the two constituents of the solution, the surface deposition occurs through simple incubation and is effective for at least 15 days in culture (Ricoult, Goldman et al. 2012). The inclusion of PEG allows the affinity of PDL to be tuned while also minimizing the passive adsorption to the substrate of biomolecules present in the cell culture medium, such as proteins in serum that may confound the functional analysis of the patterned protein. Because the RSs generated used the synthetic polymers PDL and PEG, in principal it is possible to further enhance the tunability of RSs by including biologically active proteins, peptides, or identified ECM components, such as fibronectin, collagens, and laminins. The range of cell surface affinity may also be extended beyond what we formulated by identifying other non-specific molecules that have a relatively higher or lower affinity than PDL and PEG, respectively. Furthermore, RSs could be employed experimentally that are pertinent to the organ being studied, such as to reproduce injury sites in the nervous system composed of inhibitory tenascin and sulfated proteoglycans (Schwab, Kapfhammer et al. 1993) or adhesive interactions where fibronectin and vinculin may predominate (Ghosh and Ingber 2007).

Based on the findings presented here, when patterning protein substrates, it is critical to consider the RS because the cellular responses observed may not be solely attributable to the surface-bound protein under investigation. In contrast, they may be influenced, and sometimes dictated, by a response to the RS. An efficient and informative way of representing the cell response to patterns may be via cell-surface affinity curves, similar to those employed for immunoassay binding curves (**Figure 3-11**), in which the RS acts as a competing surface, and the decrease in cell surface affinity is analogous to a decrease in the concentration of a competing species in a competitive immunoassay (Wild 2005). The slope, dynamic range and magnitude of the response extracted from these curves can serve as defining characteristics of cell-surface interactions.

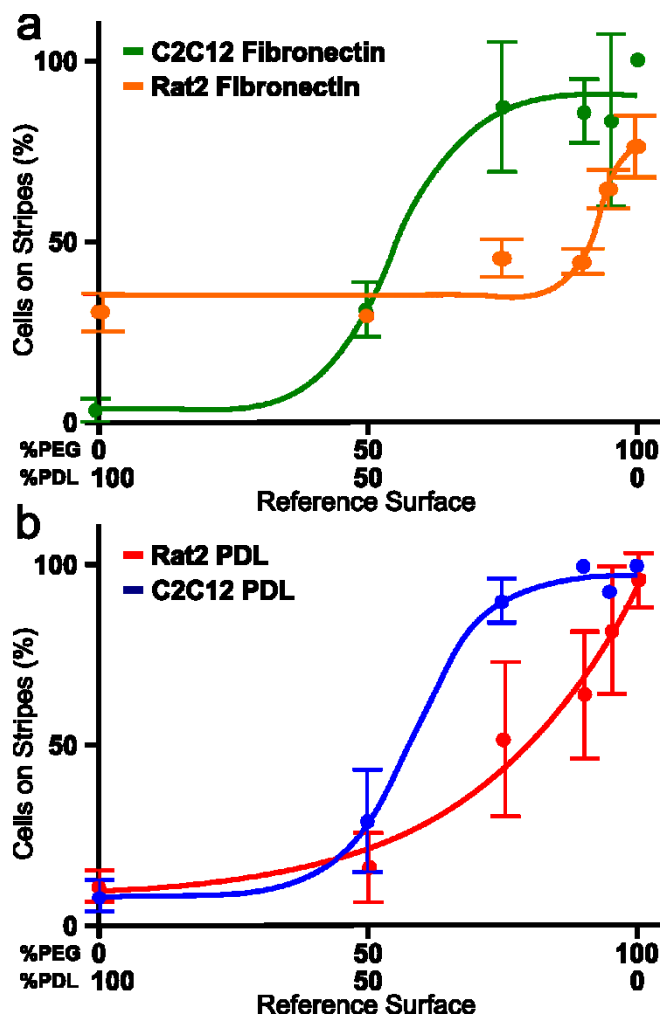


Figure 3-11. Competitive Cell-surface affinity curves. Cell-surface affinity curves of Rat2 fibroblasts and C2C12 myoblasts on printed (a) fibronectin and (b) PDL patterns established

based on the percentage of cells on the printed stripes and based on the RS (n=3-6, mean± standard error).

Patterned stripes were used in these experiments primarily due to the simplicity of the pattern facilitating the analysis of cellular responses. The stripe geometry is limited, however, as it only permits the study of a binary choice, since the concentration jumps from 0% to 100% at the stripe edge. Digital Nanodot Gradients that pattern protein spot density have been employed to extend this method to investigate directional cell migration and mechanisms of haptotaxis (Ricoult, Pla-Roca et al. 2013).

3-6 Conclusions

We define cell-surface affinity as a metric that is free of mechanistic assumptions to characterize surfaces in cell choice assays. We also introduce the term Reference Surface (RS) and provide a method to systematically tune the cell-surface affinity of the RS using varied mixtures of PEG and PDL. We demonstrate that the RS can dominate the response of both migratory cells and polarized neurons to substrate-bound protein patterns. We propose that when describing cell choice in response to a patterned protein, it must be described *relative* to the RS, *i.e.* 80 % of the cells choose fibronectin in the presence of a RS composed of 75%PEG:25%PDL. In addition, we propose that cell-surface affinity curves obtained by tuning the RS provide an accurate means to measure cellular responses to a bound cue by quantifying the magnitude, slope, and range of the response curve. Taking these issues into consideration will increase the pertinence of studies that examine the functional significance of substrate-bound proteins, lead us to re-evaluate past studies, and facilitate the collection of quantitative data relevant to cell preference. Future studies will address the possible impact of RS affinity on directional cell migration and neuronal outgrowth and guidance and may guide the interpretation of results from *in vivo* studies.

3-7 References

Adams, D. N., E. Y. C. Kao, et al. (2005). "Growth cones turn and migrate up an immobilized gradient of the laminin IKVAV peptide." Journal of Neurobiology **62**(1): 134-147.

- Calof, A. L. and A. D. Lander (1991). "Relationship between Neuronal Migration and Cell-Substratum Adhesion - Laminin and Merosin Promote Olfactory Neuronal Migration but Are Antiadhesive." Journal of Cell Biology **115**(3): 779-794.
- Curtis, A. S. G., J. V. Forrester, et al. (1983). "Adhesion of Cells to Polystyrene Surfaces." Journal of Cell Biology **97**(5): 1500-1506.
- Evans, A. R., S. Euteneuer, et al. (2007). "Laminin and fibronectin modulate inner ear spiral ganglion neurite outgrowth in an in vitro alternate choice assay." Developmental Neurobiology **67**(13): 1721-1730.
- Falconnet, D., G. Csucs, et al. (2006). "Surface engineering approaches to micropattern surfaces for cell-based assays." Biomaterials **27**(16): 3044-3063.
- Fereol, S., P. Fodil, et al. (2011). "Micropatterned ECM Substrates Reveal Complementary Contribution of Low and High Affinity Ligands to Neurite Outgrowth." Cytoskeleton **68**(7): 373-388.
- Fereol, S., R. Fodil, et al. (2009). "Prestress and Adhesion Site Dynamics Control Cell Sensitivity to Extracellular Stiffness." Biophysical Journal **96**(5): 2009-2022.
- Geiger, B., J. P. Spatz, et al. (2009). "Environmental sensing through focal adhesions." Nat Rev Mol Cell Biol **10**(1): 21-33.
- Ghosh, K. and D. E. Ingber (2007). "Micromechanical control of cell and tissue development: Implications for tissue engineering." Advanced Drug Delivery Reviews **59**(13): 1306-1318.
- Grashoff, C., B. D. Hoffman, et al. (2010). "Measuring mechanical tension across vinculin reveals regulation of focal adhesion dynamics." Nature **466**(7303): 263-U143.
- Hanke, J. H., J. P. Gardner, et al. (1996). "Discovery of a novel, potent, and Src family-selective tyrosine kinase inhibitor - Study of Lck- and FynT-dependent T cell activation." Journal of Biological Chemistry **271**(2): 695-701.
- Hood, J. D. and D. A. Cheresh (2002). "Role of integrins in cell invasion and migration." Nat Rev Cancer **2**(2): 91-100.
- Jarjour, A. A., M. Durko, et al. (2011). "Autocrine Netrin Function Inhibits Glioma Cell Motility and Promotes Focal Adhesion Formation." Plos One **6**(9).
- Kennedy, T. E., T. Serafini, et al. (1994). "Netrins are diffusible chemotropic factors for commissural axons in the embryonic spinal cord." Cell **78**(3): 425-435.

- Knoll, B., C. Weigl, et al. (2007). "Stripe assay to examine axonal guidance and cell migration." Nat Protoc **2**(5): 1216-1224.
- Larsen, M., V. V. Artym, et al. (2006). "The matrix reorganized: extracellular matrix remodeling and integrin signaling." Curr Opin Cell Biol **18**(5): 463-471.
- Lauffenburger, D. A. and A. F. Horwitz (1996). "Cell Migration: A Physically Integrated Molecular Process." Cell **84**(3): 359-369.
- Lehnert, D., B. Wehrle-Haller, et al. (2004). "Cell behaviour on micropatterned substrata: limits of extracellular matrix geometry for spreading and adhesion." Journal of Cell Science **117**(1): 41-52.
- Lemmon, V., S. M. Burden, et al. (1992). "Neurite Growth on Different Substrates - Permissive Versus Instructive Influences and the Role of Adhesive Strength." Journal of Neuroscience **12**(3): 818-826.
- Li, W., J. Lee, et al. (2004). "Activation of FAK and Src are receptor-proximal events required for netrin signaling." Nat Neurosci **7**(11): 1213 - 1221.
- Liu, G. F., H. Beggs, et al. (2004). "Netrin requires focal adhesion kinase and Src family kinases for axon outgrowth and attraction." Nature Neuroscience **7**(11): 1222-1232.
- Mai, J., L. Fok, et al. (2009). "Axon Initiation and Growth Cone Turning on Bound Protein Gradients." Journal of Neuroscience **29**(23): 7450-7458.
- Meijering, E., O. Dzyubachyk, et al. (2012). Methods for Cell and Particle Tracking. Methods in Enzymology. **504**: 183-200.
- Moore, S. W., N. Biais, et al. (2009). "Traction on immobilized netrin-1 is sufficient to reorient axons." Science **325**(5937): 166.
- Moore, S. W., J. P. Correia, et al. (2008). "Rho inhibition recruits DCC to the neuronal plasma membrane and enhances axon chemoattraction to netrin 1." Development **135**(17): 2855-2864.
- Moore, S. W. and T. E. Kennedy (2001). Dissection and Culture of Embryonic Spinal Commissural Neurons. Current Protocols in Neuroscience, John Wiley & Sons, Inc.
- Moore, S. W., X. Zhang, et al. (2012). "Netrin-1 Attracts Axons through FAK-Dependent Mechanotransduction." The Journal of Neuroscience **32**(34): 11574-11585.
- Oliva, A. A., C. D. James, et al. (2003). "Patterning axonal guidance molecules using a novel strategy for microcontact printing." Neurochemical Research **28**(11): 1639-1648.

- Ricoult, S. G., J. S. Goldman, et al. (2012). "Generation of microisland cultures using microcontact printing to pattern protein substrates." J Neurosci Methods **208**(1): 10-17.
- Ricoult, S. G., M. Pla-Roca, et al. (2013). "Large Dynamic Range Digital Nanodot Gradients of Biomolecules Made by Low-Cost Nanocontact Printing for Cell Haptotaxis." Small.
- Ridley, A. J., M. A. Schwartz, et al. (2003). "Cell migration: integrating signals from front to back." Science **302**(5651): 1704-1709.
- Roy, J., T. E. Kennedy, et al. (2013). "Engineered cell culture substrates for axon guidance studies: moving beyond proof of concept." Lab Chip **13**(4): 498-508.
- Salazar, E. P. and E. Rozengurt (2001). "Src family kinases are required for integrin-mediated but not for G protein-coupled receptor stimulation of focal adhesion kinase autophosphorylation at Tyr-397." Journal of Biological Chemistry **276**(21): 17788-17795.
- Saravia, V., S. Kupcu, et al. (2007). "Bacterial protein patterning by micro-contact printing of PLL-g-PEG." J Biotechnol **130**(3): 247-252.
- Schwab, M. E., J. P. Kapfhammer, et al. (1993). "Inhibitors of Neurite Growth." Annual Review of Neuroscience **16**: 565-595.
- Serafini, T., T. E. Kennedy, et al. (1994). "The netrins define a family of axon outgrowth-promoting proteins homologous to *C. elegans* UNC-6." Cell **78**(3): 409-424.
- Shekarabi, M., S. W. Moore, et al. (2005). "Deleted in colorectal cancer binding netrin-1 mediates cell substrate adhesion and recruits Cdc42, Rac1, Pak1, and N-WASP into an intracellular signaling complex that promotes growth cone expansion." Journal of Neuroscience **25**(12): 3132-3141.
- Shirasaki, R., C. Mirzayan, et al. (1996). "Guidance of circumferentially growing axons by netrin-dependent and -independent floor plate chemotropism in the vertebrate brain." Neuron **17**(6): 1079-1088.
- They, M., V. Racine, et al. (2005). "The extracellular matrix guides the orientation of the cell division axis." Nature Cell Biology **7**(10): 947-U929.
- Vielmetter, J., B. Stolze, et al. (1990). "Invitro Assay to Test Differential Substrate Affinities of Growing Axons and Migratory Cells." Experimental Brain Research **81**(2): 283-287.
- Vogt, A. K., F. D. Stefani, et al. (2004). "Impact of micropatterned surfaces on neuronal polarity." Journal of Neuroscience Methods **134**(2): 191-198.

- von Philipsborn, A. C., S. Lang, et al. (2006). "Microcontact printing of axon guidance molecules for generation of graded patterns." Nat Protoc **1**(3): 1322-1328.
- von Philipsborn, A. C., S. Lang, et al. (2006). "Microcontact printing of axon guidance molecules for generation of graded patterns." Nat. Protocols **1**(3): 1322-1328.
- von Philipsborn, A. C., S. Lang, et al. (2006). "Growth cone navigation in substrate-bound ephrin gradients." Development **133**(13): 2487-2495.
- Wild, D. (2005). The immunoassay handbook, Gulf Professional Publishing.
- Zhang, M., T. Desai, et al. (1998). "Proteins and cells on PEG immobilized silicon surfaces." Biomaterials **19**(10): 953-960.
- Zhang, Z. P., R. Yoo, et al. (2005). "Neurite outgrowth on well-characterized surfaces: preparation and characterization of chemically and spatially controlled fibronectin and RGD substrates with good bioactivity." Biomaterials **26**(1): 47-61.

PREFACE TO CHAPTER 4

In the previous chapter, we developed a means to control the affinity of the reference surface (RS). We used this approach to generate a range of affinities that we used to study the impact of the RS on cell response, and to identify an intermediate RS at which cells respond to patterned protein through biochemical pathways (Chapter 3). By combining this approach to control the RS with the lift-off nanocontact printing procedure to pattern substrate-bound digital nanodot gradients (Chapter 2) we developed an easy and robust method to create an *in vitro* model to investigate haptotaxis.

In the following chapter, we investigate the impact of substrate-bound gradient geometry on axonal navigation on gradients of chemotactic cues (*i.e.* netrin-1) or levels of affinity (*i.e.* polylysine). The geometrical parameters we investigate are randomness, slope, function (exponential or linear), and we readout the axonal response to variations in these parameters by calculating the outgrowth and preferred direction of growth with respect to the gradient direction. We determine that cortical neurons expressed the strongest turning response on exponential netrin-1 gradients of shallow slope with an ordered nanodot arrangement.

This chapter is a manuscript of a research article intended for submission for publication.

Acknowledgements

We thank Stephen Glasgow and Stephanie Harris for providing neurons used. We acknowledge support from CIHR (Regenerative and Nanomedicine grant, and operating grants # 114965 and # 79513 to TEK), the Canadian Foundation for Innovation and the McGill Nanotools Microfabrication Laboratory (funded by CFI and McGill University). SGR was supported by the NSERC-CREATE Integrated Sensor System and the Neuroengineering program funded by NSERC and The Molson Foundation. TEK was supported by a Scholarship from the Killam Trust and by a Chercheur Nationaux Award from the Fonds de la Recherche en Santé du Québec. DJ holds a Canada Research Chair.

CHAPTER 4

Investigating Gradient Geometry on Axonal Navigation using Digital Nanodot Gradient Arrays

Sébastien G. Ricoult,^{1,2} Grant Ongo^{2,3}, Karen Lai Wing Sun,¹ David Juncker,^{1,2,3} and Timothy E. Kennedy^{1,*}

¹McGill Program in Neuroengineering, Department of Neurology and Neurosurgery, Montreal Neurological Institute, McGill University, 3801 University Ave, Montreal, Quebec, Canada H3A 2B4

²Genome Quebec Innovation Centre, McGill University, Montréal, Quebec, Canada H3A 0G1

³Department of Biomedical Engineering,
McGill University, 740 Dr. Penfield Avenue, Montreal, Quebec, Canada H3A 0G1

4-1 Abstract

Extracellular gradients of secreted guidance factors and their role in axonal navigation have been extensively investigated using diffusible gradients, however research investigating the function of substrate-bound gradients, despite the abundance of haptotaxis *in vivo*, has been relatively limited due to technical limitations. We have developed an assay to pattern substrate-bound digital nanodot gradients to investigate the role of gradient geometry on axon turning and outgrowth. We then show that axonal navigation by different populations of neurons, the propensity of an axon to grow out and turn, differs on gradients of the chemotropic protein netrin-1. To determine if a cue that is permissive for axon outgrowth but not considered to have tropic function has the capacity to orient axon turning if patterned as a gradient, we show that gradients of poly-D-lysine effectively evoke axon turning. We then assess the extent to which the inclusion of defects in the patterned gradients, represented by non-monotonous DNGs, will disrupt the capacity of neurons to maintain an appropriate directional response. Our findings provide evidence that in response to graded distributions of netrin-1, the axons of embryonic rat neocortical neurons are most effectively guided by shallow ordered exponential monotonic gradients, with a preferred direction of growth with respect to the gradient direction that range from 17-43°. The methods and findings presented provide an effective and reliable means to

address the impact of geometry on axonal navigation.

4-2 Introduction

Cell navigation operates in response to an inhomogeneous distribution of extracellular cues. These protein cues can either be extracellular matrix (ECM) which promote cell adhesion (*e.g.* laminins, collagen, fibronectin or vitronectin) (Rozario and DeSimone 2010), or secreted chemotropic guidance cues (*e.g.* netrin-1, semaphorin, sonic hedgehog) (Dickson 2002). Long range guidance cues are distributed as gradients, which during the development of the nervous system direct axon extension to ultimately connect neurons with their targets (Tessier-Lavigne and Goodman 1996).

The netrins are a well-studied family of chemotropic axon guidance proteins (Sun, Correia et al. 2011). Binding of the receptors DCC or Neogenin to substrate-bound netrin-1 results in attraction (Xu, Wu et al. 2014). In contrast, netrin-1 binding an Unc5 homologue and DCC receptor complex evokes repulsion (Hong, Hinck et al. 1999). A ventral to dorsal gradient of netrin-1 emanating from the floor plate cells at the ventral midline of the embryonic spinal cord directs axon extension by commissural neurons, which express high levels of DCC (Kennedy, Serafini et al. 1994; Keino-Masu, Masu et al. 1996; Kennedy, Wang et al. 2006). From approximately embryonic days 9.5-11.5 in mice, these axons follow an ipsilateral circumferential trajectory extend to the floorplate, cross to the contra-lateral side and then engage a different set of molecular mechanisms to extend rostrally along the spinal cord to the brain where they will form synapses (Chedotal and Richards 2010).

Little is known regarding how axon navigation is effected by the geometry of the netrin-1 gradient, which evolves and changes as the organism develops (Kennedy, Wang et al. 2006).

To investigate axonal navigation in a simplified environment, researchers have turned to *in vitro* methods (Roy, Kennedy et al. 2013). Gradients of substrate-bound proteins can be generated using a number of different methods, however microcontact printing of proteins has the

advantage of its relative ease, low-cost and ability to rapidly decorate large surfaces with complex patterns (Kane, Takayama et al. 1999). Thus far, microcontact printing has been employed to study how the axons of DRG neurons are repelled by patterned ephrin gradients (von Philipsborn, Lang et al. 2006; von Philipsborn, Lang et al. 2007; Fricke, Zentis et al. 2011). A second study used the technique to print mixed gradients of laminin and polylysine of different slopes to investigate the parameters that best promote outgrowth (Fricke, Zentis et al. 2011). In accordance with their findings, where outgrowth could be mediated by polylysine, we recently reported that axonal navigation can be directed simply by changing the relative polylysine composition of the non-patterned surface compared to the surrounding reference surface (Ricoult, Thompson-Steckel et al. 2014). This suggests that complex polylysine gradients might be as suitable as chemotropic gradients to guide neurons to specific location, but it remains to be demonstrated.

We developed a low-cost lift-off nanocontact printing approach that allowed us to pattern protein dots down to 100 nm diameters at a very low density (Ricoult, Pla-Roca et al. 2013). By implementing designs of Digital Nanodot Gradients (DNG) where the location of each dot is controlled and changed along X and Y axis, we achieved monotonic and non-monotonic, ordered and random gradients of a record dynamic range suitable to investigate biological gradients (Ongo et al. 2014). We then created an array of 100 different DNG to simultaneously investigate a large range of geometric parameters.

Here, we employ this printing method and array to pattern gradients of netrin-1 or PDL to investigate the propensity of different gradient geometries to guide neurons. Based on these findings, we investigate how order, gradient function, and slope influence axonal navigation and identify the properties of gradient geometry that evokes the largest outgrowth and turning

response, and compare how the response varies among different neuron populations. Next, we test whether neurons can be guided by affinity gradients in the absence of chemoaffinity cues. Lastly, to determine to what extent axons maintain the capacity to orient extension despite the presence of inhomogeneity in the gradients, we examine turning in the presence of non-monotonic functions variations added as noise to the gradients.

4-3 Materials and Methods

Software: Algorithms were developed in Matlab R2013a (Natick, MA, USA). Scripts of the gradient algorithms are available for download upon request by contacting david.juncker@mcgill.ca. A spreadsheet template (Microsoft Excel 2010) of gradient parameters was imported into Matlab for processing. The output for each gradient was a text file of coordinates formatted as a Caltech Intermediate Format (CIF) file. CIFs were imported into CleWin Version 4.1 (WieWeb, MESA Research Institute at the University of Twente and Deltamask, Netherlands). Gradients were exported from CleWin as Bitmap (BMP) image files for verification of density using ImageJ 1.47 64-bit (National Institutes of Health, USA) and Matlab. The 100-gradient array was designed in L-edit (Tanner EDA, Monrovia, CA, USA) (Ongo et al., 2014).

Electron-Beam Lithography: A 4" Si wafer was coated with PMMA resist and the 100-gradient array was patterned by e-beam lithography (VB6 UHR EWF, Vistec, Montreal, QC, Canada), followed by reactive-ion etching (System100 ICP380, Plasmalab, Everett, WA, USA) 100 nm deep into the Si wafer.

Stamp Fabrication: After cleaning, the Si wafer was coated with perfluorooctyltriethoxysilane (Sigma-Aldrich, Oakville, ON, Canada) by vapor phase deposition. An accurate polymer copy of

the wafer was obtained after double replication using polydimethylsiloxane (PDMS) and a UV-sensitive polyurethane as previously described (Ricoult, Pla-Roca et al. 2013). First, a 6 mm layer of 1:10 PDMS (Dow Corning, Corning, NY, USA) was poured on the wafer inside a Petri dish, followed by degassing under vacuum in a desiccator for 10 min. Next, the PDMS was cured in an oven for 24 h at 60 °C (VWR, Montreal, QC, Canada) then peeled from the wafer. To remove uncured monomers and other extractables, the PDMS replica was submersed in 70% ethanol for 24 h then baked at 60°C for 4 h. Next, a drop of UV sensitive polyurethane (Norland Optical Adhesive 63 (NOA 63), Norland Products, Cranbury, NJ) was applied to the PDMS replica and cured by 600 W of UV light (Uvitron International, Inc., West Springfield, MA) for 30 s. The PDMS was then removed yielding an NOA replica of the original Si wafer pattern with 200 nm holes (Ricoult, Pla-Roca et al. 2013).

Nanocontact Printing: A flat PDMS stamp was cured against a perfluorooctyltriethoxysilane treated flat Si wafer. Following removal of the extractables as described above, the flat PDMS stamp was inked with a 10 µL drop of either poly-d-lysine (5 µg/ml, PDL, 70–150 kDa, Sigma–Aldrich, Oakville, ON, Canada), fluorescently labeled IgG (25 µg/ml, chicken, Invitrogen, Burlington, ON, Canada), or netrin-1 (12.5 µg/ml, produced and purified as described (Serafini, Kennedy et al. 1994) and (Shirasaki, Mirzayan et al. 1996)). A fluorescent secondary IgG was mixed into the protein ink as a fiducial marker to facilitate the localization of the nanodots. A plasma activated hydrophilic coverslip was then placed on the drop to spread the solution evenly across the surface of the hydrophobic PDMS stamp during a 5 min incubation period. After rinsing with PBS and double distilled water for 15 s each, the inked stamps were briefly dried under a stream of N₂ and immediately brought into contact with a plasma activated (PlasmaEtch

PE-50, PlasmaEtch, Carson City, NV, USA) NOA master for 5 s. The PDMS and NOA were separated and proteins in the contact regions were transferred to the NOA. The remaining proteins on the PDMS were transferred to the final substrate by printing the PDMS stamp for 5 s onto a plasma activated glass coverslip.

Backfilling: A reference surface (RSs) consisting of 75% by volume poly-L-lysine grafted polyethylene glycol (10 µg/ml, PLL(20 KDa)-g[3.5]-PEG(2 KDa), abbreviated as PEG), Surface Solutions, Dübendorf, Switzerland) and 25% poly-D-lysine (10 µg/ml, PDL, 70-150 kDa, Sigma-Aldrich, Oakville, ON, Canada) was incubated on the coverslip on a rocking plate for 15 min before washing off unbound PEG and PDL with 1xPBS (Ricoult, Thompson-Steckel et al. 2014).

Cell Culture: Embryonic rat spinal commissural neurons were isolated and cultured as described (Moore and Kennedy 2001). Embryonic rat commissural neurons and cortical neurons were seeded at 50,000 cells per coverslip or 100,000 cells per matTek dish, and grown at 37°C in 5% CO₂ for 2 DIV in neurobasal media (Invitrogen, Burlington, ON, Canada), 1% B27 (Invitrogen, Burlington, ON, Canada), 0.5% N2 (Invitrogen, Burlington, ON, Canada), 1% Penn/Strep (Invitrogen, Burlington, ON, Canada), 0.2% Fungizone (Invitrogen, Burlington, ON, Canada) and 0.25% L-glutamine (Invitrogen, Burlington, ON, Canada).

Immunocytochemistry: Cells were fixed with 4% paraformaldehyde (PFA) for 1 min, permeabilized with 0.1% triton-X 100 for 5 min, and blocked with 1% horse serum overnight at 4°C. Cells were labeled with phalloidin conjugated to Alexa Fluor 488 (1:250, Invitrogen,

Burlington, ON, Canada) and with Hoechst dye (1:10,000, Invitrogen, Burlington, ON, Canada). Protein patterns were mixed with a secondary chicken anti-goat antibody conjugated to Alexa Fluor 546 (polyclonal, 1:20, Invitrogen, Burlington, ON, Canada).

Imaging and Analysis: DNGs of fluorescently-labeled proteins were imaged by fluorescence microscopy (TE2000 microscope, Nikon, Canada and CoolSNAP HQ2 camera, Photometrics, USA). Analysis of fixed samples was conducted manually as detailed in **Figure 4-1**. Neurons with somas located either in the top or bottom 20 μm of the gradient were omitted from the analysis because the turning ability of the axon was limited by the edge of the gradient.

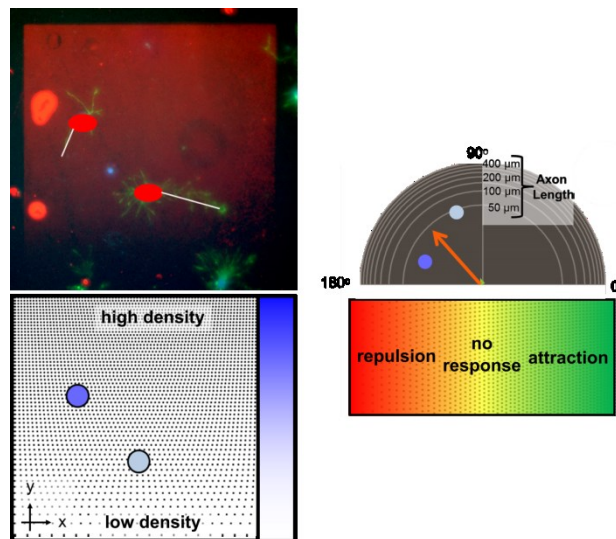


Figure 4-1. Manual analysis process flow of axonal navigation on DNGs. The Y position of neuron soma on fluorescently labeled protein DNGs (red) was first noted and based on the position of the soma, a shade of blue was attributed with dark blue attributed to somas located on the high density portion of the gradient and light on the low density end of the DNG. A line was then traced from the soma to the tip of the longest neurite and the length and angle recorded. The blue shaded dots were then plotted on a half circle log plot where each line represents 50 μm . The position of the dots represents the length of the longest neurite and the angle is indicated by

the position of the dot along the X axis, where 180° indicates strong repulsion, 90° a lack of response and, 0° indicates strong attraction. After all the dots are plotted, an average vector is calculated to determine the average response of neurons and a shade on the range of red-yellow-green applied to facilitate visualization of the neurite response.

4-4 Results and Discussion

4-4.1 Patterning substrate-bound protein digital nanodot gradients for cell assays

Two-step low-cost lift-off nanocontact printing was used to pattern protein nanopatterns on glass coverslips (Ricoult, Pla-Roca et al. 2013) (**Figure 4-2a**). First, a silicon wafer etched with the nanodot pattern was coated with a silane and replicated in PDMS to create an intermediate replica. The intermediate replica was then used as a mold to produce large pools of NOA lift-off stamps by coating the mold with the photocurable polymer and exposing it to UV light. The lift-off stamps were then contacted with flat PDMS stamps pre-inked with protein to remove protein in the contacting regions whereas in the presence of holes on the lift-off stamp, no contact is made and the protein remains on the flat PDMS stamp. This yields the protein nanopattern, and the remaining protein can be transferred onto a glass substrate through contact. The protein nanopatterns were backfilled with a 75% PEG : 25% PDL reference surface through a 15 min incubation (Ricoult, Thompson-Steckel et al. 2014). Neurons were then seeded on the patterns, fixed after 2 days of culture, and stained for filamentous actin and nuclei (**Figure 4-2b-d**). After 2 DIV, the polarized morphology of the cells with long neurites and the presence of nuclei indicate that the patterned substrates support the growth of primary neurons.

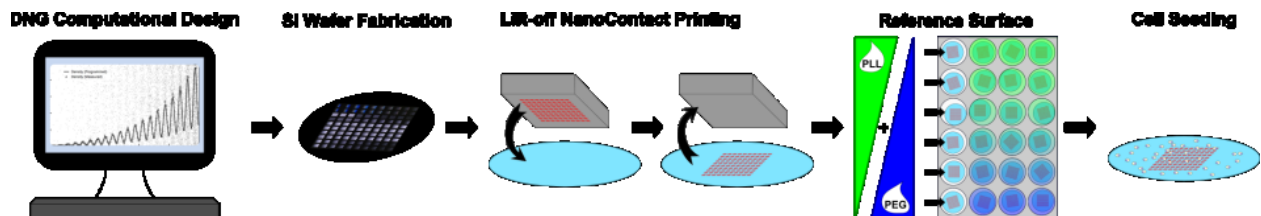


Figure 4-2. Schematic of experimental process flow. DNGs are first designed computationally using the algorithms we developed (Ongo *et al.*, 2014). Designs were then fed into a Scanning electron micrograph to etch the patterns into a Si wafer. This wafer was then used as a mold in our lift-off nanocontact printing process where NOA lift-off stamps are fabricated through a two-step replication process. PDMS intermediate stamps were first replicated from electron-beam patterned silicon wafers. These intermediate stamps are then used to create complementary replicates of the intermediate stamp, or exact replicates of the silicon wafer, out of photocurable norland optical adhesive (NOA). These lift-off NOA stamps are then used in lift-off nanocontact printing where activated lift-off stamps were contacted with protein coated flat PDMS stamps. In the regions of contact, the protein transfers to the lift-off stamp, whereas in the location of the nanoholes no contact is made, and the protein remains as a nanopattern on the flat PDMS stamp. The remaining protein on the flat stamp was then transferred to an activated glass surface through stamping. Protein patterned glass surfaces were then backfilled with a reference surface (75 % PEG : 25 % PDL) before cell seeding.

4-4.2 Axonal navigation on DNG arrays

To determine how the geometry of substrate bound gradients influences axonal navigation, which we define as the propensity of an axon to grow out and turn towards the higher printed protein density, we designed an array of 100 distinct DNGs (**Figure 4-3**) (Ongo *et al.*, 2014). The array consists of a wide range of gradients of which a key subset was employed to conduct the experiments reported herein. Axon navigation on the gradients was characterized by first

locating the position of the soma with respect to the gradient. A line was then traced from the soma to the tip of the longest neurite and the length and direction of growth relative to the gradient extracted. These values were then plotted on log plots where the dot color indicates the position of the soma on the gradient, the distance from the center corresponds to the length of the neurite, and angle of the arrow indicates the measured direction of growth relative to the gradient (**Figure 4-3**). An average vector was calculated and superposed on the log plot of each gradient and a color attributed: green indicates strong attraction, yellow no response, and red repulsion. Response plot arrays were then created where the axonal response for each of the DNGs in the array can easily be distinguished for embryonic rat cortical neurons grown on either netrin-1 (**Figure 4-4**) or PDL (**Figure 4-5**) and for embryonic rat spinal commissural neurons on netrin-1 (**Figure 4-8**).

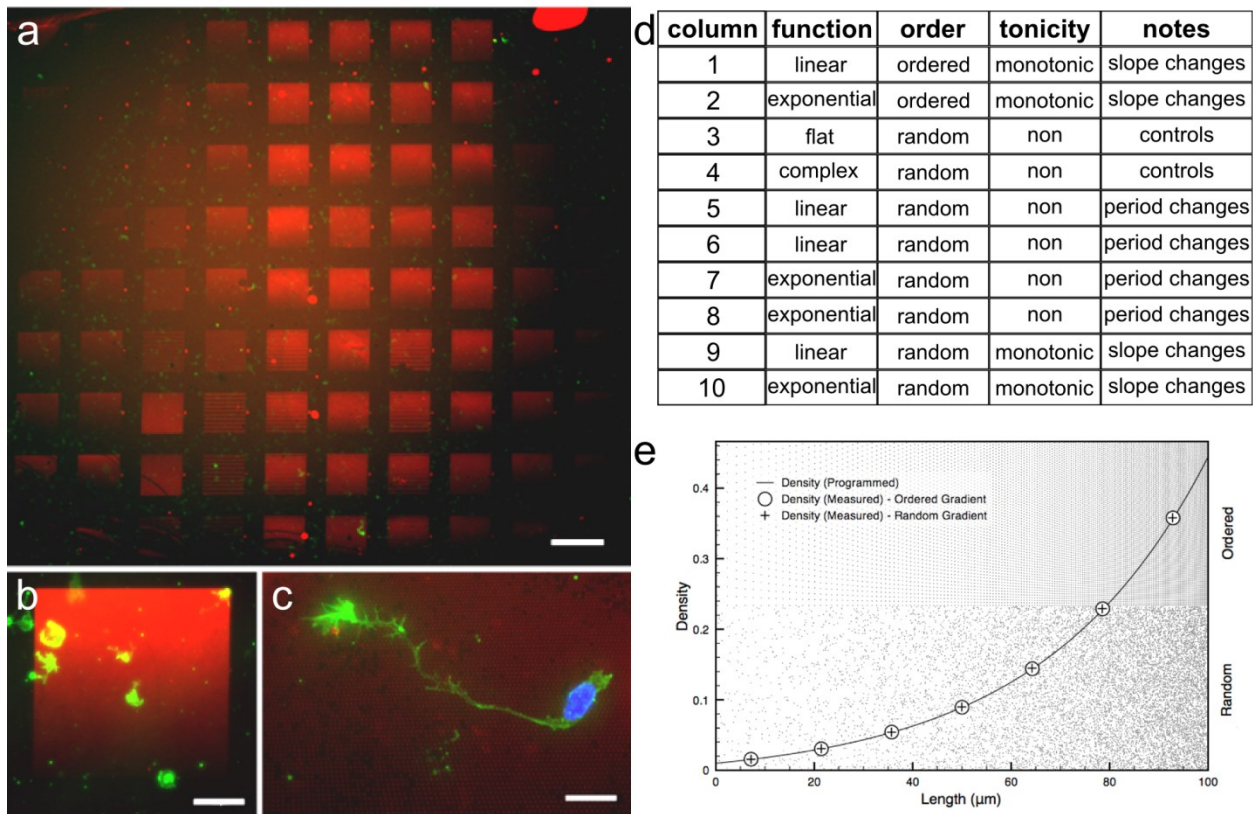


Figure 4-3. Presentation of DNG array. (a) Fluorescence image of a netrin-1 DNG array (red) seeded with neurons stained for actin (green) and nuclei (blue). (b) fluorescence image of a single gradient and (c) of a single neuron grown on the gradient. (d) table describing the gradients briefly. (e) Exemplary gradient demonstrating the concept of randomness where an ordered and random DNG follow a same exponential function. Scale bars are (a) 500 μm , (b) 100 μm , and (c) 10 μm .

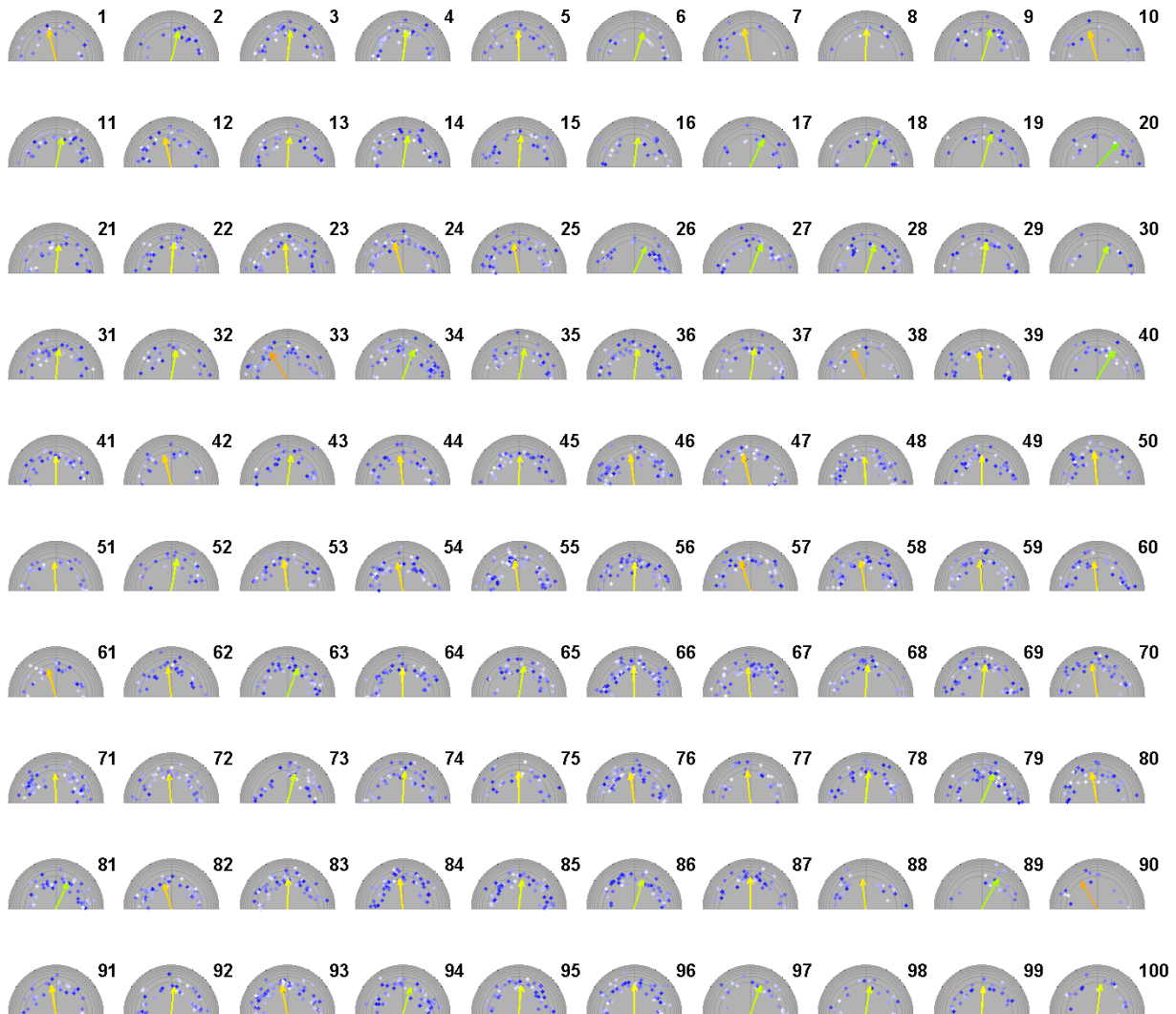


Figure 4-4. Response plots of cortical neurons to netrin-1 DNGs. The numbers represent the gradient numbers based from our gradient array, dots indicate individual neurons counted, and

the shade of blue represents the starting position of outgrowth with respect to the gradient (light blue, low density; dark blue, high density). The distance of the dots from the center indicates the length of the outgrowth, where each plotted semi-circle on the log scale indicates 50 μm . The vector direction and magnitude represents the average neuron response for that specific gradient and the color of the vector represents the response with red indicating repulsion, yellow no response, and green attraction. $n = 3,808$ neurons in 35 experiments.

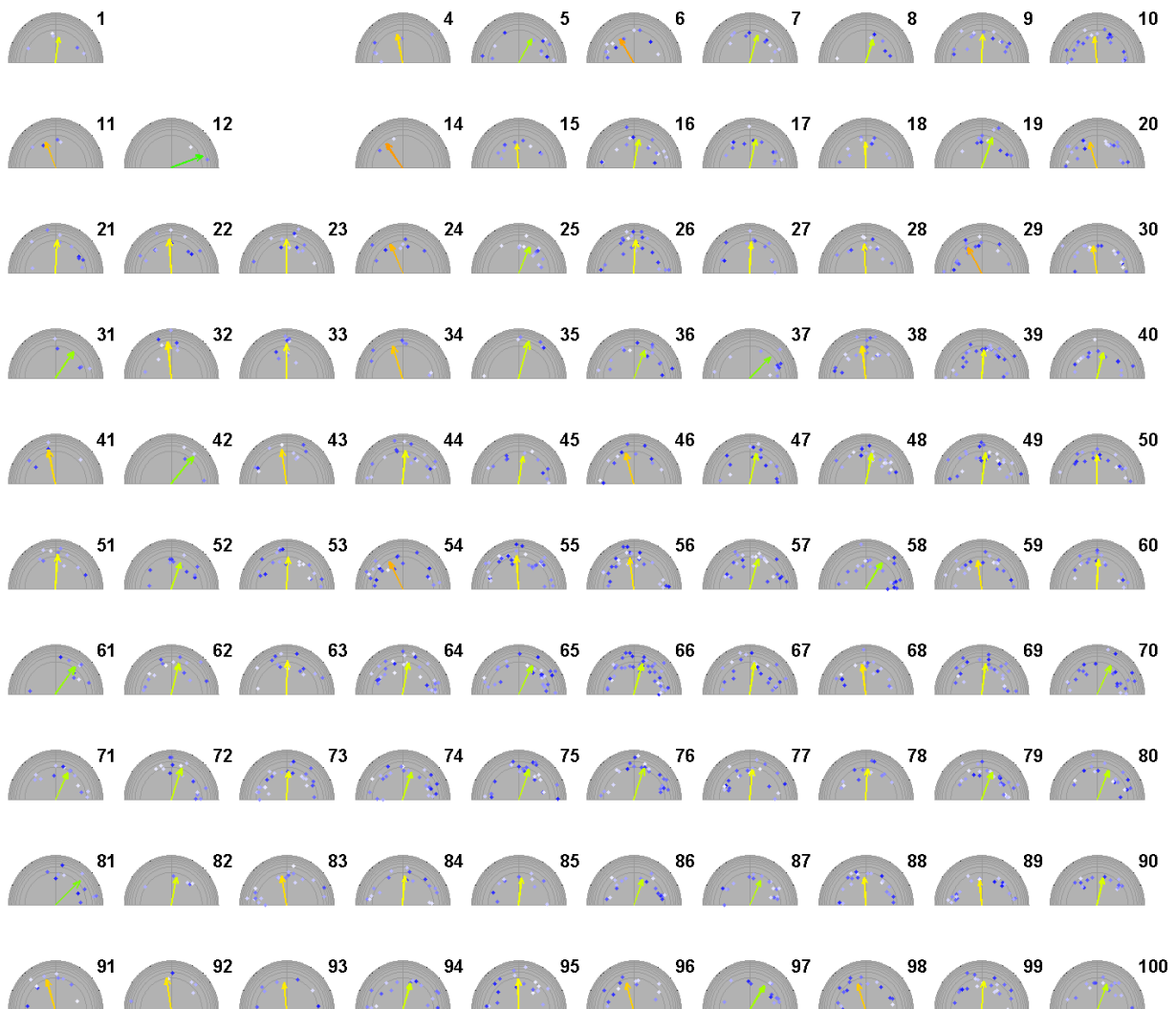


Figure 4-5. Response plots for cortical neurons to PDL DNGs. $n = 1,558$ neurons in 14 experiments.

4-4.3 Axonal outgrowth and turning are maximized on shallow ordered gradients of netrin-1

The preferred direction of growth relative to the gradient and axon outgrowth of cortical neurons were compared on gradients of different slopes ranging from steep to shallow (**Figure 4-6a**), functions following linear or exponential trends, and different levels of order (ordered or random) (**Figure 4-6b**). On netrin-1 gradients, the angle of growth of the longest neurite was the highest on exponential ordered gradients of shallow slopes, whereas on the four shallowest gradients, the angle of growth ranged from +17-43° (**Figure 4-6c**). This represents on average a 6-fold increase in the attractive response of cortical neurons to the netrin-1 DNG when the gradient is shallow in comparison to the response on steep gradients. A similar trend towards the largest response being evoked by the shallowest gradients was observed on ordered linear gradients; however, the increase was much more subdued with only a 1.25 fold increase. On random exponential gradients, the increase in attractive turning response was 7-fold, whereas on linear random gradients, the difference was insignificant. The angles of growth on shallow exponential random DNGs were only on average +9.8°, or 2.8-fold, lower than the attractive response observed on ordered exponential gradients. Cortical neuron navigation on negative control IgG gradients of the same geometry where a +43° angle of growth was observed on netrin-1 DNGs, resulted in a +15° angle of growth or a threefold decrease in turning response which confirms that the observed response stems from the patterned netrin-1 (**Figure 4-7**).

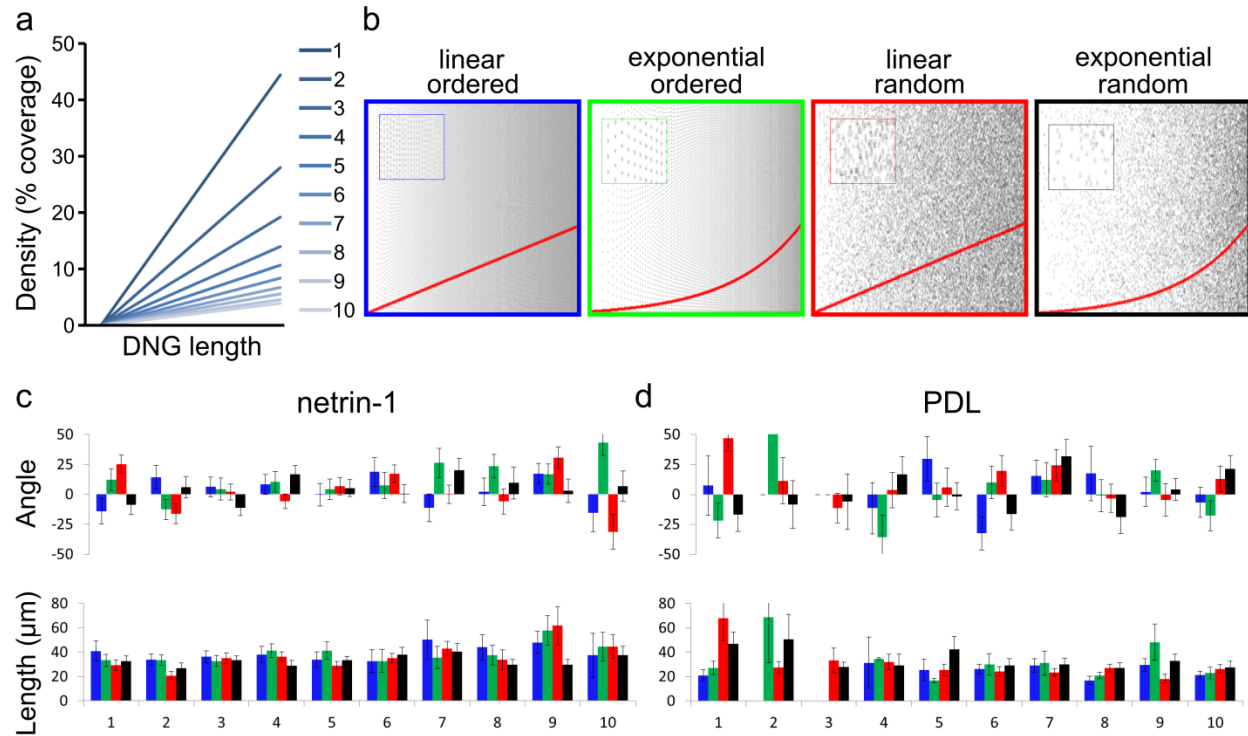


Figure 4-6. Cortical neurons make the strongest angular turn with respect to the gradient direction on shallow ordered exponential gradients of netrin-1. (a) Density curves of the 10 different gradients going from 1 with a steep slope with a maximal density of 44% coverage to shallow gradients where gradient 10 has a maximum density of 4%. (b) Schematic representation of DNGs at the steepest slope: ordered/linear (blue), ordered/exponential (green), random/linear (red), and random/exponential (black). Insets show a same magnified section of the 4 gradients. (c) Histograms of axonal turning and outgrowth for cortical neurons on netrin-1 and PDL gradients. For netrin-1 $n=15-60$ neurons/DNG and for PDL $n=2-23$ neurons/DNG, mean \pm std. err.

Comparisons of the extent of axon outgrowth on the same netrin-1 DNGs revealed that slope did not significantly affect outgrowth within the examined range of slopes. However function and outgrowth were shown to significantly impact the outgrowth length of the longest

neurite. Superior outgrowth was observed on ordered gradients with an average increase in outgrowth of 13% on linear gradients and 21% on exponential gradient. Altogether, this data suggests that axons of cortical neurons are best guided by DNGs of netrin-1 that are shallow, ordered, and exponential slopes.

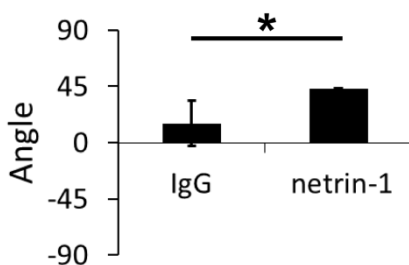


Figure 4-7. Cortical neurons turn specifically on netrin-1 DNGs. Preferred angular direction of growth of cortical neurons on ordered exponential DNG #20 composed of IgG and netrin-1. For netrin-1 n= 22 neurons/DNG and for IgG n=8 neurons/DNG, mean± std. err. * indicates statistical significance through ANOVA where $p=0.42 \times 10^{-5} < 0.05$.

4-4.4 Different neuron populations respond differently to substrate-bound netrin-1 gradients

We then assessed the navigational variance on substrate-bound netrin-1 gradients among different neuron populations. The strong response of cortical neurons observed on exponential ordered DNGs was compared to that of spinal commissural neurons (**Figure 4-8**). There was no significant difference was detected in the length of outgrowth in the axons between the two populations (**Figure 4-9**), In contrast, the preferred angle of growth with respect to the gradient of spinal commissural axons was lower than that observed with cortical neurons on the same netrin-1 DNGs, with an average angle of growth of +3° for spinal commissural neurons compared to the +14° turning observed in corticals. Furthermore, the increased turning response towards the higher density of netrin-1 observed on shallower slopes with cortical neurons was

not reproduced with spinal commissural neurons. This suggests that optimal gradient geometries will vary among neuron populations.

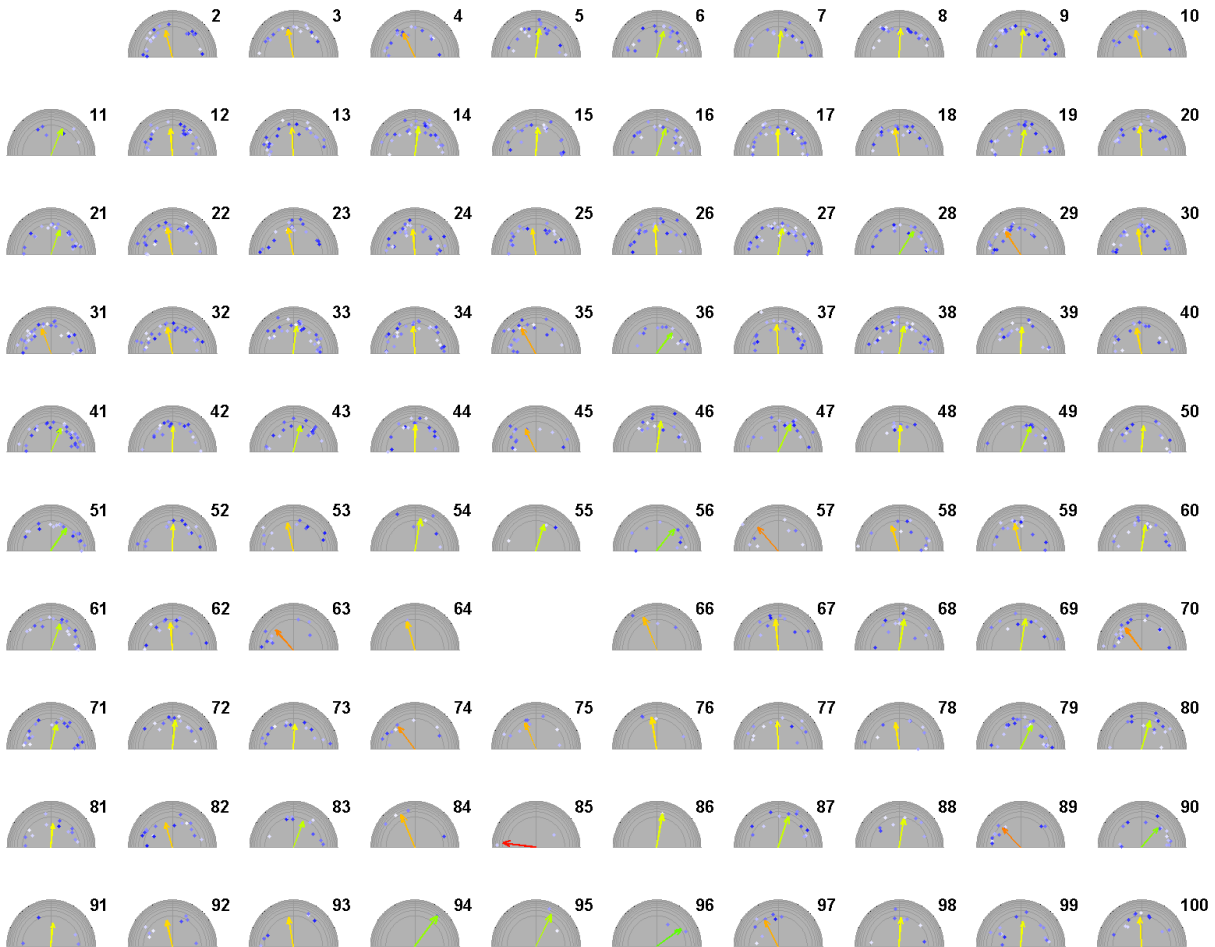


Figure 4-8. Response plots for spinal commissural neurons to netrin-1 DNGs. n=1,500 in 16 experiments.

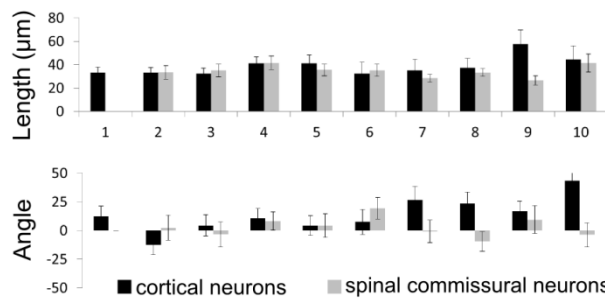


Figure 4-9. Axon navigation difference between cortical and spinal commissural neurons on netrin-1 DNGs. Corticals (black) and spinal commissural (gray) neurons were seeded on ordered exponential netrin-1 gradients of different slopes (Figure 5a) and grown for 2 DIV. The length and preferred angular outgrowth of the longest neurite for each neuron was measured and

the average for each reported in the histograms. n= 19-39 neurons/ DNG, mean± std. err.

4-4.5 Gradients of a permissive cue are sufficient to guide axonal navigation

Chemotropic responses differ critically depending on the patterned cue (Mai, Fok et al. 2009), the developmental stage of the neuron (Yam, Kent et al. 2012), and even the reference surface that surrounds the patterned surface (Ricoult, Thompson-Steckel et al. 2014). We previously demonstrated that altering the reference surface can change the cell-surface affinity, a metric free of mechanistic assumptions to characterize surfaces in cell choice assays, and thus can be employed to define the navigational route that neurons take as they travel through their environment. It remains to be shown whether gradients of molecules that are thought function merely by increasing affinity in the absence of guidance cues can be used to guide neurons to a specific target. To address this question, we patterned substrate-bound polylysine gradients and characterized the navigation of cortical neurites on these substrates (**Figure 4-6d**).

We first characterized the turning response of the cortical neurites and identified that contrary to the netrin-1 substrates, disorder resulted in a greater attractive turning response of neurites with a slight increase on linear gradients and a 2-fold increase on exponential gradients. Furthermore, the attraction on exponential gradients was superior to linear gradients with 52% and 10% increases in turning response for ordered and random gradients respectively.

Next, we characterized neurite outgrowth with no difference recorded for neurite length when comparing ordered and random DNGs. However, a significant ~20% increase in outgrowth was observed on exponential DNGs over outgrowth on linear DNGs (23% on random, 16% on ordered).

Despite the clear response of cortical neurons to affinity DNGs, the axonal response to PDL gradients in comparison to netrin-1 was inferior with an average outgrowth of 29 μm on

PDL versus the 37 μm outgrowth observed on netrin-1. Similarly, the average turning response for all the monotonic observed gradients, axons turned by $+4^\circ$ on PDL compared to $+6^\circ$ on netrin-1.

4-4.6 Non-monotonic gradients guide neurons at specific periodicity

Due to inhomogeneities in biological gradients, the gradient density slope when examining a single 2D slice is non-monotonic. The extent to which this micrometer variance impacts navigation has not been investigated and we thus designed non-monotonic gradients to test whether neurons can sense gradient direction despite the presence of variance in protein density at the microscale in the gradient.

We seeded cortical and spinal commissural neurons on non-monotonic gradients of netrin-1 or PDL ranging from 0.02% density to 44% density with 50 evenly spaced oscillations at an 8 μm periodicity and amplitude of 7.5% along the curve. The slopes followed either linear or exponential functions (**Figure 4-10**). Regardless of the patterned protein on the substrate or the neuron type, neurites extended an average of $34 \pm 1.5 \mu\text{m}$. Preferred angular growth was however significantly affected by the function of the gradient. If the gradients followed an exponential slope, neurites were relatively strongly attracted to the higher protein density with an average of $+24^\circ$, whereas on linear gradients the average turning response was -8° , representative of a weak repellent response.

In comparison to monotonic DNGs, axonal navigation observed on non-monotonic DNGs resulted in a $\sim 3\%$ decrease in outgrowth and a $\sim 31\%$ decrease in turning response. Even though an attractive response still occurred, its magnitude was weakened due to the inhomogeneity present in the gradient. This suggests that the strongest axonal response would

result from a DNG gradient deficient of variation at the nanoscale level of resolution (*i.e.* an ordered DNG) and at the microscale level of resolution (*i.e.* a monotonic DNG).

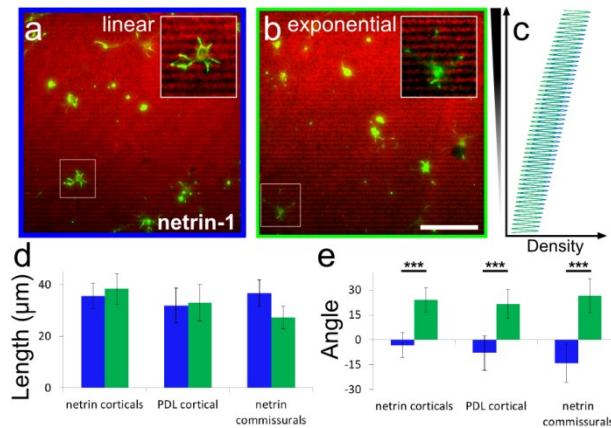


Figure 4-10. Neurons respond to non-monotonic netrin-1 and PDL gradients. Cortical neurons were grown, fixed, and stained for filamentous actin (green) on random non-monotonic gradients of netrin-1 (red) which followed either (a) linear (DNG #59) or (b) exponential functions (DNG #79) for 2 DIV. Boxes indicate the location of the cell that has been magnified in the inset. (c) Density curves along the length of the random non-monotonic gradients for the linear (blue) and exponential (green) are shown. Fluorescence decay on the edge of the gradient results from fluorescence spreading on the edge of the gradient. Neurite (d) outgrowth length and (e) preferred angular growth with respect to the gradient of cortical neurons on netrin-1 DNGs, cortical neurons on PDL DNGs, and commissural neurons on netrin-1 DNGs was compared on linear (blue) and exponential gradients (green) for both gradients investigated (n= 15-49 neurons, mean \pm std. err, *** indicates $p > 0.01$). Even though outgrowth does not differ between linear and exponential DNGs for the conditions assayed, the angle of outgrowth for each condition was significantly higher on exponential gradients. Scale bar is 100 μm .

4-5 Conclusions

Here we have used printed DNGs of netrin-1 and PDL to investigate axonal navigation *in vitro* and demonstrate that by implementing this haptotaxis assay, large data sets of the axonal navigation on each of 100 distinct gradients in our array can easily be acquired in parallel. Following confirmation that neurons do sense the netrin-1 nanopatterns, we then determined that ordered gradients maximize outgrowth, whereas shallow ordered exponential gradients maximize turning. We then provided the first report of an affinity gradient where PDL was patterned and upon which neurons responded, albeit more weakly than they did on DNGs of netrin-1. Lastly, we demonstrate that neurons maintain a weaker response to gradients despite the presence of microscopic variance introduced through a non-monotonic function. Overall we demonstrate, that ordered exponential DNGs of shallow slopes yield the strongest neurite outgrowth and preferred direction of outgrowth with respect to the gradient. Furthermore, we identify these to be key parameters for patterns of the well characterized chemotropic guidance cue netrin-1, but also for gradients of PDL, which is considered a permissive cue that increases affinity, but not a tropic guidance cue. These findings suggest that a permissive adhesive cue, when patterned as a gradient, may have the capacity to function as a tropic axon guidance cue. The validation of the method presented provides a means to rapidly address how navigation is impacted by the geometry of gradients of substrate bound cues. Lastly, the data we present serves as starting parameters upon which future studies can further tune the gradient geometry to identify the optimal gradient to drive axonal navigation.

4-6 References

- Chedotal, A. and L. J. Richards (2010). "Wiring the Brain: The Biology of Neuronal Guidance." Cold Spring Harbor Perspectives in Biology **2**(6).
- Dickson, B. J. (2002). "Molecular mechanisms of axon guidance." Science **298**(5600): 1959-1964.
- Fricke, R., P. D. Zentis, et al. (2011). "Axon guidance of rat cortical neurons by microcontact printed gradients." Biomaterials **32**(8): 2070-2076.

- Hong, K. S., L. Hinck, et al. (1999). "A ligand-gated association between cytoplasmic domains of UNC5 and DCC family receptors converts netrin-induced growth cone attraction to repulsion." *Cell* **97**(7): 927-941.
- Kane, R. S., S. Takayama, et al. (1999). "Patterning proteins and cells using soft lithography." *Biomaterials* **20**(23-24): 2363-2376.
- Keino-Masu, K., M. Masu, et al. (1996). "Deleted in Colorectal Cancer Encodes a Netrin Receptor." *Cell* **87**(2): 175-185.
- Kennedy, T. E., T. Serafini, et al. (1994). "Netrins are diffusible chemotropic factors for commissural axons in the embryonic spinal cord." *Cell* **78**(3): 425-435.
- Kennedy, T. E., H. Wang, et al. (2006). "Axon guidance by diffusible chemoattractants: A gradient of netrin protein in the developing spinal cord." *Journal of Neuroscience* **26**(34): 8866-8874.
- Mai, J., L. Fok, et al. (2009). "Axon Initiation and Growth Cone Turning on Bound Protein Gradients." *Journal of Neuroscience* **29**(23): 7450-7458.
- Moore, S. W. and T. E. Kennedy (2001). Dissection and Culture of Embryonic Spinal Commissural Neurons. *Current Protocols in Neuroscience*, John Wiley & Sons, Inc.
- Ongo, G., S. G. Ricoult, et al. (2014). "Ordered, Random, Monotonic and Non-monotonic Digital Nanodot Gradients". *Plos One*, Accepted.
- Ricoult, S. G., M. Pla-Roca, et al. (2013). "Large Dynamic Range Digital Nanodot Gradients of Biomolecules Made by Low-Cost Nanocontact Printing for Cell Haptotaxis." *Small* **9**(19): 3308-3313.
- Ricoult, S. G., G. Thompson-Steckel, et al. (2014). "Tuning cell-surface affinity to direct cell specific responses to patterned proteins." *Biomaterials* **35**(2): 727-736.
- Ricoult, S. G., G. Thompson-Steckel, et al. (2014). "Tuning cell-surface affinity to direct cell specific responses to patterned proteins." *Biomaterials* **35**(2): 727-736.
- Roy, J., T. E. Kennedy, et al. (2013). "Engineered cell culture substrates for axon guidance studies: moving beyond proof of concept." *Lab on a Chip* **13**(4): 498-508.
- Rozario, T. and D. W. DeSimone (2010). "The extracellular matrix in development and morphogenesis: A dynamic view." *Developmental Biology* **341**(1): 126-140.
- Serafini, T., T. E. Kennedy, et al. (1994). "The Netrins Define a Family of Axon Outgrowth-Promoting Proteins Homologous to C-Elegans Unc-6." *Cell* **78**(3): 409-424.
- Shirasaki, R., C. Mirzayan, et al. (1996). "Guidance of circumferentially growing axons by netrin-dependent and -independent floor plate chemotropism in the vertebrate brain." *Neuron* **17**(6): 1079-1088.
- Sun, K. L. W., J. P. Correia, et al. (2011). "Netrins: versatile extracellular cues with diverse functions." *Development* **138**(11): 2153-2169.
- Tessier-Lavigne, M. and C. S. Goodman (1996). "The molecular biology of axon guidance." *Science* **274**(5290): 1123-1133.
- von Philipsborn, A. C., S. Lang, et al. (2007). "Substrate-Bound Protein Gradients for Cell Culture Fabricated by Microfluidic Networks and Microcontact Printing." *Sci. STKE* **2007**(414): pl6-.
- von Philipsborn, A. C., S. Lang, et al. (2006). "Growth cone navigation in substrate-bound ephrin gradients." *Development* **133**(13): 2487-2495.
- Xu, K., Z. H. Wu, et al. (2014). "NEURAL MIGRATION Structures of netrin-1 bound to two receptors provide insight into its axon guidance mechanism." *Science* **344**(6189): 1275-1279.

Yam, P. T., C. B. Kent, et al. (2012). "14-3-3 Proteins Regulate a Cell-Intrinsic Switch from Sonic Hedgehog-Mediated Commissural Axon Attraction to Repulsion after Midline Crossing." Neuron **76**(4): 735-749.

CHAPTER 5

Conclusions and Summary

5-1 Summary

In this dissertation, we developed an easy and low-cost procedure to create substrate-bound protein gradients where the gradient geometry can be controlled in unprecedented ways. The procedure also ensures that cell response to the patterned protein occurs through appropriate biochemical signaling pathways and therefore minimizes the possibility of misinterpreting the acquired data. An array of 100 distinct gradients was then printed using this procedure to investigate how gradient geometry impacts axonal navigation.

In Chapter 1, we reviewed the methods that have been developed to pattern substrate-bound protein gradients and evaluate the available them based on a number of characteristics which allows us to suggest preferred methods for specific applications. We also review the axonal navigation findings that have been reported using these assays. In Chapter 2 we then developed a low-cost lift-off nanocontact printing method and new gradient designs which overcame limitations of the existing state of the art technologies and produced gradients of record dynamic range, comparable to the expected range in biological gradients. In Chapter 3, we then keyed the term reference surface for the non-patterned surface which plays a critical role in how cells respond to patterned protein. We then devised an approach whereby we mix two different solutions, one of high affinity and one of low affinity, at different ratios to identify a ratio at which cells respond to the patterned protein via appropriate biochemical pathways. Lastly, we introduced cell-surface affinity curves which better represent cell response while

contextualizing the reference surface. Altogether, these methods open up new avenues to investigate cell navigation but also other cellular mechanisms.

Finally, in Chapter 4, we combined the digital nanodot gradient design, low-cost lift-off nanocontact printing, and the approach to tune the reference surface to create an array of 100 distinct gradients which vary in geometry to address axonal navigation by embryonic rat cortical neurons and spinal commissural neurons on substrate-bound gradients composed of netrin-1 or PDL. We identified geometrical parameters at which axonal turning towards the higher protein density was maximized and a strong positive turning response of up to $+43^\circ$ observed, we demonstrated that affinity gradients in the absence of a chemotropic cue can also be used to guide neurons, despite a 33% weaker turning response in comparison to gradients of chemotropic cues. Lastly we implemented variations in the gradients via non-monotonic functions to represent the inhomogeneity of 3D biological gradients. The addition of these microscale variations led to a 31% reduction in axonal turning response.

5-2 Conclusions

We present a technically innovative haptotaxis assay composed of digital nanodot gradient designs, a low-cost lift-off nanocontact printing process, and an approach to control the reference surface. The gradients achieved using the novel designs reached an unprecedented dynamic range appropriate to study biological gradients. The ease of the low-cost lift-off nanocontact printing method makes the rapid protein nanopatterning of large surfaces available to the general scientific community for the first time. The introduction of the concept of a reference surface and the framework for quantitative cell choice assays provide a means to achieve a cell response to surface-bound protein patterns through predictable biochemical pathways. The presentation of the cell response data in cell-surface affinity curves for the first time contextualizes the reference surface. This enables cross-comparisons among different cells and different patterned proteins

which is essential in all surface-based cellular assays and might even extend into other types of bioassays. The combination of these new methods was then used to create an array of 100 distinct gradients that were used to make a number of biological findings pertaining to the impact of gradient geometry on axonal navigation. For instance, we showed that gradients with an ordered dot arrangement and a shallow exponential curve resulted in the strongest turning response observed within the geometries screened with a $+43^\circ$ angle on netrin-1 gradients. Furthermore, we provide the first report that gradients of permissive cues in the absence of chemotropic cues suffice to guide neurons, albeit to a weaker extent than chemotropic gradients. We also showed that the presence of microscale variations in the gradient decrease the axonal navigation turning response but that neurons maintain their ability to read the gradient as long as the variance remains small. The technical innovations presented here open up doors to investigate cellular biology, while the biological findings, being the first of their kind, provide a starting point for future studies where the range of gradients can be further titrated by for instance focussing on shallower gradients to potentially induce an even stronger response. Beyond the enhanced knowledge of axon navigation achieved through this work, this information might also serve towards the development of better implantable biomaterials.

5-3 Limitations

The presented setup overcomes many limitations of past methods. As a result of its low-cost and straight forward procedure, for the first time, nanopatterning becomes widely accessible among other attributes. Further studies could contribute to the betterment of the presented method in a number of ways.

The lift-off nanocontact printing method could be perfected by extending the resolution of the technique and reaching single molecule resolution which would increase the biological relevance of the patterns over the current protein clusters that are 200 nm in diameter, which

represents an aggregate of approximately 33 netrin-1 proteins for instance. Additionally, this clustering limits the level of randomness that can be replicated and it doesn't fully fulfill the needs required to study biological randomness which occurs at the single molecule scale. Furthermore, cells grow in complex environments where they are constantly simultaneously exposed to multiple proteins and this environment might induce different cell responses than exposure to single proteins does. Multiple cues could be presented in the protein nanopatterns. For instance, by aligning gradients of different proteins and geometries and sequentially printing them on a same surface. Ideally, individual dots composed of multiple proteins could be positioned in intertwined arrangements where each maintains a graded distribution. Lastly, as mentioned in Chapter 1, gradient geometries change as development of the organism progresses. Implementation of this temporal dynamic aspect in the protein nanopattern would enable the study of temporal gradient modifications and the impact it holds on axonal navigation. This could for example be achieved by patterning the DNGs on stretchable substrates that could be extended over time and change the geometry of the bound protein pattern. Alternatively, the ability to change the pattern geometry in space and time would facilitate the guidance of neurons over very large distances or it might also enable the ability to change the pattern to redirect axons that may have become misguided. One potential means to achieve this would be to pattern light-sensitive biomolecules and use a microscope to change the conformation of proteins in specific locations on demand.

To create our reference surface we use two synthetic molecules: PDL and PEG. The most obvious modification that could be implemented is their replacement with biologically relevant molecules that are commonly present in the ECM and which would better mimic the environment *in vivo* and the choices that cells are subjected to. This would require the

identification of a high affinity and a low affinity molecule that could be mixed in a similar fashion as PDL and PEG to determine an ideal RS for specific experiments. The disadvantage of implementing biologically relevant molecules in the RS is the faster degradation of the molecules, but measures could be taken to extend the lifetime of these molecules to match that of the patterned molecules.

A current limitation of the presented process is the size of the data set that is generated in a single experiment. For instance, when imaging each of the 100 DNGs with a 20x objective every 5 min over 48 hrs, a >25 GB multidimensional timelapse file was generated. Manual analysis of such large data is extremely time consuming and nearly impossible. To facilitate the analysis of such large data sets, implementation of automated analysis and data extraction processes will be needed. Such software would require the identification of the soma, axon and growth cones from brightfield images or alternatively the neurons could be stained with a vital dye such as DiI to facilitate identification (Keenan et al., 2006). Comparison of the location of the growth cone between subsequent images over time would then have to be conducted to extract parameters such as outgrowth, turning, growth cone speed, and growth cone area. Until such an automated analysis tool is implemented, progress using this technique will be limited by manual image analysis and data extraction.

A limitation of the present analysis is that, in the absence of such an automated analysis tool, results were obtained from fixed cultures where a single timepoint is captured at the end of axonal outgrowth. This process overlooks the fundamental fact that axonal navigation is a dynamic process and that many alternative facets of neuronal navigation might be revealed through dynamic analysis. To achieve reliable significance in the data, larger populations will have to be analysed, increasing the requirement for automation. It is however expected that the

development of analysis tools to extract data from timelapses series of extending axons will decrease the number of neurons that need to be analyzed by revealing the exact trajectory followed by the neuron instead of the final outgrowth vector.

5-4 Outlook

The future directions of the work presented in this dissertation are on two levels: method development and biological implementation. As mentioned above, the method could be further enhanced by developing dynamic gradients, reducing the feature size, or by developing mosaic gradients composed of multiple proteins. The method will also be implemented to advance our understanding of haptotaxis and axonal navigation. For instance, a second DNG array could be designed composed of a range of more shallow gradients which will serve to identify the minimal gradient slope that neurons can sense.

Alternatively, implementation of our assay could be directed toward the creation of substrate-bound multi-protein gradients to replicate, for instance, the pattern of guidance cues in the embryonic spinal cord where neurons are simultaneously and subsequently exposed to multiple gradients as they navigate towards their ultimate synaptic target. This would also provide the tools required to investigate the molecular mechanism that results in a cell switching its response to cues over time. Another suitable application for these multi-protein gradients would be to test whether gradients of permissive cues can compete with chemotropic gradients to guide neurons or if the pull of an affinity gradient in the opposite direction from that of a chemotropic gradient reduces the navigational response of neurons.

As described in the introduction, proteins in gradients can be either surface-bound or freely diffusible, and it is possible that the same protein be present in both states. To study how a same protein may relay different messages based on its state, it would be interesting to investigate how cells respond to the same protein in either state. Furthermore, cells could

simultaneously be exposed to opposite gradients of the same protein in both states to determine if one protein state induces a stronger cell response than the other.

The preliminary axonal navigation results provide some insight into the mechanism of haptotaxis. For instance, the validation that changes in protein nanodot density can be used to guide neurons across a 2D substrate suggests that changes in substrate-bound protein density at the nanoscale *in vivo* might play a similar role. Furthermore, the reduction in preferred direction of outgrowth with respect to the gradient when the nanodot arrangement is pseudorandom instead of ordered highlights the importance of protein arrangement at the nanoscale. Lastly, the strongest response observed on the 100 gradient geometry screen that we conducted occurred on a shallow exponential gradient with minimal and maximal densities of 0.02% and 4%, respectively. This gradient had slopes of 0.006%/μm, 0.009%/μm and 0.016%/μm at the low, middle and high density portions of the gradient. This a) confirms that cortical neurons have a very keen ability to sense gradient direction and b) suggests that growth cones might saturate faster on steeper gradients hindering their ability to sense the gradient and that even shallower gradients might induce stronger responses. Such questions as well as others can now be probed in great depth with the method presented here. Other questions that can now be probed with this assay are an in depth analysis of the cytoskeleton and receptor arrangement in the growth cone as axonal navigation takes place. Alternatively, function blocking studies could be conducted on the gradients to map out the molecular pathways at play which regulates the polarization of the growth cone and its directed motion.

The continued development of the technology introduced in this thesis by the addition of temporal control over the gradient geometry, the ability to create composite patterns, or further reducing the feature size will further increase its biological applications. These amendments to

the method will facilitate the study of cells in more complex cellular environments that are more appropriate to investigate parameters present *in vivo* such as the temporal dynamic aspect or the presence of multiple proteins. The method presented herein provides the tools required to probe haptotaxis and to extract critical information on the mechanism. With additional modifications such as the ones mentioned above, this method has the potential to become one of the go to methods to create substrate-bound protein patterns.

5-5 References

Keenan, T. M., A. Hooker et al. (2006). " Automated identification of axonal growth cones in time-lapse image sequences." *Journal of Neuroscience Methods* 151(2):232-238.

PREFACE TO APPENDIX I

This chapter was published as a manuscript in the *Journal of Neuroscience Methods* in 2012. The chapter was included as an appendix because of the relevance of the technique developed here which served as a stepping stone in the development of the nanocontact printing process (Chapter 2) as well as the work on reference surfaces (Chapter 3). The inclusion of this chapter is therefore intended to introduce the reader to the basic concept of microcontact printing before adding the necessary modifications required for patterning at the nanoscale level of resolution.

This chapter was published as a research article in *Journal of Neuroscience Methods*
(Ricoult et al., 2012).

Acknowledgements

We thank Katherine Horn for comments on the manuscript, Karen Lai Wing Sun for insightful discussion, and Ben Rappaz for assistance with imaging. Grégoire Morisse, Jenea Bin and François Beaubien provided the astrocytes and neuronal cells used in these experiments. This work was supported by the Canadian Institutes of Health Research (CIHR). SGR and JSG were supported by Jeanne Timmins Costello Studentships. SGR was also supported by the NSERC Integrated Sensor System Program. DJ holds a Canada Research Chair. TEK is a Killam Foundation Scholar and holds a Chercheur Nationaux award from the Fonds de la Recherche en Santé du Québec.

Appendix I

Generation of MicroIsland Cultures using Microcontact Printing to Pattern Protein Substrates

Sébastien G. Ricoult^{1,2,3}, Jennifer S. Goldman¹, David Stellwagen⁴, David Juncker^{1,2,3} and Timothy E. Kennedy¹

¹McGill Program in NeuroEngineering, Department of Neurology and Neurosurgery, Montreal Neurological Institute, McGill University, 3801 University Ave., Montreal, Quebec, Canada H3A 2B4; ²McGill Program in NeuroEngineering, Department of Biomedical Engineering, McGill University, 740 Dr. Penfield Avenue, Montreal, Quebec, Canada H3A 0G1; ³Genome Quebec Innovation Centre, McGill University, Montréal, Quebec, Canada H3A 1A4; ⁴Centre for Research in Neuroscience, McGill University, Montreal, Quebec, Canada H3G 1A4.

AI-1. Abstract

The capacity to isolate small numbers of neurons *in vitro* is an essential tool to study the cell biology of synapses and the development of neuronal networks by specific cell types. MicroIsland culture assays allow for single neurons, or simple neural networks, to be isolated on islands of glial cells; however, the techniques commonly used to produce microisland substrates are expensive, challenging to control, and typically result in many discarded substrates. Here, we used microcontact printing to pattern a glass surface with islands of extracellular matrix proteins known to support neural cell growth and differentiation. To promote segregation of the cells to the islands, the substrate surrounding the islands was backfilled with polyethylene glycol (PEG), forming a relatively non-permissive surface on which cell attachment is limited. Astrocytes, and subsequently hippocampal neurons, were then seeded onto the islands of patterned protein. Using this method, readily reproducible patterns of protein islands were produced that permit cell

attachment, differentiation, and growth. The technique is a rapid, inexpensive, and reliable means to generate patterned substrates appropriate for microisland cultures.

AI-2. Introduction

Since the earliest days of cell culture, researchers have attempted to reduce the complexity of *in vitro* culture conditions. MicroIsland culture techniques were developed to limit the number of cells making synaptic connections, or in the extreme, to study autaptic synapses made by one neuron onto itself (Segal et al., 1998). Initial microisland cultures isolated single neurons on a bed of heart cells. To create these islands of dissociated cardiac myoblasts and fibroblasts, a solution containing collagen was applied to a non-wetting polystyrene surface, causing the collagen solution to form beads. Drying created islands of collagen protein 300-500 μm in diameter, which were then used to segregate the myoblasts on the basis of preferential adherence to the islands of patterned protein. The myoblast islands were then used as a substrate for subsequent growth of neurons (Furshpan et al., 1986; Furshpan et al., 1976). This technique of using a non-wetting background was widely applied in studies of synaptogenesis and synapse function (Cardozo, 1993; Masuko et al., 1992), with subsequent modifications that patterned the islands using a microatomizer spray and changed the background to a thin layer of agarose (Bourque and Trudeau, 2000; Fasano, 2008; Jomphe et al., 2005; M.M. Segal, 1998). A drawback of this approach is the challenge of calibrating the spray produced by the microatomizer (Bourque and Trudeau, 2000; Fasano et al., 2008; Jomphe et al., 2005), and the production of significant waste due to the inefficiency of spraying. Although multiple techniques have been developed to isolate co-cultured cells, in general, they require specialized equipment and are not necessarily straight-forward (Goubko and Cao, 2009).

Over the past decade, microcontact printing (Bernard et al., 1998) has been increasingly applied to pattern protein substrates. The microcontact printing technique was first developed for

the field of electrical engineering to pattern a monolayer of thiols to protect portions of a layer of gold attached to a microchip from being exposed to etching solutions, in order to create gold electrodes (Kumar and Whitesides, 1993). The technique has been adapted to protein patterning and has been widely utilized for applications ranging from antigen detection (Chakra et al., 2009), to patterning gradients for studies of cell migration (von Philipsborn et al., 2007).

Novel applications of microcontact printed protein patterns have generally resulted from developing methods to print smaller patterns at increasingly higher levels of resolution. Here, to pattern substrates for microisland cell culture, we used microcontact printing to create relatively large islands, 125 μm in diameter, composed of either poly-D-lysine, fibronectin, laminin, geltrex, or netrin-1. To restrict cells to the patterned protein spots, patterned substrates were backfilled with poly-L-lysine-grafted-polyethylene glycol (PLL-g-PEG), a relatively non-permissive growth substrate. Astrocytes were first seeded onto the island array and grown to confluence on each spot. A relatively low concentration of hippocampal neurons was then seeded onto the pattern, which allowed islands containing one, or a few neurons, to be readily obtained. We demonstrate that this application of microcontact printing can be used to reliably generate reproducible islands of defined size, while decreasing the waste associated with methods commonly used to generate patterned substrates for microisland cell culture (**Figure AI-1**).

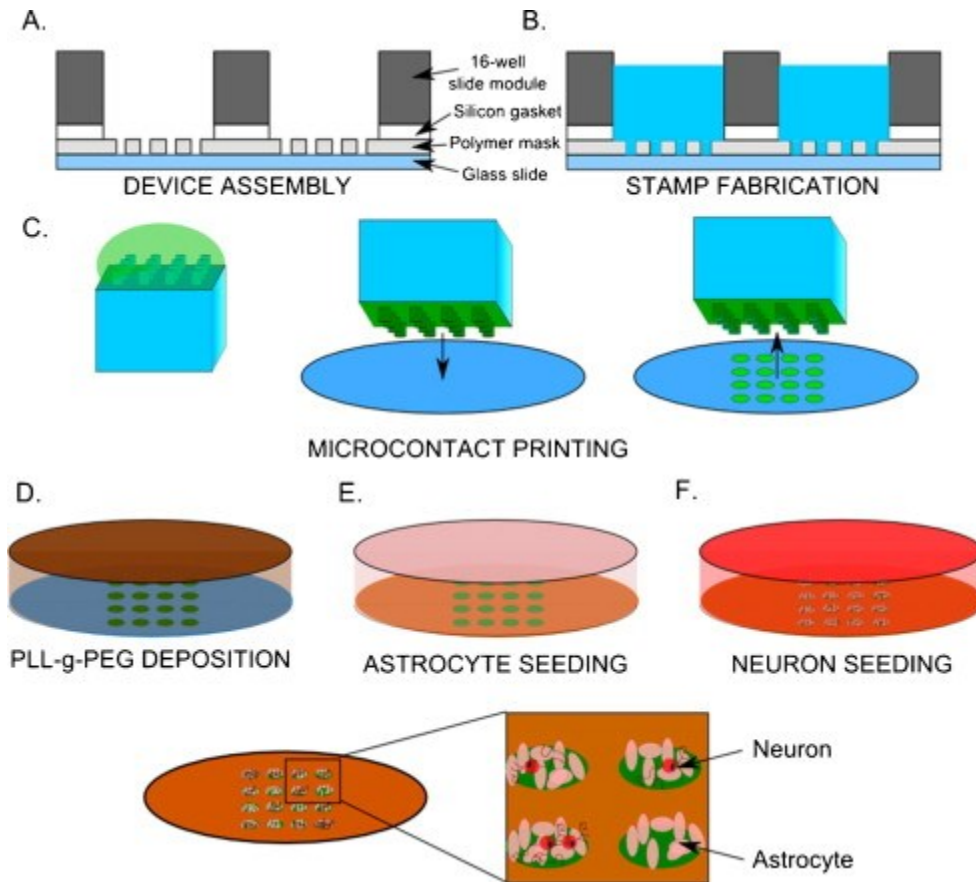


Figure AI-1. Diagram of protein patterning technology used to generate microisland cultures. (A) The device was assembled by gluing the PET polymer mask to a glass slide and overlaying a silicon gasket and slide module. (B) The wells of the slide module were then filled with mixed PDMS and cured overnight to yield stamps. (C) Next, stamps were inked with protein solution, before printing the protein onto a glass slide. (D) Once the protein was patterned onto the glass slide, the surrounding substrate was made non-permissive for cellular attachment and growth by coating with a PLL-g-PEG solution. (E) Astrocytes were grown on the substrate for 2 DIV before (F) seeding hippocampal neurons and growing them for 5-13 DIV. The technique yields cocultures of hippocampal neurons growing on isolated astrocyte microislands.

AI-3. Materials and Methods

Stamp preparation

Mold design: Arrays of circles 125 μm in diameter with a pitch of 300 μm in X and Y direction were designed in Clewin® (Wieweb Software, Hengelo, Netherlands). Upon completion, the

files were sent to Lasex (San Jose, CA, USA), where the patterns were laser-etched into 125 μm thick polyethylene terephthalate (PET) with a 501FL 3M adhesive backside.

Stamp manufacturing: Polydimethylsiloxane (PDMS) was prepared by reacting an ethylene terminated PDMS prepolymer with a poly (dimethylhydrosilane) Sylgard 184 cross linker (Dow Corning, Corning, NY, USA). The prepolymer and cross linker were mixed in a 10:1 ratio, respectively, with the help of a mixer pouring device composed of a two cartridge gun with a mixing dispensing tube (Dow Corning, Corning, NY, USA) as well as manual mixing to ensure homogeneity. The plastic protective layer was then removed from the glue side of the PET mask and the mask glued onto a clean glass slide. To ensure proper adhesion and complete removal of bubbles, the flat side of a razor blade was pressed onto the surface of the mask. In order to shape the stamps, a 16-well slide module (Grace Biolabs, Bend, OR, USA) was attached to the slide with a silicone gasket (Grace Biolabs, Bend, OR, USA). To facilitate the removal of the PDMS, a monolayer of perfluorodecyltriethoxysilane, (97%, Sigma-Aldrich, Oakville, ON, Canada) was deposited onto the surface of the assembly by evaporation in a dessicator (Bel-art, Pequannock, NJ, USA) for 30 min. Following silanization of the complex, 250 μl of the mixture was added to each well. To remove bubbles resulting from the manual mixing, the construct was first centrifuged at 1600 rpm for 5 min and then placed in a dessicator for 10 min. Any bubbles remaining at the surface were blown off with a gentle stream of compressed nitrogen gas before curing the PDMS in an oven (VWR, Ville Mont-Royal, QC, Canada) for 24 hrs at 60°C to activate the catalyst driven polymerization.

Following complete polymerization of the PDMS, the gasket was separated from the glass slide and the sealing layer peeled from the gasket exposing the cured polymer stamps. Each

stamp was then extracted from the gasket and slide module with tweezers. To remove low molecular weight PDMS and residual prepolymer present in the cured PDMS, the PDMS squares were extracted using 70% ethanol for 24 hrs followed by baking for 4 hrs at 60°C to remove ethanol by evaporation.

Microcontact printing: The quality of the stamps obtained was investigated under a microscope. The desired stamps were then placed in an ultrasonic bath containing 70% ethanol for 5 min for sterilization and then dried under a flow of nitrogen gas. After drying, the stamps were inked with 10 µl of either poly-D-lysine (5 µg/ml, PDL, 70-150 kDa, Sigma-Aldrich, Oakville, ON, Canada), netrin-1 (12.5 µg/ml, produced and purified as described (Serafini et al., 1994; Shirasaki et al., 1996)), laminin (10 µg/ml, mouse, Invitrogen, Burlington, ON, Canada), geltrex (25 µg/ml, mouse, Invitrogen, Burlington, ON, Canada) in DMEM, or fibronectin (25 µg/ml, mouse, Biopur, Bubendorf, Switzerland). A plasma cleaner (Plasmaline, Tegal, Petaluma, CA, USA) was used to remove the surface layer of organic compounds and oxidize the surface of the glass coverslips (Carolina Biologicals, Burlington, NC, USA). This renders the surface hydrophilic and allows solutions to spread on the surface of the coverslip and thereby cover the entire surface of the PDMS stamp. The solution was left at rt (~23° C) for 5 min in order for it to bind to the surface of the stamp. Once the incubation was complete, the stamp was rinsed for 15 sec with 1xPBS (Fisher Scientific, Ottawa, ON, Canada) and washed for 15 sec in double distilled water (Millipore, Billerica, MA, USA). After the two washes, the stamp was quickly dried with one strong puff of compressed nitrogen gas. The stamps were then immediately placed into contact with a plasma-activated glass coverslip for 5 sec, then peeled off and the printed coverslip immediately submerged in 1xPBS.

PEG backfill: To create a biologically inert surface where the proteins present in the serum cannot bind to the substrate, poly-L-lysine grafted polyethylene glycol (PLL(20 KDa)-g[3.5]-PEG(2 KDa), Surface Solutions, Dübendorf, Switzerland) at a concentration of 10 µg/ml in PBS was incubated on the coverslip for 15 min before washing off unbound PLL-g-PEG with 1xPBS.

Cell culture: Astrocytes were obtained from a mixed glial culture of newborn rat brain in which the oligodendrocytes were shaken off leaving behind a layer highly enriched in astrocytes (Armstrong, 1998). Astrocytes were then isolated through a 5 min exposure to trypsin at 37°C (Invitrogen, Burlington, ON, Canada) and then reseeded at a concentration of 25,000 cells per coverslip. The cells were then grown at 37°C in 5% CO₂ for 2 days in high glucose DMEM (Invitrogen, Burlington, ON, Canada), 10% Fetal Bovine Serum (Invitrogen, Burlington, ON, Canada) and 1% Penicillin/Streptomycin (Invitrogen, Burlington, ON, Canada).

Hippocampal neurons were obtained from newborn rat pups as described (Kaech and Banker, 2006) and seeded at a concentration of 1,250 cells per coverslip. The cells were then grown at 37°C in 5% CO₂ for five days in neurobasal media (Invitrogen, Burlington, ON, Canada), 1% B27 (Invitrogen, Burlington, ON, Canada), 0.5% N2 (Invitrogen, Burlington, ON, Canada), and 0.25% L-glutamine (Invitrogen, Burlington, ON, Canada). Co-cultured cells were grown in the hippocampal growth medium.

Immunocytochemistry: Cells were fixed with 4% paraformaldehyde (PFA) for 1 min, permeabilized with 0.1% triton-X 100 for 5 min and blocked with 5% milk overnight at 4°C. Astrocytes were labeled with phalloidin conjugated to Alexa Fluor 555 (1:250, Invitrogen,

Burlington, ON, Canada) and with Hoechst stain (1:10,000, Invitrogen, Burlington, ON, Canada). Protein spots were mixed with a secondary chicken anti-goat antibody conjugated to Alexa Fluor 488 (polyclonal, 1:20, Invitrogen, Burlington, ON, Canada) for visualization purposes. Astrocytes were selectively labeled using a mouse monoclonal GFAP antibody (monoclonal, 1:400, Sigma, Oakville, ON, Canada) detected with a secondary fluorescent donkey anti-mouse antibody conjugated to Alexa Fluor 488 (polyclonal, 1:500, Invitrogen, Burlington, ON, Canada). Neurons were identified using a rabbit neuronal intermediate filament (NFM) specific antibody (monoclonal, 1:1000, Millipore, Billerica, MA, USA) detected with a secondary fluorescent donkey anti-rabbit antibody conjugated to Alexa Fluor 555 (polyclonal, 1:500, Invitrogen, Burlington, ON, Canada). Alexa Fluor 555-conjugated Isolectin-IB₄ (*Griffonia simplicifolia*, 1:200, Molecular Probes Invitrogen, Burlington, ON, Canada) was used to identify microglia.

Imaging: Phase contrast and DIC imaging were conducted using an axiovert 40CFL microscope (Carl Zeiss Canada, Toronto, ON, Canada). Standard epifluorescence microscopy was performed using a 60× objective and immersion oil on a C1Si inverted fluorescence microscope (Nikon, Saint-Laurent, QC, Canada) and an Axiovert 100 using a 40× objective (Carl Zeiss, Toronto, ON, Canada).

Electrophysiology: Whole cell patch-clamp recordings were made at rt using an inverted Olympus microscope. Glass coverslips with microisland cultures of astrocytes and neurons were transferred with forceps into a recording bath containing 135 mM NaCl, 3.5 mM KCl, 1.3 mM MgCl₂, 10 mM HEPES and 20 mM D-Glucose. Neurons were identified based on pyramidal

morphology. Pipette resistances ranged from 3-5 M Ω and the internal solution contained 125 mM CsMeSO₄, 15 mM Hepes, 10 mM CsCl, 1.5 mM EGTA, 0.15 mM CaCl₂, 5 mM Phosphocreatine, 4 mM MgATP, and 0.4 mM Na₃GTP. Recordings were made in voltage-clamp mode and cells were held at -65 mV. Data was collected in p-Clamp 10.2 at 5 kHz and filtered at 1 kHz.

AI-4. Results

AI-4.1. Fabrication of stamps for microcontact printing

MicroIsland co-cultures are a powerful tool to study interactions between neurons, and between neurons and glial cells. Here we have applied microcontact printing to pattern protein substrates for microisland culture. To reduce the cost of this technique and render it more widely accessible, we designed a new method to create microcontact printing stamps that does not require a cleanroom or photolithography. This process is rendered possible by the production of laser-etched adhesive masks that can be fabricated commercially. These masks are glued onto a clean glass slide before being covered with a 16-well slide module. PDMS is then poured into the wells and cured for 24 hours to yield stamps with 118 ± 3.0 μm wide pillars (**Figure AI-2**).

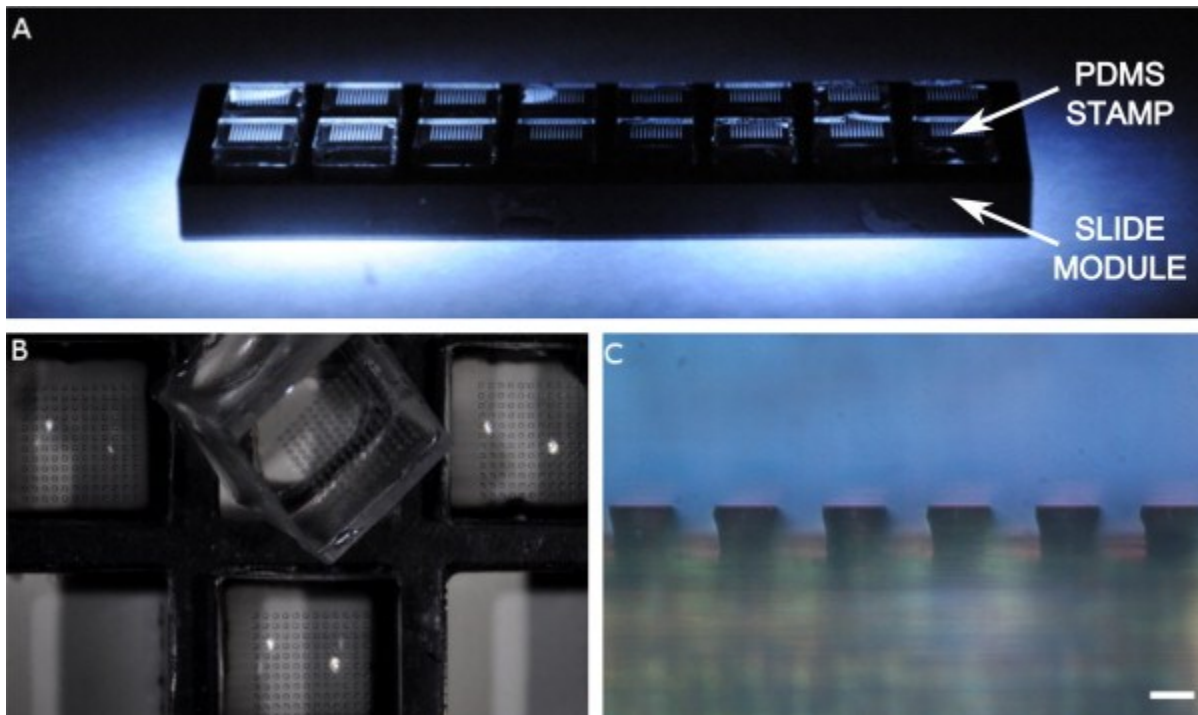


Figure AI-2. Mold and cross section of microcontact printing stamp. (A) Image of the 16-well slide module with PDMS stamps protruding from the wells. (B) Pillars on the stamps are visible. Three stamps have been extracted from the wells with one left partially inserted to illustrate the size (top center). (C) A cross section of the stamp which shows the pillars used to pattern protein islands. (20x objective, Scale bar in (C) corresponds to 100 μm).

AI-4.2. Microcontact printing and background neutralization

Microcontact printing using these stamps was employed to pattern arrays of protein islands ~ 125 μm in diameter composed of netrin-1, laminin, fibronectin, geltrex or PDL. To visualize the printed pattern, a fluorescent secondary antibody was mixed in the printing ink. Measurement of the diameter of the patterns obtained reveal a reproducible array of islands with a mean diameter of 125 ± 4.77 μm for 129 characterized islands (**Figure AI-3**). The stability of the printed islands was then tested by patterning FITC labeled PLL islands and quantifying the average fluorescence of 3×4 island arrays over a period of 15 days during which time they were stored in PBS at 4°C . Over the time period investigated, the fluorescence of the substrate islands did not change significantly, providing evidence for the stability of the patterned substrate (**Figure AI-3**). We

found that the most reproducible patterns were obtained when stamps were not reused. By contrast, reusing stamps multiple times resulted in defective printed islands with non-homogeneous protein deposition (**Figure AI-3**).

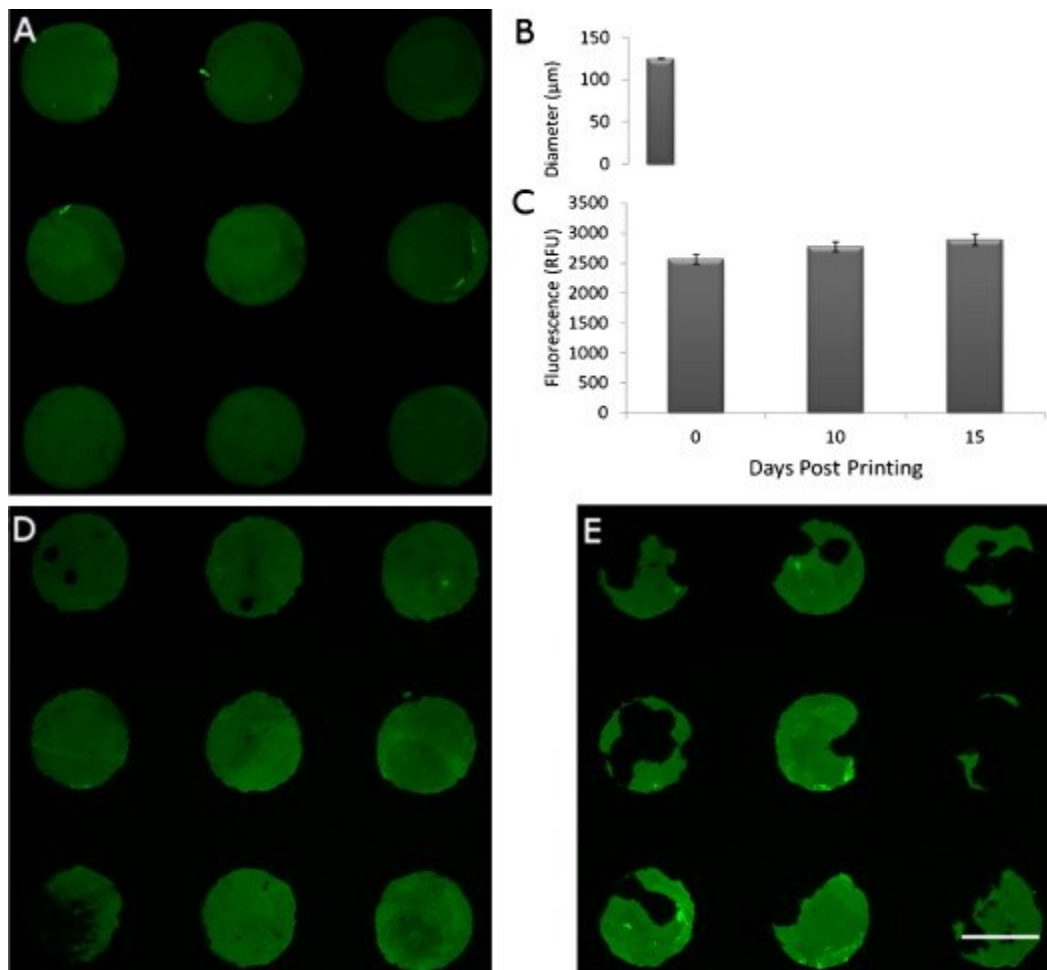


Figure AI-3. Array of microcontact printed islands. (A) 3×3 array of $125 \mu\text{m}$ diameter islands of fluorescently labeled IgG generated by microcontact printing and visualized with a $10 \times$ objective. (B) The diameter was quantified ($n = 129$ IgG islands, mean \pm SEM). (C) Islands of FITC labeled PLL were also printed, stored in the incubator in PBS buffer and imaged on days 0, 10 and 15 with a $10 \times$ objective. Relative fluorescence units (RFU) are shown over the 8 day period ($n=36$ islands per day, mean \pm SEM). The degradation of printed fluorescent antibody islands when employing the same stamp to perform multiple prints was assessed by visualizing (D) the second print and (E) the seventh print obtained with a same stamp. Scale bars correspond to $200 \mu\text{m}$.

Using this method to create protein islands, we then stamped netrin-1, laminin, fibronectin, geltrex, and PDL as patterned substrate microislands. Astrocytes were seeded onto these patterns and found to cluster on the protein islands in all conditions. Visualizing cell nuclei and the cell cytoskeleton, we quantified the number of cells per island, the cell coverage on each of the five different substrates and the extent of cell spreading on the different substrates (**Figure AI-4**). No significant difference in either measure was found for the different substrates, indicating no differential capacity for the substrates to promote astrocyte attachment and survival (ANOVA, $p\text{-value}=0.31>0.05$), however the negative control composed of stamped IgG resulted in very low levels of adhesion (ANOVA, $p\text{-value}=1.65\times 10^{-5}<0.05$).

In preliminary studies we found that proteins adsorbed onto a glass or PDL substrate from serum-containing medium or secreted by the cells reduced the selectivity of the cells for the printed islands compared to the surround. To reduce non-specific cell adhesion and proliferation to the substrate outside of the protein islands we therefore backfilled the surface with a PLL-g-PEG solution after printing. PLL-g-PEG was used, rather than other forms of PEG, such as a PEG homo-polymer, due to the PLL chain promoting adsorption to the surface. PLL-g-PEG backfilling substantially reduced the number of cells binding to the areas surrounding the printed islands; however, omitting the backfilling step resulted in complete cell coverage of the coverslip and no segregation of cells to the islands (ANOVA, $p\text{-value}=0.02<0.05$) (**Figure AI-4**).

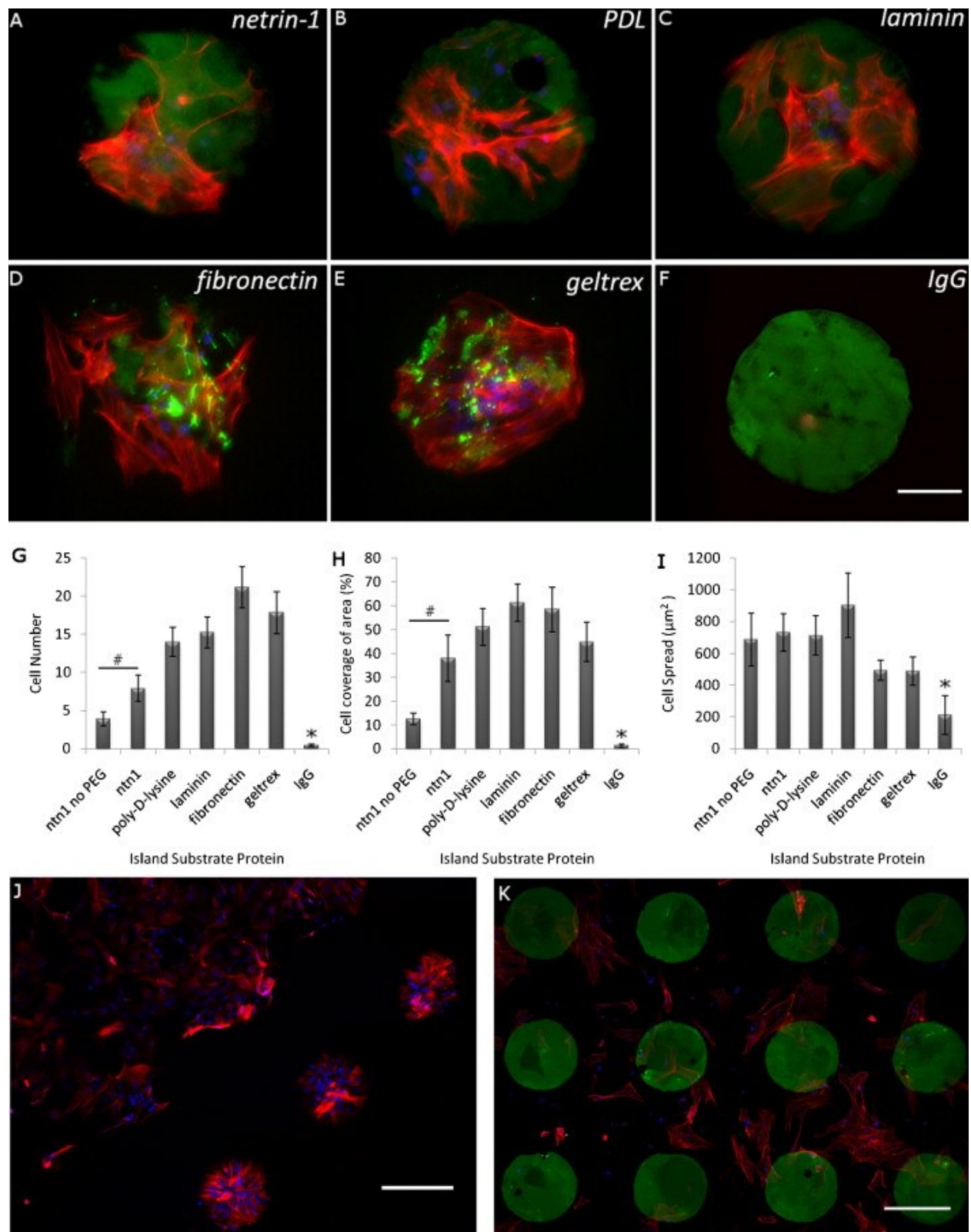


Figure AI-4. Recruitment of astrocytes to islands of different protein composition. Newborn rat astrocytes grown for 2 DIV on 125 μm diameter protein islands composed of (A) netrin-1,

(B) PDL, (C) laminin, (D) fibronectin, (E) geltrex, or (F) IgG. (G) Cell number, (H) cell coverage per island and (I) cell spread on the different substrates is indicated ($n = 12$ islands per condition, mean \pm SEM). (J) Glia segregated on islands of netrin-1 for 3 DIV. At the top left of the image, overgrowth of the astrocytes resulted in loss of isolation of the islands, where the cells have extended past the island boundaries. (K) Image of an array of islands of netrin-1 without PLL-g-PEG backfill upon which astrocytes were seeded and grown for 2 DIV. Islands were visualized by co-printing the protein of interest mixed with fluorescently labeled IgG (green) and then staining the cells with phalloidin to visualize F-actin (red) and Hoechst to label nuclei (blue). Scale bar corresponds to: 50 μm for A-F, 40 \times objective; 200 μm for J-K, 10 \times objective.

AI-4.3. Cell co-culture and optimization of cell density

To obtain a dense monolayer of astrocytes on the surface of the protein islands that does not extend past the boundaries of the islands, the cell density, as well as the time in culture, was optimized. Plating 25,000 cells on a 1.5 cm^2 substrate surface area, and incubating for 2 DIV yielded optimal coverage; however exceeding the optimal growth time period can result in overgrowth of astrocytes and loss of the isolated island structure (**Figure AI-4**). By seeding the relatively low concentration of astrocytes and carefully timing their proliferation, isolated islands were reliably and reproducibly obtained.

A discrepancy was detected in the number of Hoescht-stained nuclei detected and the number of GFAP-immunoreactive astrocytes identified on the islands, suggesting that other cell types were also present. Staining with an antibody against Isolectin IB₄, a selective marker for microglial cells, revealed the presence of a low density of microglia on the astrocyte islands (**Figure AI-5**), consistent with previous studies using microisland cultures (Fasano, 2008).

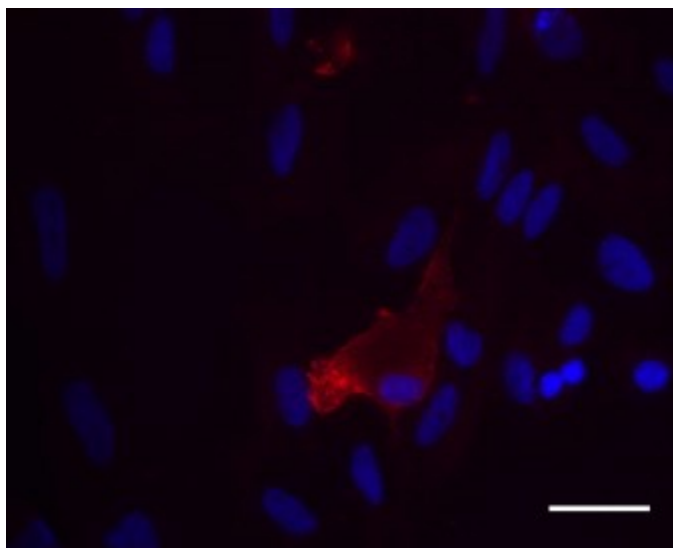


Figure AI-5. MicroIsland foundation layer includes astrocytes and microglia. Islands were stained with Isolectin IB₄ (red) to label microglia and with Hoechst (blue) to label nuclei. Scale bars correspond to 50 μ m.

By adjusting the density of neurons seeded on the coverslip, islands could readily be found that contain a single neuron. To visualize the neurons growing on the astrocyte microislands, seven days after plating the neurons, a total of 9 days after plating the astrocytes, the cultures were fixed and then stained with Hoechst dye to label nuclei, immunolabeled for glial fibrillary acidic protein (GFAP) to selectively identify astrocytes (Rodnight et al., 1997), and neuronal axons labeled using an antibody against NFM (**Figure AI-6**) (Chan et al., 2003). In the conditions described here, seeding \sim 1,250 hippocampal neurons per coverslip typically resulted in 10 – 15 % of the islands containing a single neuron.

In a separate series of experiments, we demonstrated the survival and growth of neurons without the bed of astrocytes, plating them directly on the protein islands. Over a period of 12 DIV, isolated neurons grew long neurites that remained confined to the protein island. This variation of the technique would be useful for studying neuronal function in the absence of glia (**Figure AI-6**).

To confirm the general applicability of this method to studies of synapse function, whole-cell voltage-clamp recordings were made of neurons grown on astrocyte islands following 13 DIV. The membrane currents recorded demonstrate that hippocampal neurons grown using this method are healthy and electrophysiologically active (**Figure AI-6**).

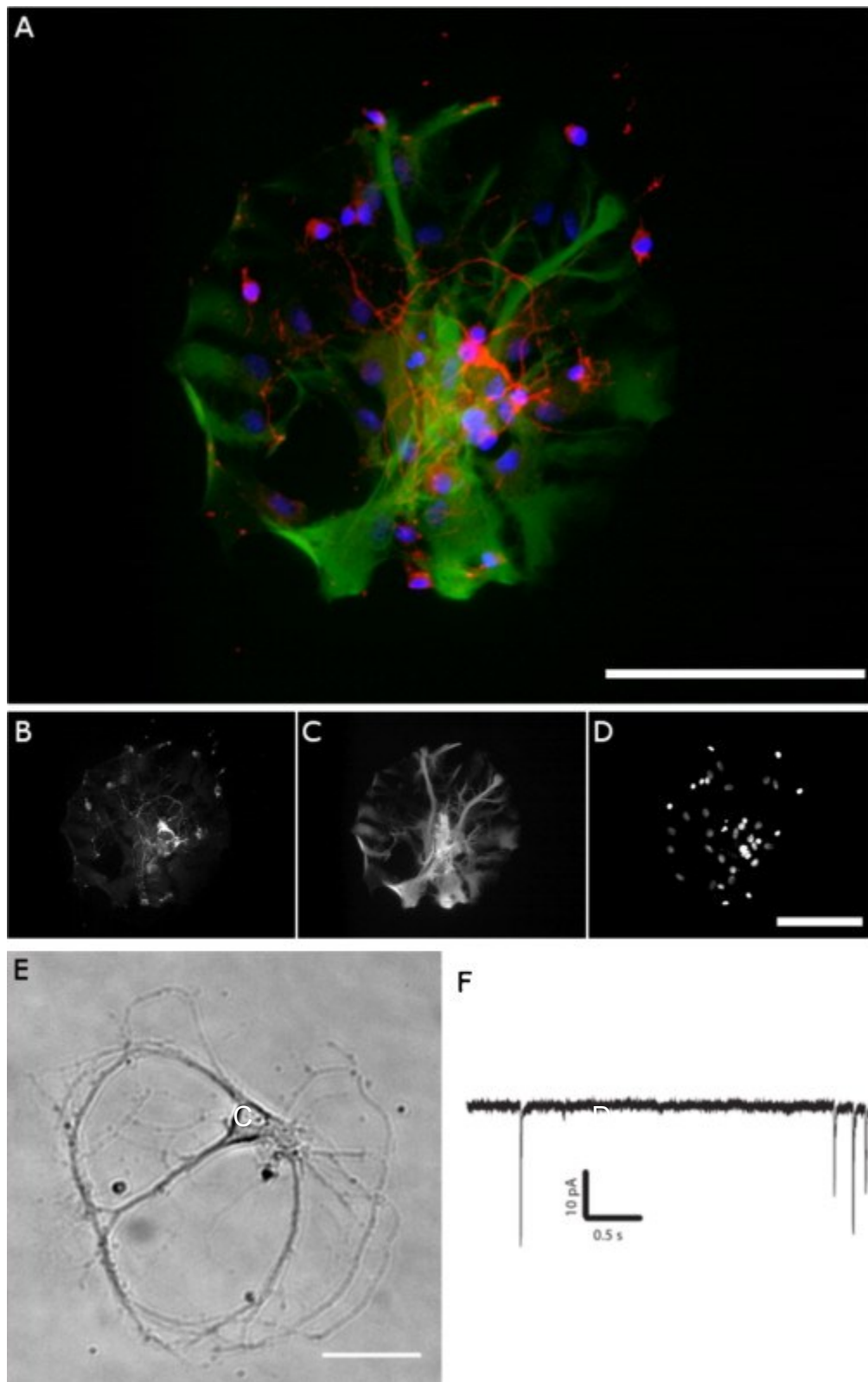


Figure AI-6. Hippocampal neurons grown on an astrocyte monolayer on printed islands of netrin-1. (A) Merged image showing the neuronal cells stained with the axonal marker NFM

(red), the astrocyte marker GFAP (green), and Hoechst stain to label nuclei (blue). Each channel is shown separately below (B) NFM, (C) GFAP, and (D) Hoechst stain. (E) DIC image of a single 125 μm diameter island on which a single hippocampal neuron was grown for 12 DIV. (F) At 13 DIV, neurons isolated on astrocyte islands were analyzed by whole-cell voltage-clamp to determine if they were electrophysiologically active. Large inward currents recorded from a pyramidal cell demonstrate the amenability of these microisland co-cultures for electrophysiological studies. Scale bars correspond to 100 μm for (A-D) and 50 μm for (E).

AI-5. Discussion

In the present study we developed a method to pattern substrates for microisland co-cultures. We show that hippocampal neurons extend long neurites in these cultures, and that these neurons form physiologically active synapses.

Standard microcontact printing techniques typically require the design of a mask for use in photolithography to produce a wafer with topography (von Philipsborn et al., 2006). This wafer is then used as a mold on which PDMS is cast and cured to produce stamps for the microcontact printing process. While this process is reliable and reproducible, it has been a limiting factor for many labs because it requires a clean room environment, as well as microfabrication expertise. However, immediate access to such a facility is no longer required, as it is now routine for custom designed wafers to be produced commercially. Once the appropriately patterned wafer has been obtained, it can be used repeatedly as the mold to produce PDMS stamps for use in microcontact printing. The generation of PDMS stamps therefore no longer requires specialized equipment or techniques.

Employing microcontact printing to pattern substrates for cell culture provides control over the geometry and precise size of the features. The relatively small variation in island size that we have documented here demonstrates that the technique yields very reproducible features. The technique is widely applicable to many proteins, as we show using netrin-1, laminin, fibronectin, geltrex, or PDL, without requiring changes in the printing procedure. Microcontact

printing exposes proteins to a variety of stresses, such as drying and mechanical forces, during the patterning process. Furthermore, some large proteins, such as fibronectin, have been reported to lose function due to denaturation during the printing process (von Philipsborn et al., 2006). Here we show cells recruited to islands composed of different extracellular matrix proteins or protein mixtures, while in contrast, islands printed with IgG, used as a negative control, did not recruit cells. These findings suggest that using the techniques employed here, the extracellular matrix proteins maintained adhesive function following printing. Insight into the printing capability of the various proteins was obtained by mixing the targeted protein with a fluorescent antibody to identify the boundaries of the island and visualize the uniformity of protein distribution across the island. Even though this is an indirect method of monitoring the protein of interest, it was sufficient to reveal that gelatin and fibronectin were not printed as efficiently as other proteins in the study. This was indicated by an uneven distribution of fluorescence across the surface of the island, perhaps resulting from protein aggregation, or in the case of gelatin which gels at room temperature, the partial formation of a gel during the printing process.

To restrict cell attachment and spreading to the island, the non-printed substrate was rendered non-permissive. The inclusion of agents to block non-specific protein binding is increasingly common in microcontact printing. We chose PLL-g-PEG due to its straightforward adsorption to the surface via the poly-lysine chain (Elbert and Hubbell, 1998) and its affinity for water (Kao et al., 2005), both of which contribute to limiting the adhesion of additional proteins to the backfilled surface. A test incubation using FITC-PLL detected binding within the boundary of the protein island, however the cellular responses indicate that access to the printed protein is not masked by PLL, consistent with PLL-g-PEG filling the substrate gaps between the printed protein islands, without a detrimental effect on the previously printed protein substrates.

By carefully monitoring the number of cells seeded and the time allowed for astrocyte proliferation *in vitro*, a layer of cells can be obtained that covers each of the substrate islands and forms the foundation for subsequent neuronal cell culture. However, if the optimal cell density is exceeded or the cells are allowed to grow for an excessive amount of time, they will saturate and grow beyond the boundaries of the island, eventually completely covering the substrate, in spite of the presence of the PEG backfill. If overgrowth of cells beyond the island boundaries is an issue, mitotic inhibitors could be added to prevent the further cell proliferation. By seeding appropriate initial numbers of cells and limiting the length of time the cells are grown *in vitro*, overgrowth can be avoided even in the absence of mitotic inhibitors. Neurons cultured on such microislands can be readily used to conduct functional studies where the interactions of a limited number of cell types can be monitored in a well defined space.

AI-6. Conclusions

The method described here provides a tool to rapidly and reproducibly pattern substrates for neuronal microisland cultures. We show that glia and neurons can be segregated to islands of netrin-1, PDL, laminin, geltrex or fibronectin, each of which supports the growth and differentiation of embryonic rat hippocampal neurons. Furthermore, we demonstrate that the neurons grown as microisland cultures are viable, healthy, and electrically active. Among the various techniques for generating microisland substrates to support neural cell culture, the method described here is straight forward, yet provides precise control over the position and size of the islands generated. Additionally it is efficient, requiring relatively limited amounts of substrate protein for patterning, and its precision and reproducibility reduce the number of defective substrates produced.

AI-7. References

- Armstrong RC. Isolation and characterization of immature oligodendrocyte lineage cells. *Methods-a Companion to Methods in Enzymology*, 1998; 16: 282-+.
- Bernard A, Delamarche E, Schmid H, Michel B, Bosshard HR, Biebuyck H. Printing patterns of proteins. *Langmuir*, 1998; 14: 2225-9.
- Bourque MJ, Trudeau LE. GDNF enhances the synaptic efficacy of dopaminergic neurons in culture. *Eur J Neurosci*, 2000; 12: 3172-80.
- Cardozo DL. Midbrain Dopaminergic-Neurons from Postnatal Rat in Long-Term Primary Culture. *Neuroscience*, 1993; 56: 409-21.
- Chakra EB, Hannes B, Vieillard J, Mansfield CD, Mazurczyk R, Bouchard A, Potempa J, Krawczyk S, Cabrera M. Grafting of antibodies inside integrated microfluidic-microoptic devices by means of automated microcontact printing. *Sensor Actuat B-Chem*, 2009; 140: 278-86.
- Chan W, Yabe J, Pimenta A, Ortiz D, Shea T. Growth cones contain a dynamic population of neurofilament subunits. *Cell Motil Cytoskel*, 2003; 54: 195-207.
- Elbert DL, Hubbell JA. Self-assembly and steric stabilization at heterogeneous, biological surfaces using adsorbing block copolymers. *Chem Biol*, 1998; 5: 177-83.
- Fasano C, Thibault D, Trudeau LÉ. Culture of Postnatal Mesencephalic Dopamine Neurons on an Astrocyte Monolayer. John Wiley & Sons, Inc., 2008.
- Fasano C, Thibault, D. and Trudeau L.E. Culture of Postnatal Mesencephalic Dopamine Neurons on an Astrocyte Monolayer. *Current protocols*, 2008; 3: 1-19.
- Furshpan E, Landis S, Matsumoto S, Potter D. Synaptic functions in rat sympathetic neurons in microcultures. I. Secretion of norepinephrine and acetylcholine. *J Neurosci*, 1986; 6: 1061.
- Furshpan E, MacLeish P, O'lague P, Potter D. Chemical transmission between rat sympathetic neurons and cardiac myocytes developing in microcultures: evidence for cholinergic, adrenergic, and dual-function neurons. *P Natl Acad Sci USA*, 1976; 73: 4225.
- Goubko CA, Cao XD. Patterning multiple cell types in co-cultures: A review. *Mat Sci Eng C-Mater*, 2009; 29: 1855-68.
- Jomphe C, Bourque MJ, Fortin GD, St-Gelais F, Okano H, Kobayashi K, Trudeau LE. Use of TH-EGFP transgenic mice as a source of identified dopaminergic neurons for physiological studies in postnatal cell culture. *Journal of Neuroscience Methods*, 2005; 146: 1-12.

Kaech S, Banker G. Culturing hippocampal neurons. *Nat Protoc*, 2006; 1: 2406-15.

Kao MJ, Tien DC, Jwo CS, Tsung TT. The study of hydrophilic characteristics of ethylene glycol. 7th International Symposium on Measurement Technology and Intelligent Instruments, 2005; 13: 442-5.

Kumar A, Whitesides GM. Features of Gold Having Micrometer to Centimeter Dimensions Can Be Formed through a Combination of Stamping with an Elastomeric Stamp and an Alkanethiol Ink Followed by Chemical Etching. *Appl Phys Lett*, 1993; 63: 2002-4.

M.M. Segal RWB, K.A. Jones and J.E. Huettner. Mass cultures and microislands of neurons from postnatal rat brain. In Goslin GBaK, editor. *Culturing nerve cells*. MIT Press: Cambridge 1998: 309–38.

Masuko S, Nakajima S, Nakajima Y. Dissociated High-Purity Dopaminergic Neuron Cultures from the Substantia-Nigra and the Ventral Tegmental Area of the Postnatal Rat. *Neuroscience*, 1992; 49: 347-64.

Rodnight R, Goncalves CA, Wofchuk ST, Leal R. Control of the phosphorylation of the astrocyte marker glial fibrillary acidic protein (GFAP) in the immature rat hippocampus by glutamate and calcium ions: Possible key factor in astrocytic plasticity. *Braz J Med Biol Res*, 1997; 30: 325-38.

Segal MM, Baughman RW, Jones KA, Huettner JE. Mass cultures and microislands of neurons from postnatal rat brain. In Goslin GBaK, editor. *Culturing nerve cells*. MIT Press: Cambridge 1998: 309–38.

Serafini T, Kennedy TE, Galko MJ, Mirzayan C, Jessell TM, Tessierlavigne M. The Netrins Define a Family of Axon Outgrowth-Promoting Proteins Homologous to C-Elegans Unc-6. *Cell*, 1994; 78: 409-24.

Shirasaki R, Mirzayan C, TessierLavigne M, Murakami F. Guidance of circumferentially growing axons by netrin-dependent and -independent floor plate chemotropism in the vertebrate brain. *Neuron*, 1996; 17: 1079-88.

von Philipsborn A, Lang S, Bernard A, Loeschinger J, David C, Lehnert D, Bastmeyer M, Bonhoeffer F. Microcontact printing of axon guidance molecules for generation of graded patterns. *Nat Protoc*, 2006; 1: 1322-8.

von Philipsborn A, Lang S, Jiang Z, Bonhoeffer F, Bastmeyer M. Substrate-Bound Protein Gradients for Cell Culture Fabricated by Microfluidic Networks and Microcontact Printing. *Science Signaling*, 2007; 2007.

PREFACE TO APPENDIX II

This chapter was published as a manuscript in *PLOS ONE* in 2014. The chapter was included as an appendix because it outlines the novel algorithms that were developed to create the DNG array that was employed in the axonal navigation studies (Chapter 4). My contributions to the manuscript are highlighted in the section detailing author contributions, but include conceptual contributions, design contributions, the patterning of the protein gradients, image analysis, and writing of the paper.

This chapter was published as a research article in *PLOS ONE*
(Ongo et al., 2014).

Acknowledgements

We acknowledge Nabila Zaman for her help with gradient algorithms, and Marta Garnelo-Abellanas and Veronique Laforte for proofreading this article. We acknowledge support from the Canadian Institutes of Health Research (CHIR, Regenerative and Nanomedicine Grant), the Imperial-McGill collaboration in Neurotechnology, the Canadian Foundation for Innovation (CFI) and the McGill Nanotools Microfabrication Laboratory (funded by CFI and McGill University). G.O. and S.G.R. were supported by the Natural Sciences and Engineering Research Council (NSERC) Collaborative Research and Training Experience (CREATE) grants for Integrated Sensors and Systems (ISS) and Neuroengineering Training Program (NTP) at McGill University. The NTP is also funded through CIHR and The Molson Foundation. G.O. was supported by the Department of Biomedical Engineering at McGill University. T.E.K. was supported by a Killam Foundation Scholar Award and a Chercheur National Award from the Fonds de la Recherche en Santé du Québec. D.J. holds a Canada Research Chair. The funders had no role in the study design, data collection and analysis, decision to publish, or preparation of the manuscript.

Appendix II

Ordered, Random, Monotonic and Non-monotonic Digital Nanodot Gradients

Grant Ongo,^{1,2} Sébastien G. Ricoult,^{2,3} Timothy E. Kennedy,³ and David Juncker^{1,2,3,*}

¹*Department of Biomedical Engineering, McGill University, Montréal, Québec, Canada;*

²*McGill University & Génome Québec Innovation Centre, McGill University, Montréal, Québec, Canada;* ³*McGill Program in Neuroengineering, Department of Neurology and Neurosurgery, Montréal Neurological Institute, McGill University, Montréal, Québec, Canada*

AII-1. Abstract

Cell navigation is directed by inhomogeneous distributions of extracellular cues. It is well known that noise plays a key role in biology and is present in naturally occurring gradients at the micro- and nanoscale, yet it has not been studied with gradients *in vitro*. Here, we introduce novel algorithms to produce ordered and random gradients of discrete nanodots – called digital nanodot gradients (DNGs) – according to monotonic and non-monotonic density functions. The algorithms generate continuous DNGs, with dot spacing changing in two dimensions along the gradient direction according to arbitrary mathematical functions, with densities ranging from 0.02% to 44.44%. The random gradient algorithm compensates for random nanodot overlap, and the randomness and spatial homogeneity of the DNGs were confirmed with Ripley's K function. An array of 100 DNGs, each $400 \times 400 \mu\text{m}^2$, comprising a total of 57 million $200 \times 200 \text{nm}^2$ dots was designed and patterned into silicon using electron-beam lithography, then patterned as fluorescently labeled IgGs on glass using lift-off nanocontact printing. DNGs will facilitate the study of the effects of noise and randomness at the micro- and nanoscales on cell migration and growth.

AII-2. Introduction

Gradients are fundamental to many phenomena of biology, from directing axonal navigation during neural development to the differentiation of stem cells in response to an injury [1,2]. Gradients may occur as either (i) free diffusion gradients, (ii) substrate-bound gradients, or (iii) a combination of both [3]. Free diffusion gradients can be generated by cell-excreted proteins that diffuse in the extracellular space. Substrate-bound gradients arise when proteins are bound to the extracellular matrix or cell membranes [4-6]. To better understand cellular haptotaxis – the directed movement of a cell or axonal growth cone along a gradient of a substrate-bound guidance cue – many techniques to generate surface-bound gradients *in vitro* have been developed [7]. Two classes of concentration gradients exist, namely continuous and digital gradients. Continuous gradients have protein concentration changing in a constant manner, and are typically produced by adsorbing molecules from a diffusible gradient. Several parameters of these gradients have been modulated, including the range and slope, which was linear, exponential or non-monotonic [8]. For example, linear gradients of the protein BDNF have been shown to modulate neuron polarization and growth [9] and linear laminin gradients have been shown to orient rat hippocampal axon specification based on slope [10]. Secondly, digital gradients which have been recently introduced, are formed by patterning small dots of protein and varying the density of the dots by changing their size [11], the spacing between them [12], or both [13]. The advantage of digital gradients is that they are deterministic, and that the local concentration can be precisely predicted since it does not rely on fluorescence measurements which may be prone to error. Digital gradients have been used to study how retinal ganglion cells identify the stop zone within graded distributions of repulsive EphrinA5 ligands [13]. However, digital gradients rarely extend over 1-2 orders of magnitude (OM), whereas it is believed that the

dynamic range of gradients *in vivo* is between 3-4 OM. To overcome these limitations, we previously developed digital nanodot gradients (DNGs), where the spacing between nanodots (200 nm in diameter) was changed in two dimensions to produce a dynamic range exceeding 3 OM. These designs were implemented using a low-cost, lift-off nanocontact printing method to pattern substrate-bound gradients of proteins and peptides. We employed these patterns for adhesion and migration studies of C2C12 myoblasts on RGD peptide and netrin-1 gradients, respectively [14]. For these experiments, gradients of $400 \times 400 \mu\text{m}^2$ were divided into 53 rectangular boxes of fixed size and density. With this approach, gradients were non-continuous and had stepwise changes in density. This is most pronounced in low-density regions where the spacing between nanodots exceeded the dimensions of the box, requiring larger box sizes and thus creating large “steps” at the bottom of the gradient. This may prove problematic as cells may fail to sense a discontinuous gradient if they fall into a region of constant density.

Noise is ubiquitous in biology [15], and modern patterning technologies can be exploited to introduce defined amounts of noise and randomness into otherwise regular patterns. The effect of randomness was evaluated in ordered arrays and repetitive patterns with a constant average density. In one study, disorder was introduced in arrays of 120 nm dots spaced 300 nm apart by randomly displacing the dot by up to 50% of the spacing to avoid overlap [16]. While this approach introduced a controlled amount of noise by restricting the maximum displacement, it was not random since dots were each contained within the original grid. Nonetheless, cellular adhesion and stem cell differentiation of osteoblasts were markedly altered as a result of increasing disorder. In another study, whole proteome analysis of cells grown on the same disordered patterns resulted in differential expression of certain proteins in the extracellular signal-regulated kinase (ERK1/2) pathway [17]. Similarly, controlled amounts of topographical

noise on nanogratings of 500 nm ridges and grooves has shown to effect PC12 neuronal cell alignment to the gratings, focal adhesion maturation and directionality [18].

Randomness and noise are also highly relevant to directed cell migration. The stochasticity of chemo- and haptotaxis has been well studied, and is apparent from the random-walk like traces of migrating cells [19]. It is well understood that biological gradients, which appear continuous, are in fact quantized since they are comprised of individual molecules adsorbed to a surface. The distribution of these molecules is not deterministic, but stochastic at the nanoscale. The engagement of receptors from migrating cells with these guidance cues has been modeled within a stochastic framework [19,20]. Random variations in the gradient also occur at the microscale *in vivo* from the local accumulation of chemo- and haptotactic molecules that form concentration puncta [21]. Gradients formed by the expression of receptors from cells embedded in a tissue may become non-monotonic as particular cells over- and under- express a receptor relative to their position in the gradient [22]. Cells navigating through such a patchwork of microscale deviations must discriminate against local maxima and minima to sense the overarching gradient slope. It has been suggested that cells alternate between periods of sensitization and desensitization and are thereby capable of maintaining an overall response to long-range gradients [23].

Random pattern generation is well established, however many patterns are not random in the mathematical sense, and often implement only an approximation of randomness to varying degrees depending on the needs of the application. Firstly, computers typically generate ‘pseudo-random’ numbers that statistically approximate the properties of true random numbers using an algorithm based on an initial ‘random seed’ – generally a random bit. If this random seed is

known, the set of pseudo-random numbers can be replicated. However, for most applications, pseudo-random numbers are indistinguishable from a true random number.

So-called random dot patterns are widely used in the reproduction of images and patterns using displays or printers that impose digitization and pixelation. Pixelation implies that pixels are positioned on a regular grid. Adjusting grayscale images to binary (black and white pixels) through half-toning is achieved by adjusting the ratio of black and white pixels in a local area, but if pixels are turned on and off according to an ordered pattern, rendering artifacts (such as Moiré patterns) arise. By locally randomizing the pixels turned on or off while matching the overall desired grayscale, it is possible to avoid such rendering artifacts. These ‘random-grid’ patterns can be generated using an array of pseudo-random values and a threshold dictated by the local grey value used to determine which pixels are black or white (**Figure AII-1**) [24]. With this approach, the value of each pixel is random, while the pixel position is fixed to an ordered grid. These random-grids have found application in the half-toning of images for display or printing [25] and the generation of random-dot stereograms for depth perception studies [26].

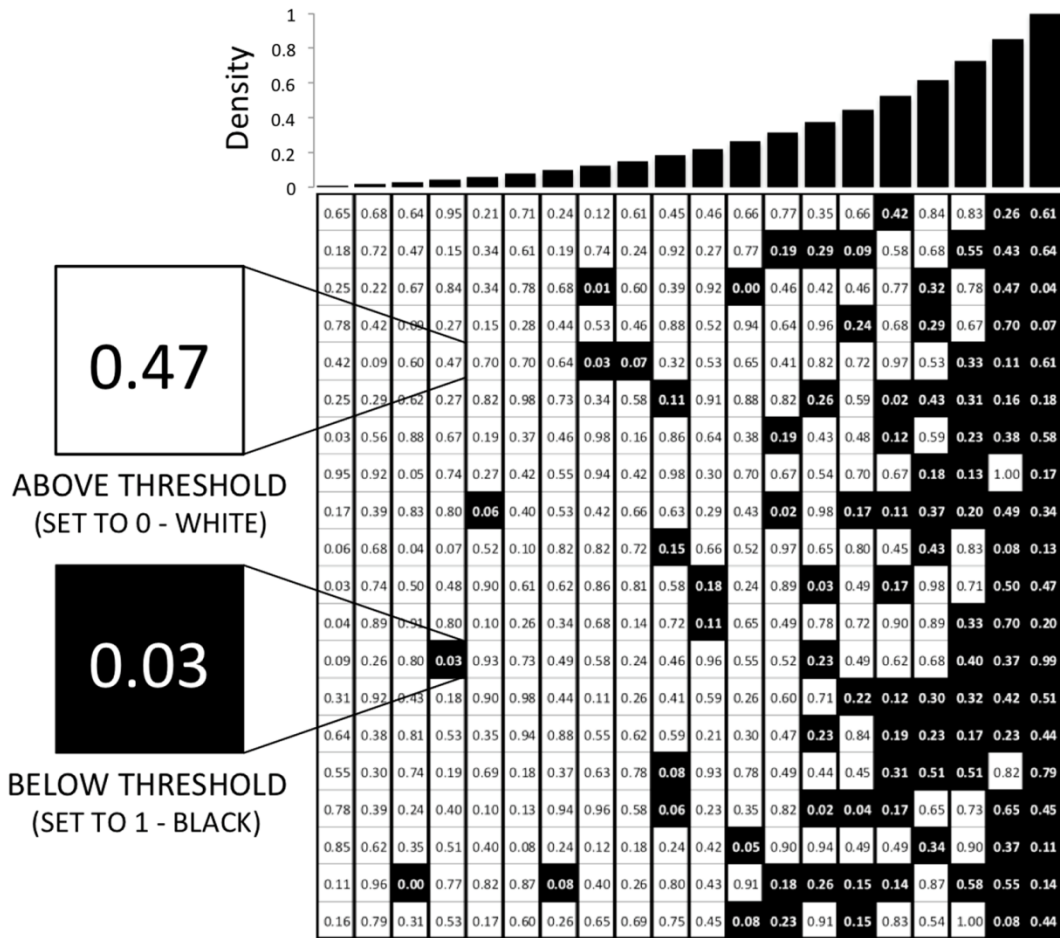


Figure AII-1. Random gradients produced by a random matrix threshold approach.

A matrix of pseudo-random numbers is generated. Values greater than or equal to the density threshold are set to 0 (white), while values less than the threshold are set to 1 (black). The binary array can then be exported directly as a bitmap image file. Each nanodot is represented by one pixel. Thus, for a $400 \times 400 \mu\text{m}^2$ sized area with $200 \times 200 \text{ nm}^2$ nanodots, a 2000×2000 matrix with 4 million values is required. This approach does not provide a fully random configuration since nanodots are aligned to a grid. While these patterns appear random to the eye, the underlying grid might be sensed at the

cellular scale. Theoretically, it is possible to further randomize the position of dots by subdividing the area, e.g. using a 50 nm grid to position and draw $200 \times 200 \text{ nm}^2$ pixels, but this would come at the cost of increased computational requirements and the possibility of overlap between adjacent dots.

Random dot patterns also comprise dot patterns where the position of the dots is not constrained to a grid as described previously, but is instead randomized within a given space. However, pseudo-random distributions of the dots, when seen from afar, can appear noisy and inhomogeneous to the eye. Therefore, algorithms involving so-called quasi random numbers (also called low discrepancy sequences) are used to create patterns with a more uniform distribution that appears visually smooth [27]. “Quasi-random” is a broad term that encompasses numbers with a disordered distribution that lie between a (pseudo-)random distribution and a regular distribution [28]; a quasi-random distribution may more closely resemble an ordered distribution than a random distribution upon closer examination. Many different algorithms have been developed to produce quasi-random numbers. As an example, for liquid crystal displays, quasi-random dot patterns without overlap are generated by mimicking molecular dynamics in which two “molecules” cannot occupy the same space [29] or by iteratively repositioning overlapping dots until overlap is minimized [27].

Both random-grid and quasi-random patterns have been optimized to produce a pleasing (macroscopic) image to the eye by introducing a controlled amount of microscale disorder, avoiding both the viewing artifacts of regular arrays and the inhomogeneity of pseudo-random dot patterns. Cells however are microscopic and sense their environment at the micro- and nanoscale. At these scales, random grid or quasi-random distributions can be significantly

different from a random one, and may not adequately reproduce the effect of a random pattern on cells. It is therefore necessary to establish an approach to produce random dot patterns that preserves randomness at the micro- and nanoscale to study the effect of random *vs.* ordered dot patterns on cell navigation.

Here, we introduce continuous DNGs eliminating the stepwise density changes of the previously reported “step” design [14] with (i) ordered and (ii) pseudo-random positioning of nanodots, as well as (iii) non-monotonic DNGs that can be implemented using either (i) or (ii). We discuss various strategies to create noisy DNGs and outline the challenges in forming random DNGs with accurate slopes, and describe a novel algorithm with pseudo-random positioning of the dots and compensating for random, but predictable, dot overlap to achieve the desired coverage. The slope of random DNGs was measured and compared to the programmed density function, and their randomness verified using Ripley’s K-function. We generated an array of 100 ordered and random $400 \times 400 \mu\text{m}^2$ large DNGs made of $200 \times 200 \text{ nm}^2$ nanodots, including monotonic and non-monotonic density curves, with a dynamic ranges spanning from 2.14 to 3.86 OM. Non-monotonic gradients produced here aim to introduce in a quantitative and repeatable manner “microscale noise” into surface-bound *in vitro* gradients. The entire array of 100 DNGs covers a 35 mm^2 area and is comprised of more than 57 million nanodots. The DNG array was patterned onto a silicon (Si) wafer by electron-beam (e-beam) lithography, and was transferred onto glass slides by lift-off nanocontact printing of fluorescently labeled IgGs [14]. The fidelity of the replication process was evaluated by overlaying the DNG design with fluorescence microscopy images of the printed IgG proteins.

AII-3. Materials and Methods

Software & Computers: Algorithms were developed in Matlab R2013a (Natick, MA, USA). Scripts of the ordered and random gradient algorithms are available upon request. A spreadsheet template (Microsoft Excel 2010) of gradient parameters was imported into Matlab for processing. The output for each gradient was a text file of coordinates formatted as a Caltech Intermediate Format (CIF) file, which is a vector graphic format and minimizes file size. CIFs were imported into CleWin Version 4.1 (WieWeb, MESA Research Institute at the University of Twente and Deltamask, Netherlands). Gradients were exported from CleWin as Bitmap (BMP) image files for verification of density using ImageJ 1.47 64-bit (National Institutes of Health, USA) and Matlab. The 100-gradient array was designed in L-edit (Tanner EDA, Monrovia, CA, USA). All software was run on a 2013 iMac computer with a 3.4 GHz Intel Core i7 processor with 32 GB 1600 MHz DDR3 memory running Windows 7 through a bootcamp partition.

Electron-Beam Lithography: A 4" Si wafer was coated with PMMA resist and the 100-gradient array was patterned by e-beam lithography (VB6 UHR EWF, Vistec, Montreal, QC, Canada), followed by reactive-ion etching (System100 ICP380, Plasmalab, Everett, WA, USA) 100 nm deep into the Si wafer.

Stamp Fabrication: After cleaning, the Si wafer was coated with perfluorooctyltriethoxysilane (Sigma-Aldrich, Oakville, ON, Canada) by vapor phase deposition. An accurate polymer copy of the wafer was obtained after double replication using polydimethylsiloxane (PDMS) and a UV-sensitive polyurethane as described in [14]. First, a 6 mm layer of 1:10 PDMS (Dow Corning, Corning, NY, USA) was poured on the wafer inside a Petri dish, followed by degassing under vacuum in a desiccator for 10 min. Next, the PDMS was cured in an oven for 24 h at 60 °C

(VWR, Montreal, QC, Canada), then peeled from the wafer. To remove uncured monomers and other extractables, the PDMS replica was submersed in 70% ethanol for 24 h then baked at 60°C for 4 h. Next, a drop of UV sensitive polyurethane (Norland Optical Adhesive 63 (NOA 63), Norland Products, Cranbury, NJ) was applied to the PDMS replica and cured by 600 W of UV light (Uvitron International, Inc., West Springfield, MA) for 45 s. The PDMS was then removed yielding an NOA replica of the original Si wafer pattern with 200 nm holes [14].

Nanocontact Printing: A flat PDMS stamp was cured against a flat-bottomed petri dish. Following removal of the extractables as mentioned above, the flat PDMS stamp was inked with a 10 μ L drop of phosphate buffered saline solution (PBS) containing 25 μ g/mL of chicken immunoglobulin G (IgG) conjugated to Alexa Fluor 488 (Invitrogen, Burlington, ON, Canada). A plasma activated hydrophilic coverslip was then placed on the drop to spread the solution evenly across the surface of the hydrophobic PDMS stamp during a 5 min incubation period. After rinsing with PBS and double distilled water for 15 s each, the inked stamps were briefly dried under a stream of N₂ and immediately brought into contact with a plasma activated (PlasmaEtch PE-50, PlasmaEtch, Carson City, NV, USA) NOA master for 5 s. The PDMS and NOA were separated and proteins in the contact regions were transferred to the NOA. The remaining proteins on the PDMS were transferred to the final substrate by printing the PDMS stamp for 5 s onto a plasma activated glass coverslip.

Imaging and Analysis: Images of the original Si master were collected using scanning electron microscopy (SEM, JEOL, Japan). DNGs of fluorescent IgGs were imaged by fluorescence microscopy (TE2000 microscope, Nikon, Canada and CoolSNAP HQ² camera, Photometrics,

USA). Images of the Si wafer were captured with a Panasonic Lumix GH3 DSLR equipped with an Olympus M. Zuiko Digital ED 60 mm macro lens. Dark field images were captured with an inspection microscope (LV150A microscope and Digital Sight DS-Fi1 camera, Nikon, Canada).

AII-4. Results and Discussion

AII-4.1. Ordered Gradient Algorithm

Ordered DNGs with continuously changing density were programmed by forming columns of nanodots with equal vertical spacing while varying the spacing between columns horizontally (**Figure AII-2B**). The density of the gradient at any point along the length l is dictated by an input density function D , and is realized by placing a single nanodot into a virtual box to form a unit cell. The dimensions d_i of the unit cell at the i^{th} column of nanodots are given by the square root of the nanodot area A_{dot} divided by the density value at the given position (Eq. 1). In this algorithm, the size of the nanodot remains constant while the dimensions of the unit cell vary for each column of nanodots along the length.

$$d_i = \sqrt{\frac{A_{dot}}{D(l)}} \quad (1)$$

The unit cell is largest at low densities and decreases at higher densities, matching the dimensions of the nanodot at a density equal to one. The unit cell dimensions for each column are calculated using an iterative approach, starting from the first column of nanodots at length zero. The position along the length for the next column of nanodots is given by the cumulative sum of unit cell dimensions (**Figure AII-2B**).

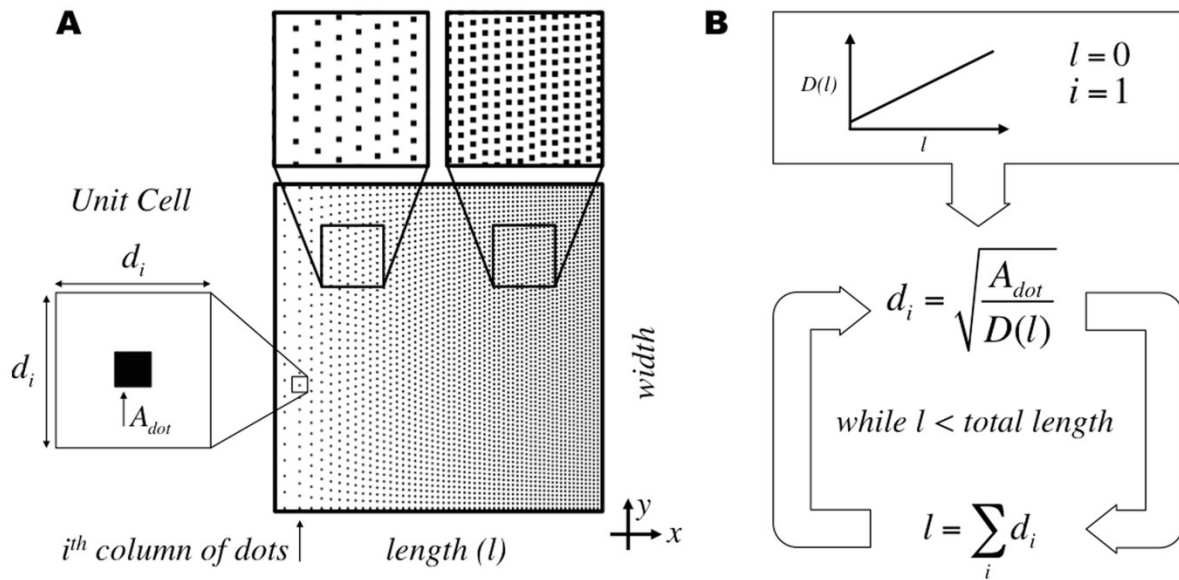


Figure AII-2. Ordered gradient algorithm for continuously changing density in Digital Nanodot Gradients (DNGs) using a unit cell approach. (A) Schematic of a linear DNG and unit cell parameters for the i^{th} column of nanodots. (B) Calculation of unit cell dimensions at each position through an iterative process using the cumulative sum of unit cell dimensions to determine position along the length.

The width of the gradient is divided by d_i to estimate the number of nanodots in the column. The value of d_i is then recalculated to equally space the integer number of nanodots along the width, ensuring that the distribution of nanodots is symmetrical. The unit cells are concatenated to form a column of points in the y direction with constant spacing as multiples of d_i . The x coordinate for each column is the position l at which the unit cell dimensions are calculated. Thus, using this algorithm it is easy to form a gradient with any slope as the size of the unit cell is directly derived from the value of the density function at a specific position. **Figure AII-3** shows a linear

density curve spanning from a minimum density $D_{min}=0.01$ to a maximum density $D_{max}=0.30$ (Eq. 2) with corresponding unit cell dimensions along the length of the gradient. Eq. 2 is normalized to span the dynamic range over the total length $L=100 \mu\text{m}$ of the gradient.

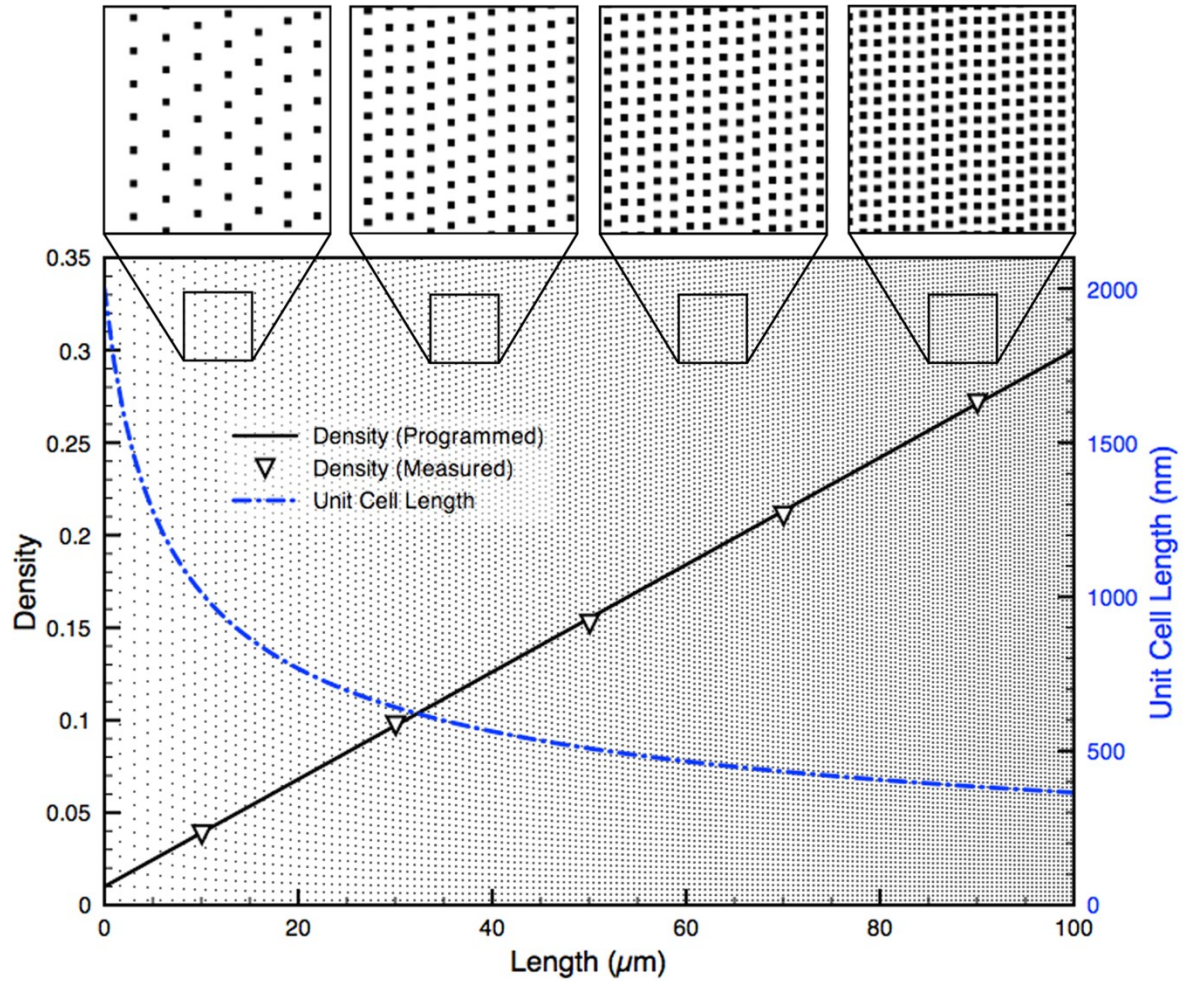


Figure AII-3. Programmed and measured density for an ordered linear DNG. A $100 \times 100 \mu\text{m}^2$ linear DNG comprised of $0.04 \mu\text{m}^2$ nanodots and spanning from 0.01 to 0.30 density. The measured density (left axis) precisely matches the programmed density ($R^2=0.9998$). The unit cell dimensions (right axis) change with the inverse square root of the density. Top insets show various spacing of nanodots at positions along the DNG.

$$D(l) = (D_{\max} - D_{\min}) \frac{l}{L} + D_{\min} \quad (2)$$

To verify that ordered gradients matched the programmed density functions, gradients were exported as bitmap images and the ratio of black to white pixels, averaged over several columns of nanodots, was used to measure density. The resulting gradients were found to match the programmed density functions with high fidelity ($R^2=0.9998$). A high fidelity match with the programmed density function was also demonstrated over a broad range of density values (0.01-0.99), and can be seen in supplementary **Figure AII-4**. Using this algorithm, a density of zero cannot be reached, as it would require an infinitely large unit cell. Consequently, when designing gradients of fixed length, the lowest density that is accessible may be limited since large unit cells are required at very low density.

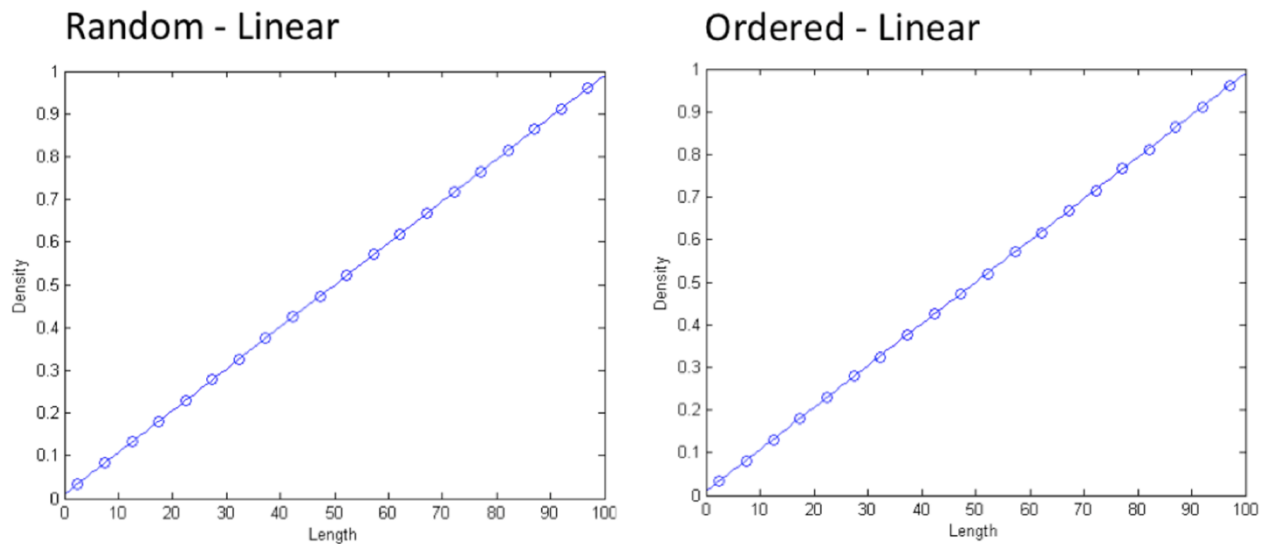


Figure AII-4. Ordered and random measured density matches programmed density over

full range. Linear gradients from densities of 0.01 to 0.99 were shown to match (dots) the programmed functions (line) with high fidelity for both ordered ($R^2 = 0.9988$) and random ($R^2 = 1.0000$) gradients. Using either approach, a high dynamic range can be achieved with near perfect match to the programmed function.

AII-4.2. Random Gradient Algorithm

Naturally occurring gradients appear continuous at the microscale, but are in fact digital at the scale of molecules and proteins. The diffusion of biomolecules is subject to Brownian motion, and is therefore expected to be random. In an effort to mimic the nanoscale noise present *in vivo*, we present an approach to produce DNGs with fully randomized nanodot positions. Similar to ordered DNGs, random gradients have increasing density along the length and constant density along the width.

Several strategies were considered to produce randomized DNGs. The first was akin to the one proposed by Dalby, *et al.* [16] and consisted of starting with a regular distribution of dots, and randomly displacing the nanodots within their “unit cell” to avoid overlap with neighboring dots. However because this approach only produces a quasi-random distribution, it was not pursued. A second approach that was considered was to start with a pseudo-random dot pattern, and then compensate for the overlap by locally moving dots. This parallels a strategy used in back-lit displays [29], however these patterns are unsuitable for our application due to the dependence on or optimization for quasi-random distributions. Whereas we don’t see fundamental obstacles in developing an algorithm to randomly redistribute overlapping dots, such algorithms tend to be computationally intensive as the position of each dot needs to be tested against each other dot,

and require multiple iterations to achieve the final distribution [27]. We thus devised a novel algorithm to create pseudo-random nanodot patterns for cell navigation that could translate arbitrary density functions into random nanodot patterns, and that was computationally economical.

The algorithm we developed compensates for the random overlap of dots by adding an excess of dots to achieve the programmed density. The algorithm first defines equally sized boxes to smoothly replicate the programmed density function without visible steps. The number of nanodots within each box was calculated based on the density function with predicted overlap at the box's position, and random x and y coordinates were generated for each nanodot. Only the nanodot coordinates were stored; the shape of the nanodots can be defined subsequently as the exported CIF file allows drawing shapes such as circles, polygons, etc. at the stored coordinates, thus making this approach flexible while reducing the file size and computation time. A consequence of the random nanodot position is that overlap between nanodots is possible. The frequency of overlap increases with density, which in turn results in a lower density than expected based on the surface area of all nanodots. However, because the distribution of the nanodots is random and the density known, the overlap is predictable, and can be compensated for so that the designed DNG matches the density function with high fidelity. For each box with area A_{box} , we first compute the probability P_{cov} that any given point in the box is covered by a nanodot of area A_{dot} (Eq. 3).

$$P_{cov} = \frac{A_{dot}}{A_{box}} \quad (3)$$

The probability $P_{not\ cov}$ that this point will *not* be covered by the nanodot is simply $1 - P_{cov}$ (Eq. 4).

$$P_{not\ cov} = \left(1 - \frac{A_{dot}}{A_{box}}\right) = \frac{A_{box} - A_{dot}}{A_{box}} \quad (4)$$

The probability that this point will not be covered by N nanodots simultaneously can then be found (Eq. 5).

$$P_{not\ cov} = \left(\frac{A_{box} - A_{dot}}{A_{box}}\right)^N \quad (5)$$

To determine the total area of the box covered by nanodots (A_{cov}), the probability that a point *will* be covered is integrated over the area of the box (Eq. 6).

$$A_{cov} = \int_{\emptyset}^{A_{box}} (1 - P_{not\ cov}) dA \quad (6)$$

$$A_{cov} = A_{box} - \frac{(A_{box} - A_{dot})^N}{A_{box}^{N-1}} \quad (7)$$

Eq. 7 can then be solved for N to determine the number of nanodots required for a given A_{cov} in each box.

$$N = \frac{\log(1 - A_{cov}/A_{box})}{\log(1 - A_{dot}/A_{box})} \quad (8)$$

Using Eq. 8 it is possible to obtain the number of nanodots required for any given density by substituting D for A_{cov}/A_{box} . As the area occupied approaches the area of the box, the number of nanodots required increases rapidly, and is infinite for a density of 1. The maximum density for a DNG was thus set to 0.9999. Without compensation, at density of 0.9999 would require 9,999 nanodots of $200 \times 200 \text{ nm}^2$ to be seeded into a $400 \times 1 \text{ }\mu\text{m}^2$ box to reach this density. When accounting for the overlap, 92,099 nanodots are required, roughly a tenfold increase. Thus, producing a typical linear gradient, ranging in density from 0.0002 to 0.4444 requires 1,061,307 nanodots and a computation time of 4.56 min (including CIF file generation). The ordered algorithm for the same linear gradient requires 885,737 nanodots and a computation time of 3.88 min. Therefore, the random gradient algorithm overall required a 19.8% increase in nanodots and a 17.5% increase in computation time using our workstation. It is expected that the time will increase for random DNGs that reach a higher density.

We compared the programmed density with the measured density of a monotonic exponential curve with decay constant k (Eq. 9) using both the ordered and random gradient generation approaches. Eq. 9 is normalized to span the dynamic range over the length of the gradient. The random gradients produced with this algorithm were found to follow the programmed curve with high fidelity ($R^2 = 0.99986$), and accurately match the measured density of ordered gradients produced with the same input function (**Fig. AII-5**).

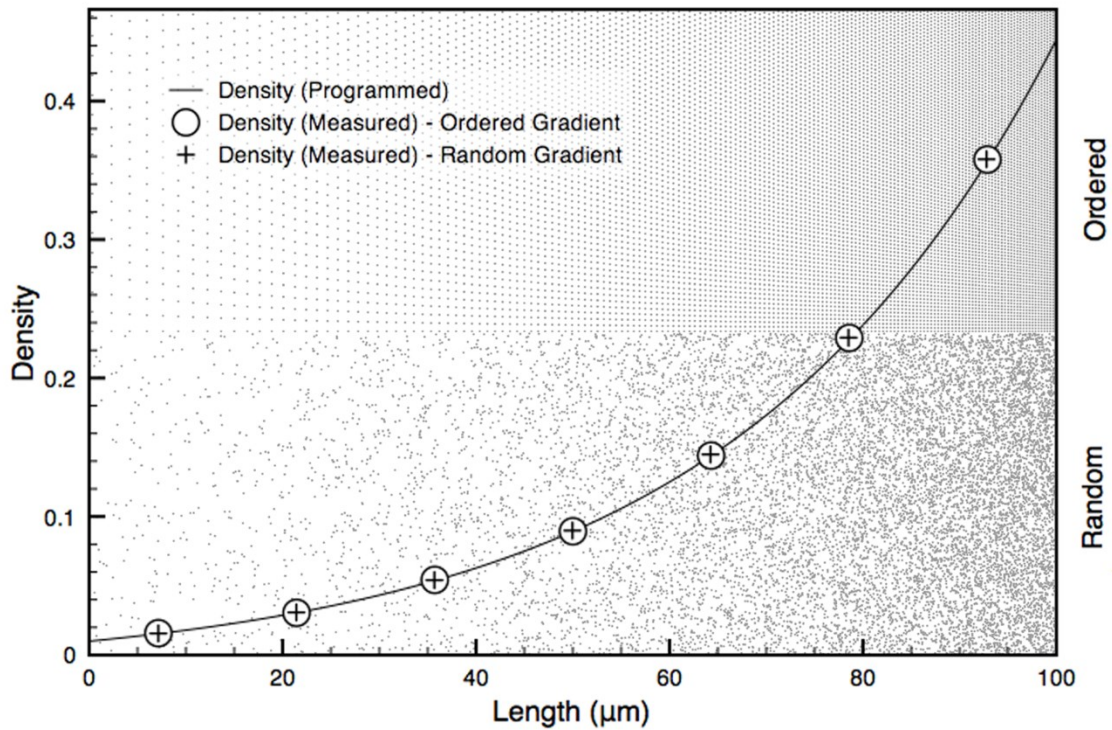


Figure AII-5. Ordered and random DNGs superposed with their programmed exponential density function and actual, measured density. A $100 \times 100 \mu\text{m}^2$ exponential ($k=3$) DNG spanning from a density of 0.01 to 0.30 is shown in ordered (top half) and random (bottom half) form. The random DNG was programmed by subdividing it into $1 \mu\text{m}$ wide boxes with random seeding of nanodots and compensating for overlap. The measured density follows the programmed exponential curve with high fidelity for both ordered ($R^2=0.99996$) and random ($R^2=0.99986$) DNGs.

$$D(l) = (D_{\max} - D_{\min}) \frac{e^{\frac{k}{L}l} - 1}{e^k - 1} + D_{\min} \quad (9)$$

The distribution of neighboring nanodots can be parsed to verify whether it satisfies the conditions of randomness. Since density changes along the length of the DNG, randomness can only be assessed in the direction of constant density, perpendicular to the gradient. The randomness along each box was verified using Ripley's K function based on the number of nanodots N_{p_i} within a distance s from the i^{th} point p_i taken over the sum of all points n and normalized by the area λ (Eq. 10).

$$K(s) = \frac{1}{n} \sum_{i=1}^n N_{p_i}(s) / \lambda \quad (10)$$

For a homogenous, random Poisson distribution, the expected value of Eq. 10 is πs^2 . Deviations from πs^2 indicate regions of clustering or dispersion [30]. Using the coordinates of nanodots from the DNGs, $K(s)$ was found to lie within a 95% confidence interval obtained from 10 simulations of randomly distributed coordinates at the same density. This suggests the nanodots are spatially homogenous and randomly distributed compared to ordered gradients, which lie outside the confidence interval (**Figure AII-6**).

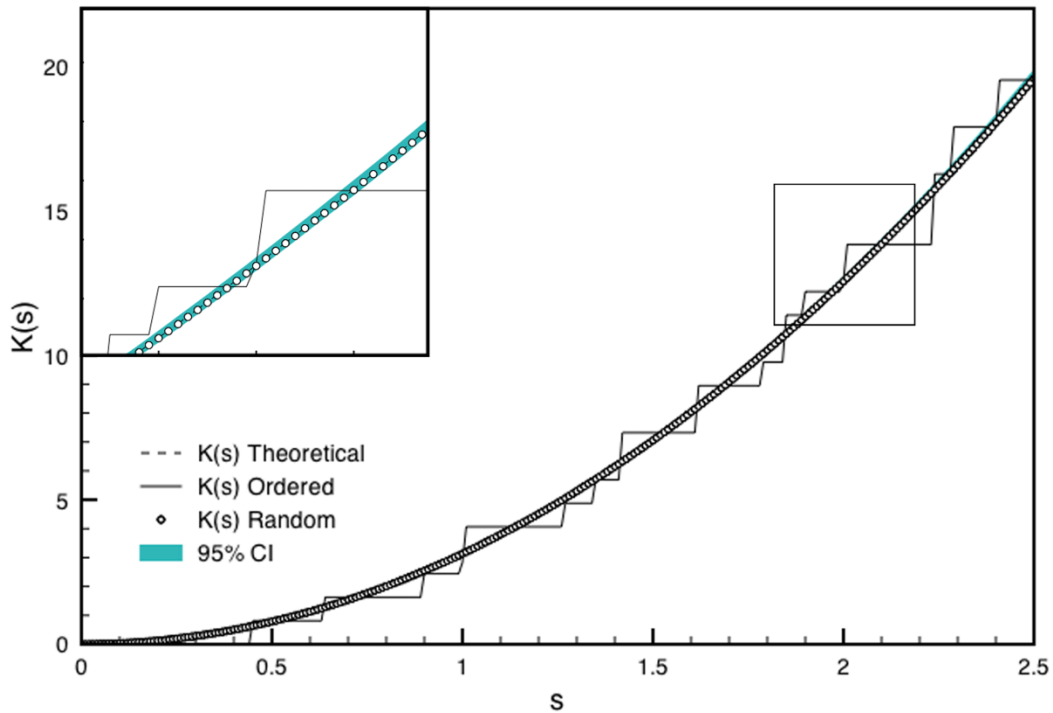


Figure AII-6. Ripley's K analysis for randomness and spatial homogeneity of a sample box produced with the ordered and random DNG algorithms. $K(s)$ for ordered and random gradients for a $10 \times 400 \mu\text{m}^2$ box at 0.20 density are shown. A 95% confidence interval was calculated as 1.96 times the standard deviation of $K(s)$ from 10 simulations of randomly distributed points at 0.20 density. The inset shows a magnified portion of the graph indicated by the box.

AII-4.3. Non-monotonic gradients

We have shown that linear and exponential gradients can be produced using either the ordered or random algorithms. These curves are monotonic, meaning they only ever increase or decrease.

Given the approaches outlined here, more complex gradients can be easily generated from any input density function, specifically non-monotonic curves. To study the ability of cells to recognize an average gradient in a non-monotonic environment, we propose linear and exponential gradients that are superposed with sinusoidal functions with either constant amplitude, or with linear or exponentially changing amplitude. In the anticipation of future cell experiments, we also programmed a series of sinusoids with varying frequency and amplitude, while having an average slope of zero to act as negative controls.

Here, we demonstrate the flexibility of the algorithms with the production of non-monotonic gradients. One such gradient produced is a sinusoid with exponentially increasing amplitude superposed with an exponential gradient (**Figure AII-7**). Eq. 11 gives the input density function for such a curve, where A is the amplitude, B is the number of oscillations, and k_1 and k_2 are the decay constants for the average gradient and amplitude of the sinusoid, respectively.

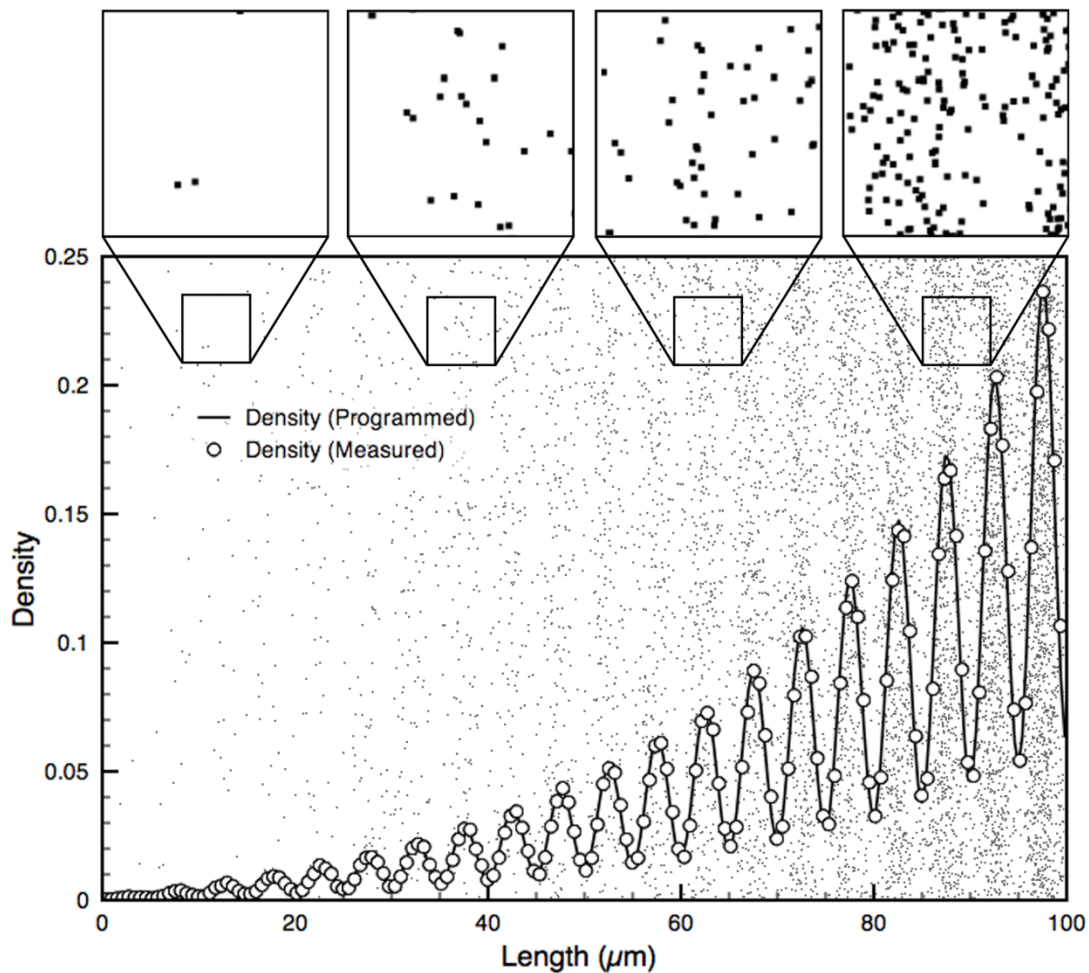


Figure AII-7. Non-monotonic random DNG superposed with its density function and actual, measured density. A $100 \times 100 \mu\text{m}^2$ non-monotonic DNG. The programmed density function (line) is a sinusoid ($A=0.10$, $B=20$) with an average exponential trend ($k_1=3$) and exponentially increasing amplitude ($k_2=3$). Measured density from bitmap (circles) accurately follows the programmed function ($R^2=0.9988$). Insets show close-up views of nanodots and reveal increasing overlap of nanodots at higher densities.

$$D(l) = (D_{\max} - D_{\min}) \frac{e^{k_1 \frac{l}{L}} - 1}{e^{k_1} - 1} + A \sin\left(2\pi B \frac{l}{L}\right) \frac{e^{k_2 \frac{l}{L}} - 1}{e^{k_2} - 1} + D_{\min} \quad (11)$$

AII-4.4. One-Hundred-Gradient Array

The flexibility of the gradient algorithms and the fabrication method discussed below was leveraged by producing an array of 100 distinct gradients within a 35 mm² area (**Figure AII-8**). The array is comprised of 20 ordered and 80 random gradients, with densities ranging from 0.0002 to 0.4444 for a maximum dynamic range of 3.85 OM. For ordered gradients, this corresponds to a maximum pitch of 14.8 μm at low density, and 100 nm at high density. The minimum density is limited by the size of the cell and its capacity to sense the gradient, *i.e.* the cell will not sense the gradient if dot spacing exceeds one third the size of the cell, which we previously assessed using the migratory response of C2C12 myoblasts [14]. The maximum density is defined by the resolution of e-beam lithography, which limits the minimum pitch to 100 nm. To address how randomness affects cell navigation, 20 gradients (10 linear and 10 exponential) were produced as both ordered (#1-20) and random (#81-100) gradients. This portion of the array will serve to address gradient sensing mechanics for cell migration that may arise from either (i) the absolute concentration of the gradient at a given location or (ii) the concentration ratio between the cell's leading and trailing edges.

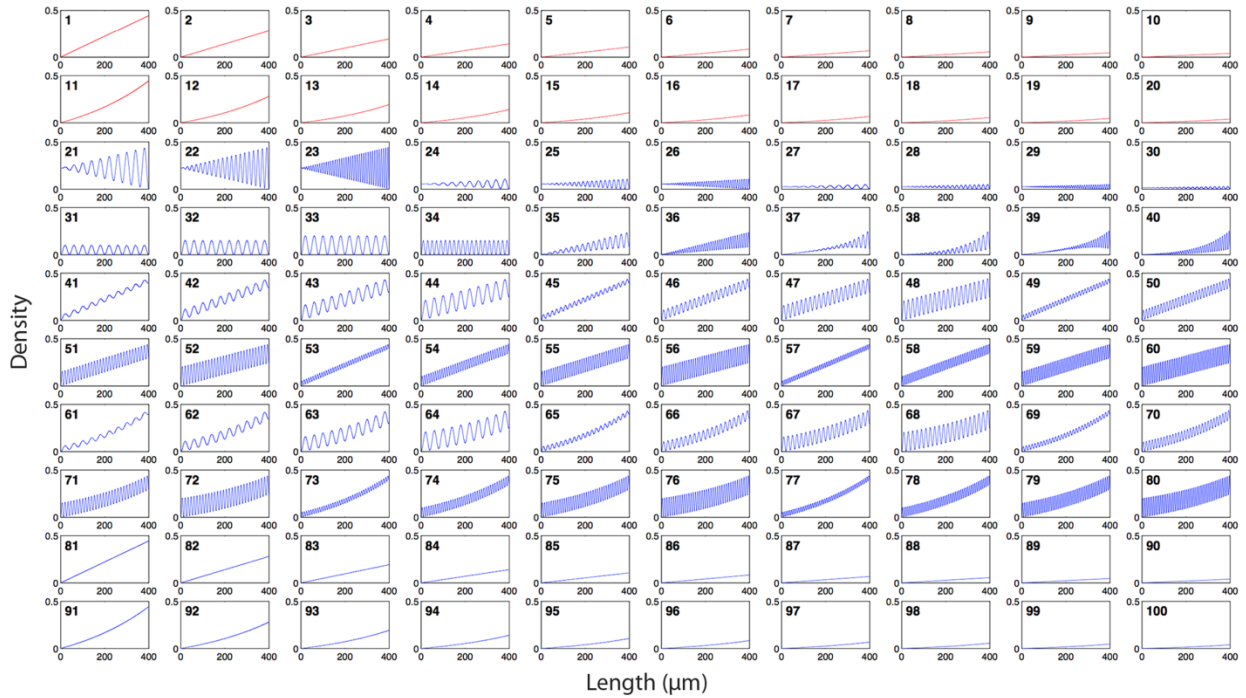


Figure AII-8. Density functions of the array of 100 DNGs. Each box shows the density function of one gradient. Functions 1-20 were produced with the ordered gradient algorithm (red), and functions 21-100 were produced with the random gradient algorithm (blue). Functions 1-10 and 81-90 are linear. Functions 11-20 and 91-100 are exponential. Functions 21-34 are sinusoidal with no slope (controls), where 21-30 have linearly increasing amplitude and 31-34 have constant amplitude. Functions 35-36 feature a linear slope superposed with a sinusoid that has constant amplitude. Functions 37-40 feature an exponential slope superposed with a sinusoid that has exponentially increasing amplitude. Functions 41-60 have a constant slope superposed with a sinusoid of constant amplitude. Functions 61-80 are exponential slopes superposed with sinusoids of constant amplitude.

The other 60 gradients are non-monotonic and random. These consist of 14 sinusoids with no average slope (#21-34) that serve as controls. These vary in frequency and amplitude, and may have constant or increasing amplitude along their length. Controls for ordered gradients were designed in our prior work. The remaining 46 gradients (#35-80) have sinusoidal curves with various levels of complexity. These include sinusoids with linearly (#41-60) and exponentially (#61-80) increasing average density, and non-monotonic functions with linearly increasing amplitude and average density (#35-36) and exponentially increasing amplitude and average density (#37-40) to demonstrate the flexibility of this new approach in gradient generation. As discussed, the sinusoidal curves with different amplitude and frequency may introduce obstacles for cells trying to sense the overarching gradient, and replicate effects that may occur due to cell “mosaicism” in a controlled manner.

AII-4.5. Gradient Array Fabrication

The hundred-gradient array was etched 100 nm deep into a Si wafer by e-beam lithography (**Figure AII-9**). The integrity of individual dots for ordered and random gradients was confirmed by scanning electron microscopy (SEM) (**Figure AII-10**).

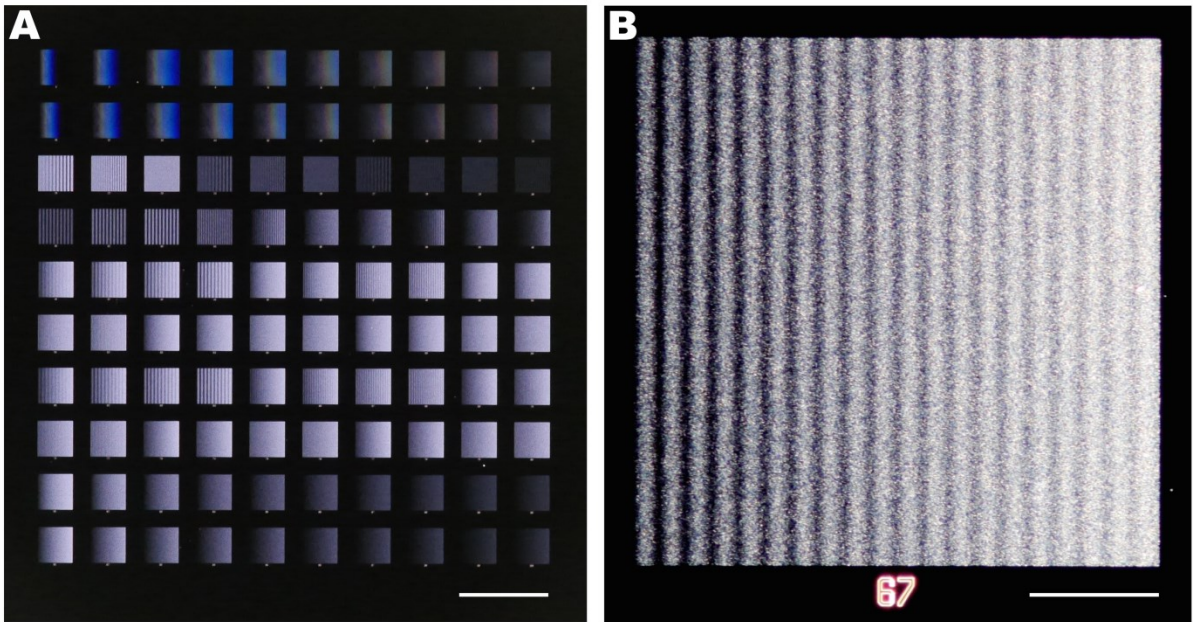


Figure AII-9. Optical images of the 100-gradient-array. The 100 DNGs were patterned into a Si wafer using e-beam lithography. (A) Image of all gradients; scale bar is 1 mm. (B) Dark-field image of DNG 67 which is a random sinusoid with exponentially increasing average density; scale bar is 100 μm .

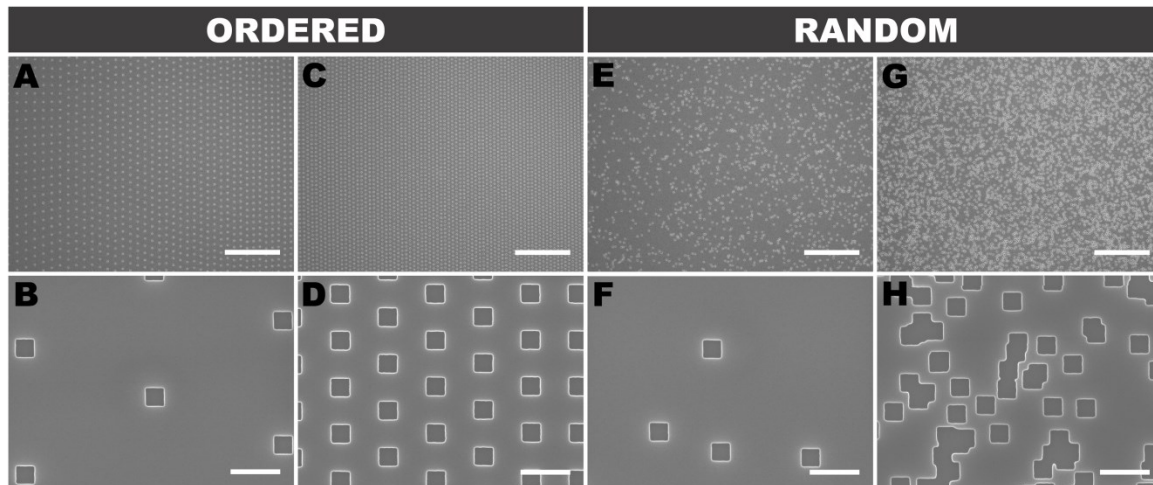


Figure AII-10. Nanodot distribution in ordered and random DNGs. SEMs of ordered (A-D) and random (E-H) exponential gradients at low (A,B,E,F) and high (C,D,G,H) densities. (H) highlights the random overlap between nanodots that is compensated for by the random DNG algorithm. Scale bars are 10 μm (top row) and 500 nm (bottom row).

To translate the etched Si wafer into substrate-bound protein gradients, we employed lift-off nanocontact printing [14]. First, a PDMS intermediate replica was produced, followed by a second replication into low-cost Norland Optical Adhesive. A flat PDMS stamp was inked with a protein solution, and through contact with the plasma-activated NOA lift-off stamp, a monolayer of protein was selectively removed from the surface of the flat stamp leaving behind the digital nanodot protein pattern. Next, the flat PDMS stamp was brought into contact with a plasma-activated glass slide to transfer the DNG pattern. To confirm the accuracy of the replication and printing process, images of the design and the printed protein DNG were digitally overlapped and compared (**Figure AII-11**), revealing a high fidelity between the two patterns.

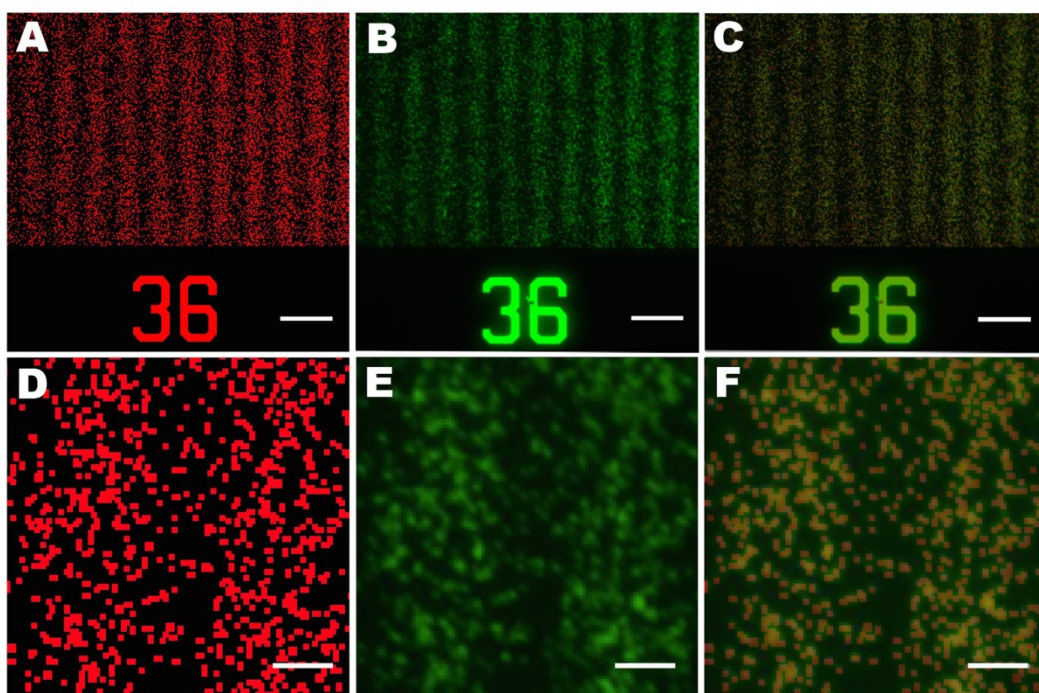


Figure AII-11. The printed nanodot pattern accurately replicates the design. Bitmap image of the programmed design colored in red (A, D) compared with a fluorescent image of nanocontact printed IgG by lift-off (B, E, green) and merged (C, F). In the inset (E), out of ~1000 spots, 21 are missing, indicating that the replication works well. Scale bars A-C are 10 μm , scale bars D-F are 2 μm .

The pattern overlay in **Figure AII-11** was characterized by thresholding the printed image with boundaries of 31 and 255 in ImageJ and comparing it to the bitmap image (**Figure AII-12**). The total number of nanodots is difficult to determine owing to the random overlap, but we estimate that there are ~1000 spots, and using the above threshold, 21 were lacking from the print. Overall, the transfer process is thus accurate to ~98% in this example. Dust particles on the Si wafer or on the intermediate PDMS replica, or mechanical damage due to the replication process

could account for the absence of these protein dots. While the fidelity of the replication and printing process is high, it might be improved further by employing more durable polymers during the replication process as well as by working in a cleanroom environment throughout.

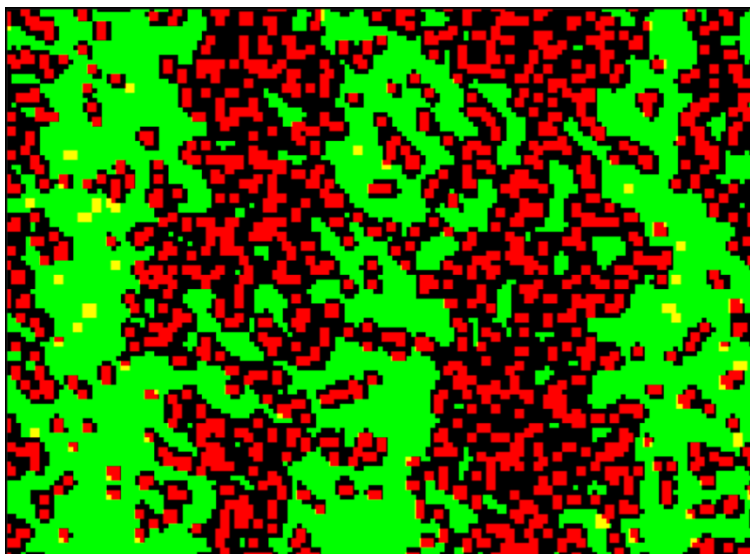


Figure AII-12. Image processing procedure to assess alignment of the DNG design and print. The fluorescent image of nanocontact printed IgG was first thresholded in ImageJ with boundary values of 31 and 255. The image was then transformed to binary and the binary values inverted to facilitate visualization. The edited fluorescent image (green) was then merged with the bitmap (red) and yellow dots, indicative of non-printed dots, were counted to determine to what extent the print matched the design.

AII-5 Conclusion

Patterned substrate-bound protein gradients are a valuable tool to study a number of biological processes such as neuronal development or regeneration. The novel algorithms presented here, providing pseudo-randomness at a scale commensurate to the cellular level, can provide control over geometry and noise in DNGs. Combined with high-throughput patterning, an array of one hundred DNGs with linear, exponential, and non-monotonic slopes featuring 57 million spots

over an area of 35 mm² can be patterned at once in a matter of minutes. The diversity of DNGs shown here will help study and quantify the mechanisms by which cells sense and navigate through immobilized gradients. There are many opportunities for refining digital nanodot patterns. Firstly, to mimic the self-repellent nature of proteins adsorbing to surfaces, it might be useful to develop an algorithm that prevents, or limits, the overlap of nanodots. Secondly, whereas here two curves were superposed in one direction, such curves might be generated in two perpendicular directions to create a two-dimensional navigation landscape to better mimic the local accumulation of guidance cues as puncta. Thirdly, it might be possible to program density functions that introduce clusters of noise that more accurately replicate the noise and mosaicism imposed by individual cells *in vivo* which can extend over tens of micrometers. Fourthly, it should be possible to pattern overlapping DNGs of different proteins that run in the same, or different directions, as well as produce any type of navigational landscapes that are found *in vivo* simply by converting the recorded densities into digital nanodot patterns, following the trend of rapid prototyping of replicas of living tissues [31]. Before expanding the nanodot patterning, it will be important to test and validate the current DNGs and establish the optimal conditions along with the suitable non-patterned reference surfaces for each study [32].

AII-6 References

1. McLaughlin T, O'Leary DDM (2005) Molecular gradients and development of retinotopic maps. *Annu Rev Neurosci* 28: 327-355.
2. Chung BG, Flanagan LA, Rhee SW, Schwartz PH, Lee AP, et al. (2005) Human neural stem cell growth and differentiation in a gradient-generating microfluidic device. *Lab on a Chip* 5: 401-406.

3. Goodman CS (1996) Mechanisms and molecules that control growth cone guidance. *Annual Review of Neuroscience* 19: 341-377.
4. Kim BK, Lee JW, Park PJ, Shin YS, Lee WY, et al. (2009) The multiplex bead array approach to identifying serum biomarkers associated with breast cancer. *Breast Cancer Res* 11: R22.
5. Lander AD, Nie Q, Wan FYM (2002) Do morphogen gradients arise by diffusion? *Developmental Biology* 247: 471-471.
6. Gurdon JB, Bourillot PY (2001) Morphogen gradient interpretation. *Nature* 413: 797-803.
7. Keenan TM, Folch A (2008) Biomolecular gradients in cell culture systems. *Lab on a Chip* 8: 34-57.
8. Joanne Wang C, Li X, Lin B, Shim S, Ming G-l, et al. (2008) A microfluidics-based turning assay reveals complex growth cone responses to integrated gradients of substrate-bound ECM molecules and diffusible guidance cues. *Lab on a Chip* 8: 227-237.
9. Mai J, Fok L, Gao HF, Zhang X, Poo MM (2009) Axon Initiation and Growth Cone Turning on Bound Protein Gradients. *Journal of Neuroscience* 29: 7450-7458.
10. Dertinger SKW, Jiang XY, Li ZY, Murthy VN, Whitesides GM (2002) Gradients of substrate-bound laminin orient axonal specification of neurons. *Proceedings of the National Academy of Sciences of the United States of America* 99: 12542-12547.
11. Von Philipsborn AC, Lang S, Bernard A, Loeschinger J, David C, et al. (2006) Microcontact printing of axon guidance molecules for generation of graded patterns. *Nature Protocols* 1: 1322-1328.

12. Coyer SR, García AJ, Delamarche E (2007) Facile Preparation of Complex Protein Architectures with Sub-100-nm Resolution on Surfaces. *Angewandte Chemie International Edition* 46: 6837-6840.
13. von Philipsborn AC, Lang S, Loeschinger J, Bernard A, David C, et al. (2006) Growth cone navigation in substrate-bound ephrin gradients. *Development* 133: 2487-2495.
14. Ricoult SG, Pla-Roca M, Safavieh R, Lopez-Ayon GM, Grütter P, et al. (2013) Large Dynamic Range Digital Nanodot Gradients of Biomolecules Made by Low-Cost Nanocontact Printing for Cell Haptotaxis. *Small* 9: 3308-3313.
15. Raser JM, O'Shea EK (2005) Noise in gene expression: Origins, consequences, and control. *Science* 309: 2010-2013.
16. Dalby MJ, Gadegaard N, Tare R, Andar A, Riehle MO, et al. (2007) The control of human mesenchymal cell differentiation using nanoscale symmetry and disorder. *Nature Materials* 6: 997-1003.
17. Kantawong F, Burgess KEV, Jayawardena K, Hart A, Burchmore RJ, et al. (2009) Whole proteome analysis of osteoprogenitor differentiation induced by disordered nanotopography and mediated by ERK signalling. *Biomaterials* 30: 4723-4731.
18. Tonazzini I, Meucci S, Faraci P, Beltram F, Cecchini M (2013) Neuronal differentiation on anisotropic substrates and the influence of nanotopographical noise on neurite contact guidance. *Biomaterials* 34: 6027-6036.
19. Dickinson R, Tranquillo R (1993) A stochastic model for adhesion-mediated cell random motility and haptotaxis. *Journal of Mathematical Biology* 31: 563-600.
20. Smith JT, Elkin JT, Reichert WM (2006) Directed cell migration on fibronectin gradients: Effect of gradient slope. *Experimental Cell Research* 312: 2424-2432.

21. Weber M, Hauschild R, Schwarz J, Moussion C, de Vries I, et al. (2013) Interstitial Dendritic Cell Guidance by Haptotactic Chemokine Gradients. *Science* 339: 328-332.
22. Sweetser DA, Birkenmeier EH, Hoppe PC, McKeel DW, Gordon JI (1988) Mechanisms underlying generation of gradients in gene expression within the intestine: an analysis using transgenic mice containing fatty acid binding protein-human growth hormone fusion genes. *Genes & Development* 2: 1318-1332.
23. Ming GL, Wong ST, Henley J, Yuan XB, Song HJ, et al. (2002) Adaptation in the chemotactic guidance of nerve growth cones. *Nature* 417: 411-418.
24. Pappas TN (1994) Digital Halftoning Techniques for Printing. *Icps '94: The Physics and Chemistry of Imaging Systems - Is&T's 47th Annual Conference, Vols I and II*: 468-471.
25. Ulichney R (1987) *Digital halftoning*: MIT press.
26. Dev P (1975) Perception of Depth Surfaces in Random-Dot Stereograms - Neural Model. *International Journal of Man-Machine Studies* 7: 511-528.
27. Imamichi T, Numata H, Mizuta H, Ide T (2011) Nonlinear Optimization to Generate Non-Overlapping Random Dot Patterns. *Proceedings of the 2011 Winter Simulation Conference (Wsc)*: 2414-2425.
28. Dalal IL, Stefan D, Harwayne-Gidansky J (2008) Low Discrepancy Sequences for Monte Carlo Simulations on Reconfigurable Platforms. *2008 International Conference on Application-Specific Systems, Architectures and Processors*: 108-113.
29. Chang JG, Su MH, Lee CT, Hwang CC (2005) Generating random and nonoverlapping dot patterns for liquid-crystal display backlight light guides using molecular-dynamics method. *Journal of Applied Physics* 98.

30. Kiskowski MA, Hancock JF, Kenworthy AK (2009) On the Use of Ripley's K-Function and Its Derivatives to Analyze Domain Size. *Biophysical journal* 97: 1095-1103.
31. Derby B (2012) Printing and Prototyping of Tissues and Scaffolds. *Science* 338: 921-926.
32. Ricoult SG, Thompson-Steckel G, Correia JP, Kennedy TE, Juncker D (2014) Tuning cell–surface affinity to direct cell specific responses to patterned proteins. *Biomaterials* 35: 727-736.